Gold nanorod photoluminescence : applications to imaging and temperature sensing

Carattino, A.

Citation

Carattino, A. (2017, March 9). *Gold nanorod photoluminescence : applications to imaging and temperature sensing*. *Casimir PhD Series*. Retrieved from https://hdl.handle.net/1887/46596

Author: Carattino, A.
Title: Gold nanorod photoluminescence : applications to imaging and temperature sensing
Issue Date: 2017-03-09

GOLD NANOROD PHOTOLUMINESCENCE

APPLICATIONS TO IMAGING AND TEMPERATURE SENSING

GOLD NANOROD PHOTOLUMINESCENCE

APPLICATIONS TO IMAGING AND TEMPERATURE SENSING

Proefschrift

ter verkrijging van
de graad van Doctor aan de Universiteit Leiden,
op gezag van de Rector Magnificus prof. mr. C. J. J. M. Stolker,
volgens besluit van het College voor Promoties,
te verdedigen op donderdag 9 maart 2017
klokke 13:45 uur

door

Aquiles CARATTINO

geboren te Buenos Aires (Argentinië)
in 1986

Promotor: Prof. dr. M. A. G. J. Orrit

Promotiecomissie: Prof. dr. N. H. Dekker (TU Delft)
Prof. dr. A. F. Koenderink (FOM Institute AMOLF)
Prof. dr. E. R. Eliel
Prof. dr. M. P. van Exter
Dr. ir. S. J. T. van Noort
Prof. dr. T. Schmidt

Keywords: Gold Nanorods, Luminescence, Imaging, Anti-Stokes, Temperature

Printed by: Gildeprint

Front & Back: Cover art design by Camila Carattino.

FSC
www.fsc.org
MIX
Paper from
responsible sources
FSC® C012854

Casimir PhD Series, Delft-Leiden 2017-03

ISBN 978-90-8593-288-8

An electronic version of this thesis can be found at
`https://openaccess.leidenuniv.nl/`.

The work described in this thesis is part of the research programme of the Foundation for Fundamental Research on Matter (FOM), which is part of the Netherlands Organisation for Scientific Research (NWO).

Voor mijn ouders en mijn zus

PREFACE

Behind every thesis lies a story that involves much more people than the mere author whose name is on the cover. This book is the conclusion of four years of work in the MoNOS group at the physics institute in Leiden, where I have focused on the study of single gold nanorod luminescence and its possible applications.

The project was framed within a larger collaboration with three more groups from biophysics, biology and chemistry. The aim of the project was utilizing single gold nanorods as labels in the nucleus of cells, focusing into the study of the glucocorticoid receptor. My part in the collaboration was the understanding of the mechanisms that give rise to the luminescence of single gold nanorods, crucial for the imaging and tracking in living cells. Even if my work was not biophysical, I always kept an eye into the biological applications of my research.

A Friday afternoon idea, triggered by postdoc Saumyakhanti Khatua evolved into what now is chapter 2 of this booklet. He asked me if it was possible to monitor the etching process of gold by cyanide ions in single gold nanoparticles. The first trial showed already something interesting: single particles on glass were behaving completely different than in bulk suspension. More importantly, to answer the question it was clear that we needed better software to control the setup.

Ferry Kruidenberg, a bachelor student at the time, joined the group to help develop the software even further. He designed the core layout of the program and the first graphical user interface. Together we learned about version control, instrumentation and programming patterns. Simultaneously, a master student, Irina Komen, joined the group to start working on an optical tweezer. Together we managed to obtain photothermal signals from single nanoparticles that were trapped in water and glycerol. However, the final objective was to study the fluorescence enhancement of a dye in the vicinity of the rod while away from any other surface, thus preventing sticking of the molecules to the coverslip.

Even if the results on the optical tweezer didn't fit into this thesis, while characterizing the emission from different nanoparticles an interesting phenomenon appeared: emission at higher energies than the excitation energy, the anti-Stokes emission. This emission proved to be reasonably efficient, sometimes even comparable to the Stokes-shifted counterpart. The detection of anti-Stokes luminescence was consistent between different samples and under different conditions.

Anti-Stokes luminescence opened the door to two different approaches. Firstly it was possible to exploit the emission at shorter wavelengths to suppress the background when imaging under biological conditions. Cells are known to fluoresce under laser irradiation and therefore dim emitters such as small nanoparticles are hard to distinguish from the background. After discussing with Veer Keizer, a PhD candidate in biology belonging to the same project, we embarked into the exploitation of the anti-Stokes emission for imaging. These ideas led to Chapter 3 and its publication in the Biophysical Journal. It was very well received by the reviewers, one of them qualified the findings as a “very important breakthrough”.

However, there was more in the anti-Stokes emission than solely the application to imaging. If the emission depends on temperature, it can be used as a nano-thermometer. Photothermal therapy is a fertile subject that relies on locally increasing the temperature to kill specific cells. This is achieved by shining a laser onto gold nanoparticles inside or in the vicinity of those cells. However there are so far no ways of controlling the temperature of the particles. Studying the anti-Stokes emission can be a solution to a long standing problem in the medical and biological sciences.

To prove the usefulness of the method, the measurements were performed in a temperature variable flow cell. An air spaced objective was needed to avoid altering the temperature of the observed area, which in turn lowered the collection efficiency. At higher temperatures (around $60\,^{o}$C) the setup drifts several micrometers and therefore an accurate control of temperature and a proper tracking of the particles was needed.

Chapter 4 shows that it is indeed possible to determine the absolute temperature of single nanoparticles just by measuring their anti-Stokes spectrum. The method does not require any form of *ad-hoc* calibration and can be easily implemented in any confocal microscope coupled with a spectrometer. These findings can have a major impact on photothermal therapy and in material sciences, where the question of the temperature reached by the particles has been open for more than 20 years. Testing the method in real situations is the next logical step but was outside the time frame of the thesis.

With the experience built on the anti-Stokes luminescence, characterizing the scattering of single gold nanoparticles at different temperatures did not prove to be particularly challenging. Since the first inception of the computer software until the last version, that allowed to acquire all the data in Chapter 5, almost 4 years had passed.

This work summarizes a lot of effort by a lot of people. It neglects all the failed experiments and frustrations. It is important to remind that failure is only a relative measure; while we learn something either of nature or of ourselves, we are being successful.

Aquiles Carattino
Leiden, March 2017

CONTENTS

1

INTRODUCTION

Gold nanorods are ideal candidates for complementing fluorophores in labelling applications. The presence of the surface plasmon resonance generates large absorption and scattering cross sections, thus making the detection of single nanoparticles possible under a light microscope. In this introduction we will review the current status of light microscopy, particularly of fluorescence microscopes. We will introduce some properties of gold nanoparticles including the plasmon resonance and we will focus into the luminescence emission. Finally we will briefly introduce the experimental chapters of this thesis, that correspond to applications of the luminescence ranging from imaging to temperature sensing.

1.1. LIGHT MICROSCOPY

MICROSCOPES have become indispensable tools in material science and biology. The first microscopes developed by Antoni Van Leeuwenhoek in the XVII century were aimed at studying fabrics; it didn't take long however to discover that nature was hiding amazing details beyond what the bare human eye could see. The first microscope builders focused into developing better lenses in order to obtain sharper images and therefore being able to observe even smaller structures.

With the development of the wave theory of light a fundamental limitation for optical microscopes appeared: the diffraction limit. Abbe realized that no matter how good a lens is, there will always be a limit to how much it is possible to focus light. This limit is determined mainly by the wavelength of the employed light beam and by the maximum acceptance angle of the lens. Shortening the wavelength of the sources is therefore a possible strategy to increase the resolution of a microscope.

Particles with wavelengths shorter than optical wavelengths, such as electrons, opened the possibility to investigate much smaller structures[1]. Notably in the field of virology the electron microscope provided the evidence that researchers were long looking for: the existence of particles smaller than what optical microscopes were able to resolve. Electron microscopes are a very powerful tool but they require special sample preparations that don't allow the study of biological processes *in vivo*.

With a similar strategy, the resolution of optical microscopes can be increased with the use of ultraviolet sources. Some biological samples show emission of light at longer wavelengths when irradiated with UV light, nowadays simply referred to as autofluorescence. In 1911 German physicist Oskar Heimstädt used the the emission from bacteria to build the first fluorescence microscope[2]. The difficulties to focus enough UV light into the sample and the low efficiency in collecting the emission made him skeptical of the success of his design. He ended his work stating[3],

> If and to what degree fluorescence microscopy will widen the possibilities of microscopic imaging only the future will show.

Fluorescence however was not a new phenomenon. It was first observed and characterized during the second half of the 19th century. The pioneering works of Stokes showed that some materials when irradiated with short wavelengths emit light at longer ones. Only in the 1930s did the first applications of fluorescent materials start to emerge for biological applications. Fluorophores were employed to stain biological samples, allowing to easily detect tissue components or bacteria. Oskar Heimstädt could rest assured that his invention was starting to revolutionize biology.

The following decades witnessed a phenomenal increase in technical developments, including the advancement of epi-illimuniation, the confocal microscope and the improvement of filters and light sources. The dichromatic mirror, the final key element of a fluorescence microscope, was introduced in 1967[4]. The wealth of information that could be retrieved thanks to fluorescence and its simple implementation were crucial for the success of the fluorescence microscope and its establishment as a standard tool in almost any biological or material science laboratory. Fluorescence microscopes however do not overcome the diffraction limit.

At the end of the XX century a major breakthrough occurred in the field of optics: the detection of a single-molecule fluorescence in 1990[5]. Single molecules opened the door to determine material properties that would have been hidden by ensemble averaging. The first studies were performed at low temperature (few Kelvins) and gave access to properties not only of the fluorescence of molecules themselves but also of the hosting matrices, mainly polymers and crystals. Single molecules are the bridge between the diffraction limit of far field optics and the atomic scale properties of materials.

Single-molecule microscopy also changed the way imaging can be performed. If two fluorophores are separated further away than the diffraction limit, their centers can be determined with a precision that scales as $\approx 1/\sqrt{N}$, with N the number of recorded photons. The possibility of localizing single molecules beyond Abbe's limit shows how useful single-molecule detection could be. For example, tracking of single molecules[6] could be used to study diffusion with unprecedented spatial and temporal resolutions.

In relevant biological samples, however, the density of fluorophores is such that they are not further apart than the diffraction limit. In the late 1990s it was found that the fluorescence of molecules can be switched on and off by irradiating them with specific wavelengths[7]. This led to the development of a wide variety of techniques that rely on switching on and off molecules[8], and therefore they can be individually localized[9]. Post processing the information of each fluorescent molecule allows to reconstruct images with a spatial resolution an order of magnitude higher than the diffraction limit[10].

Molecules, however, show two phenomena known as blinking[11] and bleaching[12]. At room temperature it is impossible to prevent fluorophores from going to dark states, meaning that their fluorescence signal will disappear. Blinking characterizes the process by which fluorescence disappears for a comparatively short period of time. If the molecule undergoes an irreversible transition to a dark state, the process is called bleaching. Blinking and bleaching put a hard limit to the experiments that can be performed with single molecules, since they cannot be observed for extended periods of time. Tracking is limited to few seconds, and imaging is limited to few frames.

As single-molecule detection allowed to bridge the length mismatch between visible light and biologically relevant scales, new agents that can fill the gap between biologically relevant time scales and fluorophores' observation times are of utmost importance. In this direction different approaches were taken, including the use of scattering instead of fluorescence[13], the use of semiconductor quantum dots[14] and of metallic nanoparticles[15]. The latter are the focus of this thesis and of the next few sections.

1.2. GOLD NANOPARTICLES

Metallic nanoparticles have been utilized for a very long time. In a fortuitous way Romans dispersed gold salts into oxide mixtures that then they melted to obtain red-coloured glass; the beautiful Lycurgus cup[16] is the only surviving complete example of an artifact made out of such glasses. Nanoparticles in the glass have preserved their optical properties for centuries and can still be admired today. In medieval times the technique was rediscovered and became common in the fabrication of red-coloured glasses for churches throughout Europe.

The explanation of the phenomenon however only came one century ago. Gustav Mie in 1908 calculated the scattering of a plane wave incident on spherical particles[17] by fully solving Maxwell's equations. This solution is known today as Mie scattering. The original paper compared measured and calculated scattering spectra of gold nanospheres; both experiments and theory show a peak at around 550 nm. The weaker interaction with light of longer wavelengths explains the reddish color of colloidal gold nanoparticle suspensions.

The peak observed in the spectra is related to a resonance of the oscillating conduction electrons on the surface of the metal and is known as plasmon resonance. For particles much smaller than the incident wavelength, a simplification of the Mie formalism can be made by considering only the first order electrostatic approximation. In this case the polarizability of a nanosphere of volume V is given by[18]

$$\alpha_{\text{sphere}} = 3\epsilon_0 V \frac{\epsilon(\omega) - \epsilon_m}{\epsilon(\omega) + 2\epsilon_m} \tag{1.1}$$

where ϵ_0 is the permittivity of vacuum, $\epsilon(\omega)$ is the permittivity of the metal as a function of the incoming excitation frequency ω and ϵ_m is the permittivity of the surrounding medium. The absorption cross section can thus be calculated as $\sigma_{\text{abs}} = k\text{Im}(\alpha)$ and the scattering as $\sigma_{\text{scatt}} = k^4|\alpha|^2/(6\pi)$.

From equation 1.1 it is possible to see that a resonance will appear when $\text{Re}(\epsilon(\omega)) = -2\epsilon_{\text{m}}$. It is important to note that the energy at which this resonance appears is therefore dependent not only on the particle's material properties but also on the surrounding medium's optical constants. In the case of elongated nanoparticles, some correction factors can be introduced to the polarizability. Several computer packages[19–21] exist to calculate with a great precision absorption and extinction cross sections of arbitrary geometries and therefore it is not worth entering into the specifics of the calculations[1].

It is important to point out, however, that while nanospheres have resonances that slightly change with their radius, elongated particles such as nanorods present a longitudinal resonance that strongly depends on their aspect ratio. The more elongated particles will have resonances with lower energies. Moreover particles with resonances to the near infrared region show a narrower resonance[22], making them interesting candidates for sensing applications. In biological conditions, nanoparticles with resonances towards longer wavelengths are particularly relevant because cells are typically transparent to near-infrared wavelengths.

A standard procedure to obtain gold nanoparticles is synthesis through wet chemical methods[23]. Even in the best of cases there will be a dispersion of shapes in the sample. The differences between nanoparticles can be observed on electron micrographs, but also optically. Slightly different particles will show different resonances[24] and this becomes more significant for elongated particles. Minute changes in shape will lead to different plasmonic resonances, that can be observed under the microscope. In a sample of such particles it is unlikely that two of them will have the exact same resonance. Dimers and clusters will therefore have a characteristic signature since more than one resonance will be observed in general.

The distribution of resonance energies has another important advantage: studying properties that depend on the resonance does not require a new synthesis nor changing

---

[1] A complete description of how to calculate the plasmon resonance with the ADDA package can be found at: https://www.aquicarattino.com/science/plasmon-resonance/

the sample. Once the nanoparticles are immobilized on a substrate it is possible to characterize them individually, select the ones with particular resonances and perform the rest of the experiments on them. All the chapters in this thesis show results that were gathered through the study of different particles in the same sample and under the same exact conditions: from chemical reactions in chapter 2 to electron phonon coupling in chapter 5 and anti-Stokes luminescence in chapters 3 and 4.

Besides the geometrical factors, nanoparticles also show a broad distribution of their quantifiable properties. For example, the quantum yields of nanoparticles that are apparently equivalent (similar in size, same resonance energy) can differ from each other by almost an order of magnitude[25]. In every chapter of this thesis variations from particle to particle can be observed. Chapter 2 shows that the etching rates can vary from particle to particle, in chapter 5 we have observed that the broadening rates when increasing temperature can differ from particle to particle. It means that particles differ from each other more than what an optical or scanning electron microscopes can resolve. The only way of validating the observed results is therefore through accumulating significative statistics on single-particle measurements.

1.3. LUMINESCENCE FROM GOLD NANOPARTICLES

Light emission from gold and copper was first observed by Mooradian[26] in 1969. In his work, electrons and holes in the metal were excited with visible light and the emission was observed at longer wavelengths. Strikingly, the emission quantum yield (i.e. the number of emitted photons per absorbed photon) that he estimated was in the order of 10^{-10}. In subsequent years several studies showed that this low number could be increased with the presence of sharp edges[27] or tips[28], but still it would be much lower than the typical fluorescence yield of organic dyes, on the order of few percent at least.

When transitioning from bulk gold to nanoparticles, the interaction of light with metals will be highly influenced by the presence of the plasmon resonance[29]. On one hand nanoparticles will have large absorption cross sections in specific wavelength regions, as explained in the previous section. On the other hand the emission spectrum will also be enhanced for frequencies around the plasmon resonance. Previous work has already shown a big overlap between the scattering and the emission spectra of gold nanoparticles[25].

The emission quantum yield of single gold nanoparticles is several orders of magnitude higher than bulk values partly due to the presence of sharp structures such as edges and tips. Typical quantum yield values are in the order of 10^{-6}[25], several orders of magnitude lower than those of organic dye molecules, but the absorption cross section can be in the order of $10^{-2}\,\mu\text{m}^2$, 6 orders of magnitude higher than those of dye molecules. The combination of both factors makes it possible to use luminescence to detect single gold nanoparticles in a standard fluorescence microscope.

The photoluminescence of gold nanoparticles can be excited mainly through two different approaches. It is possible to use a short wavelength laser, e.g. 532 nm, to excite interband transitions in gold[30], as well as the plasmon resonance of spheres or the transverse plasmon resonance of rods. The emission from particles can be collected after placing a notch or long pass filter in the detection path to prevent the excitation light to reach the detectors. Illuminating with a short wavelength allows one to collect the entire plasmonic emission, but doesn't fully exploit the advantage of the larger absorption cross section that the resonance provides.

The other approach to observe luminescence from nanoparticles is to excite them close to their resonances. In this way it is possible to benefit from the higher absorption cross section leading to lower excitation powers. Recent studies have shown that the emission quantum yield does not change significantly between exciting at the resonance and exciting with a shorter wavelength around 532 nm[31]. However, the photoluminescence itself is also coupled to the plasmon; if excited in resonance, the emission will be concentrated around the excitation wavelength[32]. Detection filters may therefore block an important part of the emission spectrum.

Throughout this thesis luminescence will refer to all the emission from a nanoparticle at different wavelengths than the excitation wavelength and that scales linearly with the excitation power. Luminescence makes it is possible to observe single gold nanoparticles under a conventional fluorescence microscope. A notch or long pass filter in the detection path efficiently blocks the excitation light while allowing the luminescence emission to go through. Moreover it is possible to select nanoparticles with resonances at wavelengths at which no other sources absorb or emit, effectively lowering the background.

For dye molecules the Stokes shifted fluorescence can be understood as a consequence of energy conservation: a photon of a given energy excites the electrons of a material that subsequently relax back by emitting another photon, by transferring energy in the form of heat to the medium or a combination of both. It is expected therefore that the emitted photon has a lower energy than the incident one. This is always valid unless the excited electrons can somehow gain energy from the medium before relaxing back radiatively. If this happens, the process is called anti-Stokes and the emitted photons possess a higher energy than the excitation.

When excited at resonance, gold nanoparticles exhibit anti-Stokes luminescence with intensities that can be compared to the Stokes shifted emission. In brief, the mechanism proposed for the emission of photons with higher energies is the interaction of electrons and holes with phonons in the gold lattice before they recombine radiatively. Note that in this process the interaction with other thermal charge carriers is also possible. Assuming that the anti-Stokes emission from gold nanoparticles depends only on the population of phonons, the general shape of the emission is expected to be

$$\bar{I} \approx \left(\exp\frac{\hbar\omega}{k_B T} - 1\right)^{-1}. \tag{1.2}$$

where ω is the frequency of the emitted photon, k_B is Boltzmann constant and T is the temperature.

Notably in equation 1.2 the only adjustable parameter is temperature. If properly characterized, the anti-Stokes emission spectrum should provide a way to estimate the absolute temperature of the particles without any previous calibration.

1.4. APPLICATIONS OF GOLD NANOPARTICLES

1.4.1. TUNING THE RESONANCE OF GOLD NANOPARTICLES

The previous two sections highlighted different strategies for detecting single gold nanoparticles such as nanospheres or nanorods. The principal characteristic of the particles is their localized surface plasmon resonance. The resonance wavelength (or energy) will be given by the geometry of the particle and by the surrounding medium's properties, such as its refractive index. The geometry of the particles is determined during the synthesis procedure, where the average length and width can be tuned. However, when the particles are deposited on a substrate, their resonance is already determined.

Chapter 2 focuses into tuning the plasmon resonance *in-situ*, once they are immobilized on a substrate and optically characterized. Currently two approaches exist for tuning the plasmon resonance after synthesis: (1) it is possible to tune the refractive index of the medium using an electric or magnetic field[33]. (2) It is possible to induce shape modifications of the nanoparticles either through chemical[34–38] or physical means[25, 39, 40]. In the majority of the reports a blue shift of the plasmon resonance has been observed.

In the case of chemical etching of the nanoparticles, almost all works have focused on bulk measurements in suspension. The tips of the particles tend to be more reactive because they are less protected by the surfactants that prevent aggregation of particles. This leads to an anisotropic reaction that slowly transforms elongated particles into spheres and that softens sharp edges or tips, yielding an overall blue-shift of the resonance.

Chapter 2 shows that through well known chemistry between gold and cyanide ions it is possible to induce a red-shift of the plasmon. This is modelled through an isotropic etching of the particles, and a good agreement between calculations and experiments is obtained. The main difference with previous work is the absence of a capping agent on the particles' surface. Controllably changing the shape of nanoparticles is of great importance for experiments where a specific resonance is needed.

1.4.2. IMAGING THROUGH DETECTION OF ANTI-STOKES EMISSION

Gold nanoparticles are ideal candidates for labelling biological samples because they prove to be innocuous to the cell[41] but also because they can be observed for extended periods of time[28, 42]. One of the drawbacks of gold nanoparticles is their low quantum yield. Since the absorption cross section of the particles scales as their volume, detecting smaller particles in presence of background requires a specific approach.

To overcome these difficulties, several techniques have been developed for imaging gold nanoparticles, including two-photon excited luminescence[43], photothermal heterodyne detection[44] and interferometric detection[45]. Each of these methods is useful but their operation requires dedicated setups and a high level of expertise.

Chapter 3 of this thesis shows that it is possible to image gold nanorods in biologically relevant conditions through detection of their anti-Stokes emission. By placing a short-pass filter in the detection path the background level is reduced significantly, while the luminescence signal from the particles remains high. This is valid even for cells stained with ATTO 647N, a dye with high quantum yield that absorbs light of the same wavelengths as the rods. In these conditions it is not possible to observe any single nanoparticle through conventional Stokes-shifted emission while the anti-Stokes scheme presents a signal-to-background ratio higher than 10.

The technique presented in chapter 3 can be readily implemented in any conventional microscope by the addition of the appropriate filters. It does not require any special operation nor infrastructure. Moreover any data analysis tool for tracking, imaging, centroid extraction, etc. of single labels can readily be implemented without further modifications.

1.4.3. GOLD NANOPARTICLES AS NANO-THERMOMETERS

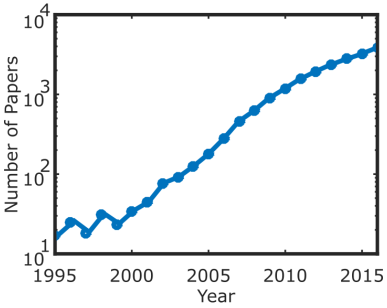

Figure 1.1: Number of papers published containing the terms Plasmonic Photo Thermal Therapy since 1995. Note the logarithmic scale in the y-axis.

During the past two decades there has been an increasing interest in gold nanoparticles as possible agents for medical treatments[46–48]. The strong interaction between particles and light makes them ideal candidates not only for labelling but also for releasing heat into very localized environments [46, 47, 49, 50]. This simple approach can be used for instance to induce death of cancer cells and is normally referred to as Plasmonic Photo Thermal Therapy (PPTT or PTT depending on the author). Figure 1.1 shows the number of papers published in this field since 1995. The increase in the number of publications is more than exponential, and depicts the relevance this technique is gaining over time.

After decades of research there is however almost no information regarding the temperatures that need to be reached by the nanoparticles to induce cell death. Much less is available at a single-particle/single-cell level. Moreover the field of thermometry at the nanoscale is subject to a heated debate[51, 52] since some experimental findings[51] contradict expected values from thermodynamic considerations[53].

Chapter 4 of this thesis focuses into the characterization of the mechanisms that give rise to anti-Stokes luminescence. Discarding multi-photon processes, photons with higher energies than the excitation energy require interactions with thermal baths. In a nanoparticle electrons and holes can interact with phonons before recombining radiatively, as discussed in section 1.3.

By carefully fitting the luminescence spectra of single gold nanorods and nanospheres with a function similar to equation 1.2 it is possible to extract the surface temperature of the particles. The method presented in chapter 4 does not depend on any ad-hoc calibration and can be performed in any confocal microscope with a coupled spectrometer. The chapter shows the increase in temperature with increasing laser powers and also shows the changes that the luminescence spectra undergo when increasing the medium's temperature.

The calibration-free procedure is a major improvement over previous techniques in the field of nano-thermometry. The results from the chapter can have a significant impact on an emerging community that addresses one of the most pressing health issues of our time.

1.4.4. PLASMON DAMPING AS A FUNCTION OF TEMPERATURE

Luminescence is not the only method for detecting gold nanorods with an optical microscope. Gold nanoparticles have a large scattering cross section coinciding with the plasmon resonance. Exciting nanoparticles with white light allows one to record the scattering spectra in any confocal microscope coupled to a spectrometer. Since the resonance itself is affected by the surrounding conditions[54, 55], it is possible for example to use it for studying changes in the refractive index of the medium. However the plasmon resonance energy is not the only interesting property of the nanoparticles; the plasmon damping rate can also be used to detect changes in the surrounding conditions.

In principle there are four main mechanisms responsible for damping of the plasmons[22, 56, 57]: electron-phonon coupling, electron-surface interactions, electron-electron collisions and radiative damping. Out of those only the coupling with phonons shows an appreciable dependence on temperature[54, 55]. Therefore studying the dependence of the plasmon width with temperature could lead to an alternative approach to measure temperature changes.

Chapter 5 focuses on the characterization of the plasmon resonance of single gold nanorods at various temperatures. In the range of temperatures studied (between 293 K and 350 K), the plasmon width increases linearly with temperature. The broadening is assigned to an increase in the electron-phonon damping rate, and the observations can be understood through the Debye model of phonons. Measuring the broadening of the resonance can then be related to changes in temperature of the surrounding medium.

The scattering of gold nanorods is much more efficient than their luminescence, not only because of their large scattering cross section but also because of the low quantum yield of their emission. Therefore the powers needed for recording scattering spectra are much lower than the ones employed when exciting the luminescence of the particles. These lower powers enable studies of the plasmon resonance without inducing a significative increase of temperature. However the broad distribution of widths and broadening rates found in the studies of chapter 5 does not allow to perform an absolute temperature measurement but only to measure a relative change. This is similar to other experiments performed with quantum dots[51] and therefore expands the toolbox of available techniques for thermometry at the nanoscale.

1.5. ONE PROGRAM TO RULE THEM ALL

All modern laboratories rely on computer equipment to perform measurements, ranging from integrated micro controllers to powerful computers. A micro controller, for example, is responsible for maintaining a stable temperature of a heating plate; a fast computer on the other hand can analyze data online in high throughput experiments and take decisions on the fly. Experiments performed at CERN and in other particle physics accelerators heavily rely on computers to discard millions of non-interesting events and save the relevant ones. However, for the average experimentalist there is a big gap between what is needed and what is available.

Flexible, open source programs to control experiments are hard to find in the Internet if they exist at all. The absence of a solution generates a double negative effect: researchers find themselves reinventing the wheel more often than desired and experiments are based on what can be done and not on what is desired to be done. For example, a simple home-built confocal microscope requires a dedicated computer program to run, which can take months to develop. Commercial software normally lacks the flexibility that new science needs, limiting the creativity of researchers while planning experiments.

All the chapters of this thesis relied on a flexible computer program that allowed to plan complex experiments building on software rather than being limited by it. The program has been made open source and can be found on Github[2]. It started to be developed for simplifying repetitive tasks such as refocusing on a particle or triggering a spectrometer. Later it evolved into a fully functional graphical user interface (GUI) for performing and visualizing 2D and 3D scans, acquiring fast timetraces, monitoring an optical tweezer and communicating with serial devices as well as over the network. The latest developments of the software open the possibility to define an application programming interface (API) for easy integration with applications on smartphones or to control several independent setups through the local network or also through the Internet.

Chapter 2 shows results where several particles were analyzed while being etched with potassium cyanide. Studying several nanoparticles under the same conditions is crucial for characterizing the dependence with the plasmon resonance and to discard any systematic error. Refocusing on the particles by hand is too slow for processes that happen as fast as the ones shown in the chapter and therefore the experiments wouldn't have been possible without a specialized computer program.

Chapter 3 shows the scanning capabilities of the software for imaging purposes. Moreover the specific program for acquiring the power dependence plots can be written in about 20 lines of code. When varying the temperature of the sample as done in chapters 4 and 5, being able to refocus on a reference particle to compensate for the drift of the setup was of utmost importance.

The software even if developed with an optical microscope in mind, can be easily extended to other configurations. Choosing Python as the programming language provides platform independence; it can run without inconvenience on several Windows versions, Mac OS and Linux. The main objective of the program is to provide a lower level layer on which to build creative solutions to complex problems.

REFERENCES

[1] G. A. Kausche, E. Pfankuch, and H. Ruska, *Die Sichtbarmachung von pflanzlichem Virus im ubermikroskop,* Naturwissenschaften **27**, 292 (1939).

[2] O. Heimstädt, *Das Fluoreszenzmikroskop,* Z. Wiss. Mikrosk. **28**, 330 (1911).

---

[2] https://github.com/aquilesC/SmartScan

[3] N. Rusk, *Milestones in light microsopy: The fluorescence microscope,* Nature (2009), 10.1038/ncb1941.

[4] J. S. Ploem, *The use of a vertical illuminator with interchangeable dichroic mirrors for fluorescence microscopy with incident light,* Z. Wiss. Mikrosk. **68**, 129 (1967).

[5] M. Orrit and J. Bernard, *Single pentacene molecules detected by fluorescence excitation in a p -terphenyl crystal,* Phys. Rev. Lett. **65**, 2716 (1990).

[6] T. Schmidt, G. J. Schutz, W. Baumgartner, H. J. Gruber, and H. Schindler, *Imaging of single molecule diffusion.* Proc. Natl. Acad. Sci. **93**, 2926 (1996).

[7] W. E. Moerner, R. M. Dickson, A. B. Cubitt, and R. Y. Tsien, *On/off blinking and switching behaviour of single molecules of green fluorescent protein,* Nature **388**, 355 (1997).

[8] E. Betzig, G. H. Patterson, R. Sougrat, O. W. Lindwasser, S. Olenych, J. S. Bonifacino, M. W. Davidson, J. Lippincott-Schwartz, and H. F. Hess, *Imaging Intracellular Fluorescent Proteins at Nanometer Resolution,* Science (80-.). **313**, 1642 (2006).

[9] T. Dertinger, R. Colyer, G. Iyer, S. Weiss, and J. Enderlein, *Fast, background-free, 3D super-resolution optical fluctuation imaging (SOFI),* Proc. Natl. Acad. Sci. **106**, 22287 (2009).

[10] W. E. Moerner, *New directions in single-molecule imaging and analysis,* Proc. Natl. Acad. Sci. **104**, 12596 (2007).

[11] M. Orrit, *Chemical and physical aspects of charge transfer in the fluorescence intermittency of single molecules and quantum dots,* Photochem. Photobiol. Sci. **9**, 637 (2010).

[12] R. Zondervan, F. Kulzer, M. A. Kol'chenk, and M. Orrit, *Photobleaching of Rhodamine 6G in Poly(vinyl alcohol) at the Ensemble and Single-Molecule Levels,* J. Phys. Chem. A **108**, 1657 (2004).

[13] J. Ortega-Arroyo and P. Kukura, *Interferometric scattering microscopy (iSCAT): new frontiers in ultrafast and ultrasensitive optical microscopy,* Phys. Chem. Chem. Phys. **14**, 15625 (2012).

[14] A. P. Alivisatos, W. Gu, and C. Larabell, *Quantum dots as cellular probes,* Annu. Rev. Biomed. Eng. **7**, 55 (2005).

[15] X. Huang, S. Neretina, and M. A. El-Sayed, *Gold nanorods: from synthesis and properties to biological and biomedical applications,* Adv. Mater. **21**, 4880 (2009).

[16] D. J. Barber and I. C. Freestone, *An investigation of the origin of the colour of the Lycurgus Cup by analytical transmission electron microscopy,* Archaeometry **32**, 33 (1990).

[17] G. Mie, *Beiträge zur Optik trüber Medien, speziell kolloidaler Metallösungen,* Ann. Phys. **330**, 377 (1908).

[18] C. F. Bohren and D. R. Huffman, *Absorption and scattering of light by small particles* (John Wiley & Sons, 2008).

[19] M. A. Yurkin and A. G. Hoekstra, *The discrete-dipole-approximation code ADDA: Capabilities and known limitations,* J. Quant. Spectrosc. Radiat. Transf. **112**, 2234 (2011).

[20] A. F. Oskooi, D. Roundy, M. Ibanescu, P. Bermel, J. D. Joannopoulos, and S. G. Johnson, *MEEP: A flexible free-software package for electromagnetic simulations by the FDTD method,* Comput. Phys. Commun. **181**, 687 (2010).

[21] B. T. Draine and P. J. Flatau, *Discrete-Dipole Approximation For Scattering Calculations,* J. Opt. Soc. Am. A **11**, 1491 (1994).

[22] C. Sönnichsen, T. Franzl, T. Wilk, G. von Plessen, J. Feldmann, O. Wilson, and P. Mulvaney, *Drastic Reduction of Plasmon Damping in Gold Nanorods,* Phys. Rev. Lett. **88**, 077402 (2002).

[23] L. Vigderman, B. P. Khanal, and E. R. Zubarev, *Functional gold nanorods: Synthesis, self-assembly, and sensing applications,* Adv. Mater. **24**, 4811 (2012).

[24] K. Lindfors, T. Kalkbrenner, P. Stoller, and V. Sandoghdar, *Detection and Spectroscopy of Gold Nanoparticles Using Supercontinuum White Light Confocal Microscopy,* Phys. Rev. Lett. **93**, 037401 (2004).

[25] M. Yorulmaz, S. Khatua, P. Zijlstra, A. Gaiduk, and M. Orrit, *Luminescence quantum yield of single gold nanorods.* Nano Lett. **12**, 4385 (2012).

[26] A. Mooradian, *Photoluminescence of metals,* Phys. Rev. Lett. **22**, 185 (1969).

[27] G. T. Boyd, Z. H. Yu, and Y. R. Shen, *Photoinduced luminescence from the noble metals and its enhancement on roughened surfaces,* Phys. Rev. B **33**, 7923 (1986).

[28] M. B. Mohamed, V. Volkov, S. Link, and M. A. El-Sayed, *The 'lightning' gold nanorods: fluorescence enhancement of over a million compared to the gold metal,* Chem. Phys. Lett. **317**, 517 (2000).

[29] E. Dulkeith, T. Niedereichholz, T. Klar, J. Feldmann, G. von Plessen, D. Gittins, K. Mayya, and F. Caruso, *Plasmon emission in photoexcited gold nanoparticles,* Phys. Rev. B **70**, 205424 (2004).

[30] M. Beversluis, A. Bouhelier, and L. Novotny, *Continuum generation from single gold nanostructures through near-field mediated intraband transitions,* Phys. Rev. B **68**, 1 (2003).

[31] Y. Cheng, G. Lu, Y. He, H. Shen, J. Zhao, K. Xia, and Q. Gong, *Luminescence Quantum Yields of Gold Nanoparticles Varying with Excitation Wavelength,* Nanoscale , 2188 (2015).

[32] R. Sundararaman, P. Narang, A. S. Jermyn, W. a. Goddard III, and H. a. Atwater, *Theoretical predictions for hot-carrier generation from surface plasmon decay,* Nat. Commun. **5**, 5788 (2014).

[33] P. A. Kossyrev, A. Yin, S. G. Cloutier, D. a. Cardimona, D. Huang, P. M. Alsing, and J. M. Xu, *Electric field tuning of plasmonic response of nanodot array in liquid crystal matrix,* Nano Lett. **5**, 1978 (2005).

[34] N. R. Jana, L. Gearheart, S. O. Obare, and C. J. Murphy, *Anisotropic Chemical Reactivity of Gold Spheroids and Nanorods,* Langmuir **18**, 922 (2002).

[35] J. Rodríguez-Fernández, J. Pérez-Juste, P. Mulvaney, and L. M. Liz-Marzán, *Spatially-directed oxidation of gold nanoparticles by Au(III)-CTAB complexes.* J. Phys. Chem. B **109**, 14257 (2005).

[36] E. Carbó-Argibay, B. Rodríguez-González, J. Pacifico, I. Pastoriza-Santos, J. Pérez-Juste, and L. Liz-Marzán, *Chemical Sharpening of Gold Nanorods: The Rod-to-Octahedron Transition,* Angew. Chemie **119**, 9141 (2007).

[37] C. K. Tsung, X. Kou, Q. Shi, J. Zhang, M. H. Yeung, J. Wang, and G. D. Stucky, *Selective shortening of single-crystalline gold nanorods by mild oxidation,* J. Am. Chem. Soc. **128**, 5352 (2006).

[38] W. Ni, X. Kou, Z. Yang, and J. Wang, *Tailoring longitudinal surface plasmon wavelengths, scattering and absorption cross sections of gold nanorods,* ACS Nano **2**, 677 (2008).

[39] S. Link, C. Burda, B. Nikoobakht, and M. A. El-Sayed, *Laser-Induced Shape Changes of Colloidal Gold Nanorods Using Femtosecond and Nanosecond Laser Pulses,* J. Phys. Chem. B **104**, 6152 (2000).

[40] Y. Horiguchi, K. Honda, Y. Kato, N. Nakashima, and Y. Niidome, *Photothermal reshaping of gold nanorods depends on the passivating layers of the nanorod surfaces,* Langmuir **24**, 12026 (2008).

[41] N. Lewinski, V. Colvin, and R. Drezek, *Cytotoxicity of nanopartides,* Small **4**, 26 (2008).

[42] J. Pérez-Juste, I. Pastoriza-Santos, L. M. Liz-Marzán, P. Mulvaney, J. Perezjuste, I. Pastorizasantos, L. Lizmarzan, and P. Mulvaney, *Gold nanorods: Synthesis, characterization and applications,* Coord. Chem. Rev. **249**, 1870 (2005).

[43] B. van den Broek, B. Ashcroft, T. H. Oosterkamp, and J. van Noort, *Parallel Nanometric 3D Tracking of Intracellular Gold Nanorods Using Multifocal Two-Photon Microscopy,* Nano Lett. **13**, 980 (2013).

[44] S. Berciaud, D. Lasne, G. Blab, L. Cognet, and B. Lounis, *Photothermal heterodyne imaging of individual metallic nanoparticles: Theory versus experiment,* Phys. Rev. B **73**, 045424 (2006).

[45] F. Ignatovich and L. Novotny, *Real-Time and Background-Free Detection of Nanoscale Particles,* Phys. Rev. Lett. **96**, 013901 (2006).

[46] A. M. Gobin, M. H. Lee, N. J. Halas, W. D. James, R. A. Drezek, J. L. West, M. Gobin, M. H. Lee, N. J. Halas, W. D. James, R. A. Drezek, and J. L. West, *Near-Infrared Resonant Nanoshells for Combined Optical Imaging and Photothermal Cancer Therapy,* Nano Lett. **7**, 1929 (2007).

[47] X. H. Huang, I. H. El-Sayed, W. Qian, and M. a. El-Sayed, *Cancer cell imaging and photothermal therapy in the near-infrared region by using gold nanorods,* J. Am. Chem. Soc. **128**, 2115 (2006).

[48] S. Huo, S. Jin, X. Ma, X. Xue, K. Yang, A. Kumar, P. C. Wang, J. Zhang, Z. Hu, and X.-J. Liang, *Ultrasmall Gold Nanoparticles as Carriers for Nucleus-Based Gene Therapy Due to Size-Dependent Nuclear Entry,* ACS Nano **8**, 5852 (2014).

[49] X. Huang, P. K. Jain, I. H. El-Sayed, and M. A. El-Sayed, *Plasmonic photothermal therapy (PPTT) using gold nanoparticles,* Lasers Med. Sci. **23**, 217 (2008).

[50] L. R. Hirsch, R. J. Stafford, J. A. Bankson, S. R. Sershen, B. Rivera, R. E. Price, J. D. Hazle, N. J. Halas, and J. L. West, *Nanoshell-mediated near-infrared thermal therapy of tumors under magnetic resonance guidance.* Proc. Natl. Acad. Sci. U. S. A. **100**, 13549 (2003), arXiv:0008204 [cond-mat] .

[51] J.-M. Yang, H. Yang, and L. Lin, *Quantum Dot Nano Thermometers Reveal Heterogeneous Local Thermogenesis in Living Cells,* ACS Nano **5**, 5067 (2011).

[52] M. Suzuki, V. Zeeb, S. Arai, K. Oyama, and S. Ishiwata, *The 10ˆ5 gap issue between calculation and measurement in single-cell thermometry,* Nat. Methods **12**, 802 (2015).

[53] M. K. Sato, M. Toda, N. Inomata, H. Maruyama, Y. Okamatsu-Ogura, F. Arai, T. Ono, A. Ishijima, and Y. Inoue, *Temperature Changes in Brown Adipocytes Detected with a Bimaterial Microcantilever,* Biophys. J. **106**, 2458 (2014).

[54] M. Liu, M. Pelton, and P. Guyot-Sionnest, *Reduced damping of surface plasmons at low temperatures,* Phys. Rev. B **79**, 035418 (2009).

[55] A. Konrad, F. Wackenhut, M. Hussels, A. J. Meixner, and M. Brecht, *Temperature Dependent Luminescence and Dephasing of Gold Nanorods,* J. Phys. Chem. C **117**, 21476 (2013).

[56] C. Novo, D. Gomez, J. Perez-Juste, Z. Zhang, H. Petrova, M. Reismann, P. Mulvaney, and G. V. Hartland, *Contributions from radiation damping and surface scattering to the linewidth of the longitudinal plasmon band of gold nanorods: a single particle study,* Phys. Chem. Chem. Phys. **8**, 3540 (2006).

[57] M. Hu, C. Novo, A. Funston, H. Wang, H. Staleva, S. Zou, P. Mulvaney, Y. Xia, and G. V. Hartland, *Dark-field microscopy studies of single metal nanoparticles: understanding the factors that influence the linewidth of the localized surface plasmon resonance,* J. Mater. Chem. **18**, 1949 (2008).

2

In situ TUNING OF GOLD NANOROD PLASMON THROUGH OXIDATIVE CYANIDE ETCHING

Single gold nanorods exhibit great opportunities for bio-sensing, enhanced spectroscopies and photothermal therapy. A key property of these particles is the surface plasmon resonance, that is strongly dependent on their shape. Methods for tuning this resonance after the synthesis of the particles are of great interest for many applications. In this work we show that, through very well known chemistry between gold atoms and cyanide ions, it is possible to tune the surface plasmon of single 25×50 *nm rods by more than* 100 *nm towards longer wavelengths. This is achieved by slowly etching gold atoms from the surface of the particles, preserving their specific optical properties.*

This chapter has been published in Physical Chemistry Chemical Physics 18, 15619-15624 (2016).

2.1. INTRODUCTION

GOLD nanoparticles exhibit large absorption and scattering cross sections with resonances ranging from the visible to the near-infrared. This property is closely related to the surface plasmon, a collective oscillation of conduction electrons that depends on the shape of the particles. For gold nanorods (AuNR) the surface plasmon resonance (SPR) wavelength depends on the aspect ratio (AR) of the particle and can be found between 540 nm for spheres with AR of 1 to beyond 800 nm for elongated particles. The SPR of gold particles can be observed by recording their scattering or luminescence spectrum[1]. Both show a near exact overlap for a large range of wavelengths[2].

The surface plasmon presents great opportunities in (bio-) sensing[3], enhanced spectroscopies [4], photothermal therapy[5] and for concentrating light below the diffraction limit[6]. Success in many of these applications requires precise and *in situ* control over the nanoparticles' plasmon resonance energy. For example, maximum fluorescence[7] or Raman enhancement[8] is achieved when the nanoparticles' plasmon resonance is tuned to the excitation laser wavelength. As another example, efficient photothermal therapy requires the nanoparticles' SPR to be tuned to the near-IR to minimize the damage to healthy cells[9].

Typically the SPR is tuned by carefully manipulating the shapes of nanoparticles during their synthesis. Particularly useful are the rod-shaped particles, whose resonance can be found between 600 nm and beyond 1000 nm, depending on their aspect ratios. Adjusting the concentrations of gold seeds and silver nitrate during the seed-mediated growth[10] is the usual way for producing particles with different resonances. Many other nanoparticle shapes such as nanoprisms, nanorice, nanocubes, nanoshells, etc. have been synthesized with their plasmon resonances covering the entire spectral range from visible to near-IR[11]. Wet-chemical synthesis methods, however, generally yield a broad distribution in nanoparticle sizes and/or shapes, hindering precise and reproducible experiments that need a particular resonance. Furthermore, these methods do not provide any *in situ* adjustment of the SPR, any change of which requires a new synthesis.

For the past decade, single-particle experiments have provided insight into processes that would have been averaged out in bulk experiments. For instance, pump and probe experiments on single particles avoid assumptions regarding size distributions of the sample[12, 13]. Nonlinear processes such as second (or third) harmonic generation can be studied when the particles' plasmon is well characterized and single-particle experiments allow to overcome the inhomogeneous broadening of a sample in suspension[14, 15]. Enhanced spectroscopies normally rely on well defined structures fixed on a substrate[16]. Most of these experiments will benefit from techniques that allow to tune *in situ* the plasmon resonance and geometry of specific particles once they are immobilized on a substrate and optically characterized.

Recently, new methods have been developed to tune nanoparticles' SPR after their synthesis. These approaches can be divided into two broad categories: (1) The first group of methods tune the refractive index of the medium using an electric or magnetic field[17]. The advantage of these methods is that the SPR shift is reproducible and reversible. However the tuning range is rather limited and continuous tuning within this range is difficult to achieve. (2) The other set of approaches rely on controllably inducing shape modifications of the nanoparticles to tune the plasmon resonance through chemical

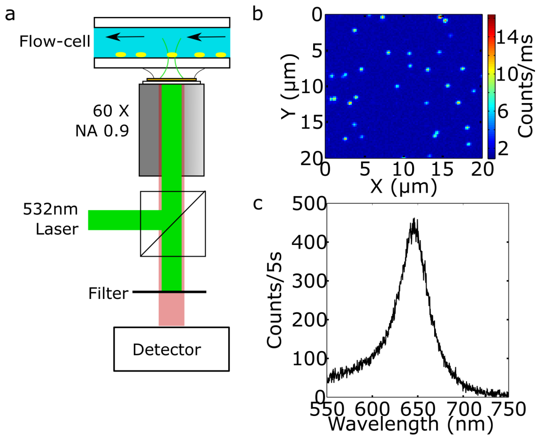

Figure 2.1: Experimental setup and examples of observations. a) Simplified schematic of the confocal microscope employed during the measurements. b) A typical 1-photon luminescence raster scan of the sample immersed in water, before etching and c) luminescence spectrum of a single rod.

or physical means. For example, thermal reshaping was induced by illuminating the nanoparticles with an intense, pulsed [18, 19] or continuous laser[2]. Increasing the particles' temperature therefore leads to changes in shape, favoring those conformations with a lower surface energy (i.e. spheres over rods, etc.). Chemical reshaping is also possible and was the focus of several studies[20–24]. In those cases, the capping agent will induce different reactivities on the sides than on the tips of the particles; because of a higher curvature[25] the tips are normally more susceptible to chemical reactions, leading to an anisotropic reshaping shortening the long axis or softening any high-curvature region. Both in the case of laser-induced or chemical-induced reshaping the outcome is usually a blue-shift of the surface resonance peak.

In this work we present a new approach for precise and *in situ* tuning of plasmon resonances of single gold nanorods isolated and immobilized on a glass surface. A nanorod's plasmon resonance is tuned over 130 nm, starting from 650 nm up to 780 nm. Our method exploits well-known chemistry between gold and cyanide ions (CN^-) to controllably etch gold atoms from the nanoparticle and thereby change its aspect ratio. We note that unlike many of the previous studies, here we observe a SPR red shift on gold nanorods. We also verified the resuts from scanning electron microscopy (SEM) images of the particles and by simulations based on the discrete dipole approximation method. Contrary to previous works where the etching was preferred at the tips, we attribute the red shift to isotropic etching of gold nanorods from all sides resulting in an increase of aspect ratio.

2.2. EXPERIMENTAL METHOD

Gold nanorods were synthesized by following standard seeded-growth method[26]. The average size of nanorods was 50 nm × 25 nm and their SPR is located at 620 nm in water (refer to the Supplementary Information for SEM images and bulk extinction spectra of nanorods as synthesized).

Single-particle measurements were done on a home-built confocal microscope (Figure 2.1a). A 532 nm laser was used for exciting the particles. The excitation power was 300 μW at the back aperture of the objective (Olympus 60×, NA0.9 air). Since the laser employed is not in resonance with the longitudinal plasmon, the power dissipated by the particles is not high enough as for showing thermal reshaping. After several minutes of irradiation the plasmon position didn't show any shift. Typical powers needed for reshaping are in the range $1-5$ mW[2]. The luminescence signal was filtered with two 532 nm notch filters and was detected by either an avalanche photodiode or a liquid-nitrogen-cooled CCD-spectrometer (Acton 500i). The images were acquired by scanning the sample across the tightly focused laser beam using a XYZ piezo scanning stage (PI Nano Cube). Figure 2.1b shows a typical result from a raster scan. Each bright spot corresponds to a single nanoparticle.

Samples were prepared by spin-casting a suspension of AuNR on clean coverslips. Afterwards the slides were thoroughly rinsed with Milli-Q water and placed in an ozone cleaner for one hour to eliminate any trace of the surfactant (cetyltrimethylammonium bromide, CTAB.) To perform the measurements, the samples were mounted on a flowcell and the initial spectra were taken with the rods immersed in Milli-Q water. Figure 2.1c shows an example of the luminescence spectrum of a single particle. Having this initial characterization allowed us to discard clusters of rods[27] from the study.

Of each sample, approximately 10 different particles were selected. Afterwards a solution of KCN was flowed into the sample chamber and spectra of each particle were acquired consecutively after focusing on each one. The time resolution varies according to the exposure time and number of particles studied; in this work a spectrum of each particle was taken at least every minute. Concentrations of KCN ranging from 10 μM to 80 μM were employed with different samples.

2.3. RESULTS

Figure 2.1b shows a typical one-photon-excited luminescence image of gold nanorods isolated on a glass surface and covered with water. Single-particle spectra display a narrow Lorentzian lineshape[27] while clusters show additional features or a broad spectrum. Figure 2.1c shows a typical spectrum originating from a single nanoparticle. In the samples analyzed more than 90% of the diffraction-limited bright spots originate from single gold nanorods.

Figure 2.2 shows the one-photon luminescence spectra of a gold nanorod immersed in 20 μM KCN at intervals of 70 s. We clearly observe a gradual red shift of the nanorod's plasmon resonance by more than 100 nm over a time interval of 300 s. The left inset of Fig. 2.2 shows the integrated intensity of the particle as a function of time. It is possible to observe a decrease of the intensity by a factor 4 during the same interval in which the shift was observed. Fitting each spectrum with a Lorentzian function allows to extract the resonance wavelength at each recorded time. A more detailed analysis shows that the nanorod's plasmon resonance wavelength varies almost linearly with time as shown in the right inset of Fig. 2.2a

We note the presence of an additional shoulder peak at 650 nm which is more prominent for the less intense curves. We attribute this shoulder to Raman scattering by the O-H stretching modes of water, between 3000 cm^{-1} and 3600 cm^{-1}. Excitation at 532 nm

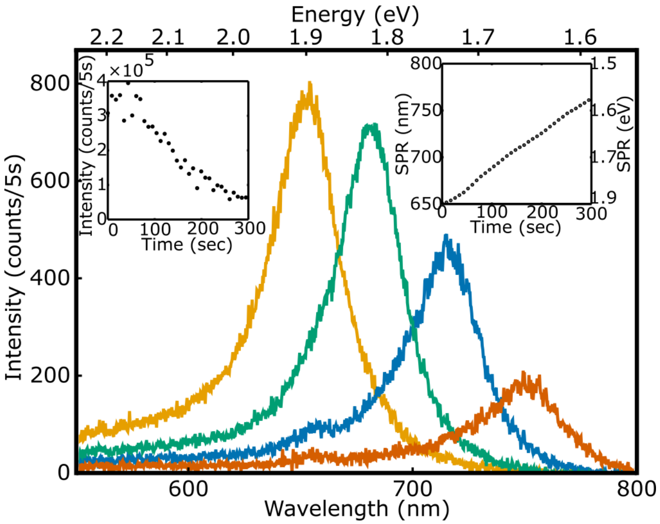

Figure 2.2: One-photon-excited luminescence spectra of gold nanorods immersed in 20 μM KCN. The different curves show the plasmon shift of a single rod. Each shown spectrum was acquired at 70 s intervals. The insets display the integrated intensity of the peak and the resonance wavelength as functions of time, respectively. b) Timetrace of the peak wavelength for 10 different particles immersed in 20 μM KCN. The green solid curve is the average of all the particles.

produces Stokes emission between roughly 630 nm and 650 nm, as observed directly on the background spectrum shown in Figure S3. This Raman band is not completely eliminated upon subtraction of the background spectrum from that of the particle. This non-additivity of the spectra indicates that water Raman scattering is significantly enhanced by the near-field of the nanorod[28].

All the studied nanorods present the same qualitative behavior. Our results are summarized in Fig. 2.3, which shows the shift of plasmon resonance wavelength as a function of time for ten different rods (dashed lines). Each nanorod shows a red shift of the plasmon resonance wavelength which varies almost linearly with time irrespective of the initial resonance wavelength. The rate of SPR shift, however, varies significantly from particle to particle. The highest observed rate was 15 nm/minute while the lowest one was 2 nm/minute. The green curve in Figure 2.3 is the average of all the shifts; since spectra of each particle were acquired sequentially, we interpolated the values of the shift at intermediate times to compute the average.

The reaction between gold and potassium cyanide is well known and is used for gold mining, electroplating, etc. Gold reacts with aqueous CN^- ions in presence of oxygen to form $\mathrm{Au(CN)}_2^-$, which is soluble in water. The reaction can be written as follows

$$4\,\mathrm{Au} + 8\,\mathrm{CN}^- + \mathrm{O}_2 + 2\,\mathrm{H}_2\mathrm{O} \leftrightarrows 4\,\mathrm{Au(CN)}_2^- + 4\,\mathrm{OH}^-$$

In our experiment the formation of $\mathrm{Au(CN)}_2^-$ results in gold etching from the nanorods, as has been reported previously[22].

The etching of gold atoms from a nanorod has two effects: Firstly, the nanorods' volume will decrease gradually with reaction time. This is consistent with our observation

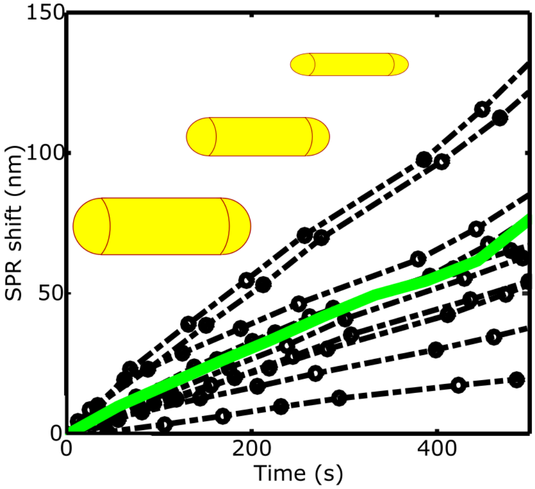

Figure 2.3: Timetrace of the peak wavelength for 10 different particles immersed in 20 μM KCN. The green solid curve is the average of all the particles. The diagram shows the isotropic etching of a nanorod, leading to a higher aspect ratio.

that the one-photon-excited luminescence intensity decreases with time. Secondly, the aspect ratio of a nanorod can either decrease or increase depending on the preferred direction of etching. The Nanorod aspect ratio will decrease with time if the reaction happens preferably at the tips. This is indeed the case for nanorods protected with CTAB and dispersed in solution[22]. CTAB binds more weakly to the tips than to the sides and therefore leaves the tips more susceptible for chemical reactions[29]. The consequent decrease of aspect ratio yields a blue shift of the plasmon resonance[30]. If etching happens isotropically from both sides and tips, an overall increase of the nanorod's aspect ratio results, as is depicted schematically in Fig. 2.3. This is the more likely scenario in our experiment as the nanorods' surface does not have any protective CTAB bilayer.

Numerical simulations based on the discrete dipole approximation were performed to assess the hypothesis that the red shift of the plasmon resonance is due to isotropic nanorod etching. The initial dimensions of the particles were fixed at 25 nm × 50 nm which coincide with the median values of the distribution of sizes of our nanoparticles (see SI). Simulations are carried out in etching steps of 0.5 nm. Figure 2.4 shows the calculated scattering spectra of the particle at different etching steps. We clearly observe a red-shift of the plasmon resonance wavelength, in concordance with what was observed in our experiment. The first inset of the figure shows the decrease of the maximum scattering cross section spectrum as a function of etched thickness.

Comparing experimental and simulated data can be achieved by fixing the value of the etching rate. In our case the best approximation to the particle shown in Figure 2.2 is achieved by setting the etching rate to 1 nm/min. Comparison to simulations for different nanorods would in principle allow us to check the consistency of the assumption of a constant etching rate for all rods. Indeed, both volume and aspect ratio of the rod can be determined by comparison of experimental data to simulations. A new comparison after

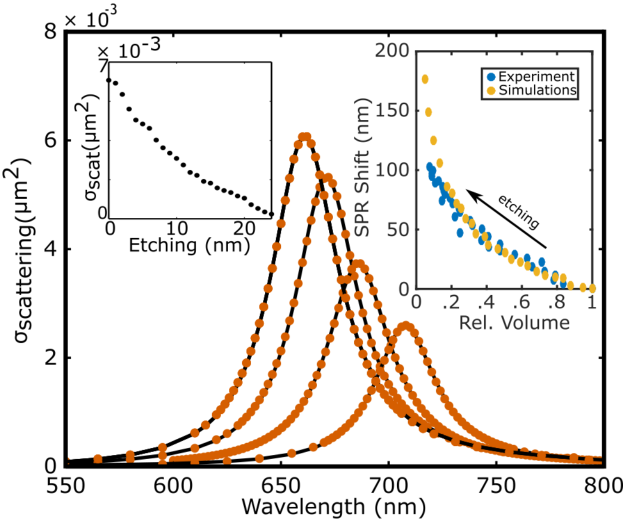

Figure 2.4: Examples of the curves obtained at different simulations steps. The black curves are fits with Lorentzians. The left inset shows the maximum scattering cross section as function of etching. The right inset displays the plasmon shift of experimental and simulated data as the relative volume of the particle diminishes.

a given etching time would give the changes in volume and aspect ratio, which should be consistent with the same etching rate for all rods. In the present work, however, we did not attempt this analysis. We simply used the relative volume as a scaling factor to compare simulations and experiments, as is shown in the right inset of Figure 2.4.

The luminescence intensity of gold nanorods is roughly proportional to their volume. It is possible therefore to calculate the relative volume of a particle by comparing the total luminescence intensity at a given instant and at a reference time. We employed the initial intensity as the reference, therefore the SPR shift increases while the relative volume decreases as depicted by the arrow in the inset of Figure 2.4. The volume of the simulated particle can be directly computed from the geometrical parameters. The inset shows a remarkable agreement between the simulations and the experimental data. For smaller relative volumes (less than 0.1) the recorded spectra are 10 times less intense than the initial one, giving rise to a less accurate positioning of the resonance peak.

Figure 2.5 shows simulated plasmon shift rates for three different series of nanorods. In each series particles have the same initial volume, but different initial plasmon resonance, spanning from 600 nm to 780 nm. The first series corresponds to 5 particles with a volume of 6800 nm^3 (red), the second to 7 particles of 20000 nm^3 (green) and the third to 6 of 25000 nm^3 (blue). The shift rate is defined as the plasmon shift given by etching a thickness of 0.5 nm away from the particle. It can be observed that for larger particles the shift is slower than for smaller ones at the same initial resonance. On the other hand it is also possible to observe that red-shifted particles present a larger shift rate.

The results in Fig. 2.5 are easier to understand considering that the plasmon resonance is closely related to the aspect ratio of the particles (length divided by diameter). Small particles will exhibit a bigger change in aspect ratio when subjected to the same amount

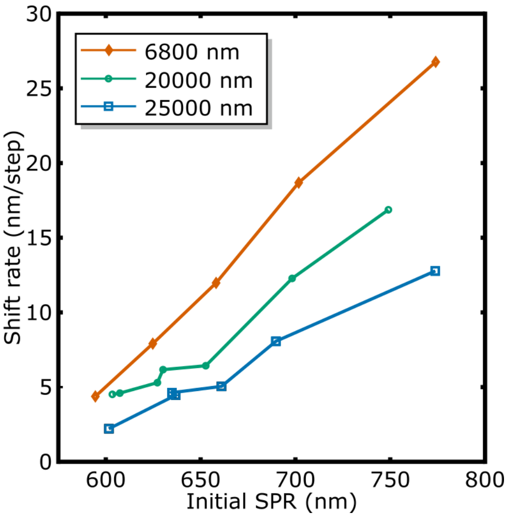

Figure 2.5: Shift rate as a function of the initial plasmon resonance for different particles. The lines correspond to particles with the same initial volume but different initial aspect ratios. As expected from an isotropic etching, larger particles will present a slower plasmon shift and more elongated particles will have a faster one.

of etching than bigger particles. This explains why smaller particles show a higher shift rate than more massive ones. On the other hand, volume is not the only factor to take into account. Particles with a higher initial aspect ratio (longer resonance wavelength) will show a faster change in aspect ratio when subjected to the same amount of etching. The interplay between both volume and initial aspect ratio can account for the big variability observed experimentally. This is also supported by the distribution of particle sizes and aspect ratios observed in the SEM images (see A.2.)

Figure 2.6 shows the measured FWHM of the plasmon peak for several nanorods immersed in 20 μM KCN as a function of the resonance shift. Note that the plot shows the width of the resonance in units of energy and not in units of wavelength. Because of the nonlinear relation between them, the peak width expressed in wavelength depends on the peak position rendering difficult the comparison of widths during the shift. At the beginning of the reaction there is a decrease of the width. Then it stabilizes for shifts between 75 nm and 100 nm. After this point, as the volume of the particles is largely reduced, it is no longer possible to reliably extract information from the spectra. The inset of Fig. 2.6 shows the FWHM obtained from the simulations for a 25 nm × 50 nm nanorod. The simulated spectrum is slightly narrower than the measured one but the trends are similar.

The initial decrease of the resonance FWHM observed in the experiments may be due to the elimination of defects from the surface of the particles. However, the simulated width that doesn't take into account any surface impurities shows a similar decrease. This behavior can be explained by the decrease of both the radiative and non-radiative damping mechanisms during the etching process. The radiation damping scales as the volume of the particle[31] and therefore will decrease while the cyanide etches gold atoms

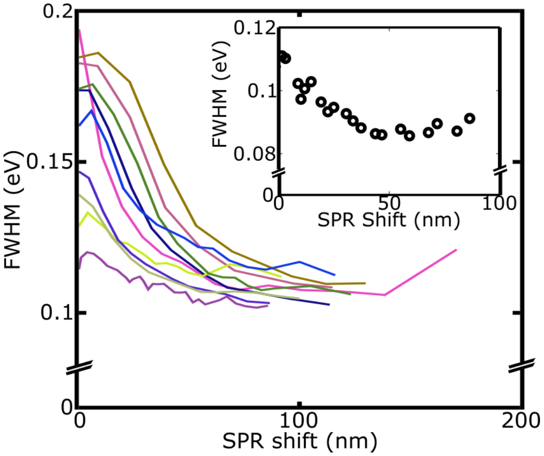

Figure 2.6: Measured plasmon FWHM of different particles immersed in 20 μM KCN as a function of their plasmon shift. The inset shows the results from the simulations carried out with the ADDA package. b) SPR Shift as a function of time for particles with the same initial SPR at different KCN concentrations.

from the particle. On the other hand we observe that the energy distance between the longitudinal plasmon peak and interband transitions in gold increases during the etching process. Therefore the non-radiative damping mechanisms in the particle may also become less efficient[1]. Both effects combined can account for the diminishing plasmon width that is observed.

Figure 2.7 shows the plasmon peak shift as a function of time for various KCN concentrations for particles with a plasmon peak at roughly 630 nm. As shown for the simulations (Figure 2.5), the etching rate depends on the initial SPR, therefore it is important to choose particles that are similar to each other. The time-traces of the peak position clearly show that the shift rate is proportional to the concentration of KCN. For every concentration a shift of at least 100 nm was observed. It is important to note that the behavior of the FWHM in all the cases is similar and it resembles the results shown in Figure 2.7.

Samples of the same nanorods were prepared for scanning electron microscopy (SEM) imaging by drop-casting the same solution of rods. SEM images were acquired before the etching, after 2 min immersion in KCN and after 4 min. In each case we observed that when particles are isolated from each other, the rod shape is preserved. In aggregates of particles this no longer holds and rods start to lose their shape (see Supporting Information for SEM images.) Calculating the distribution of sizes of the particles shows a slight increase in the aspect ratio but this shift is smaller than the width of the distribution.

The simulations also allow us to estimate the volume of gold etched away from a particle by unit of time. For a typical case as the one depicted in Figure 2.7 it is possible to obtain an etching rate of 0.5 nm/ min for the 10 μM timetrace. Assuming an atomic radius of gold of 144 pm[32] we obtain that the reaction rate can be as low as 700 atoms per second. From the simulations and these estimates it is possible to approximate the plasmon shift for every etched atom. In the same conditions as before, it would be $0.2 \cdot 10^{-3}$ nm/atom, several orders of magnitude smaller that the sensitivity of our

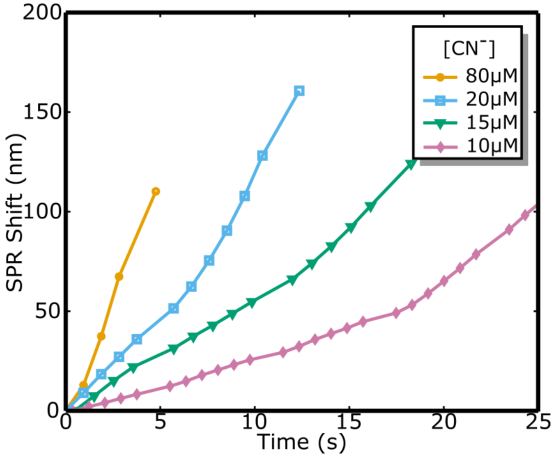

Figure 2.7: SPR Shift as a function of time for particles with the same initial SPR at different KCN concentrations.

experiments.

The same experiments performed in solution (see SI) show a different behavior of the plasmon resonance. As reported by other groups [22, 25] the rods reshape into spheres. The presence of CTAB can explain this trend: the tips will be more exposed and therefore react more quickly, yielding a net decrease in aspect ratio. In our single-particle experiments CTAB was removed both by rinsing the samples with water and by placing them in an ozone cleaner. However, the glass surface supporting the rods has to be taken into account. In principle there is a side of the rods in contact with the surface that will be less, or not, exposed to KCN. Etching in this case wouldn't be isotropic and would flatten the rods. Neither the optical nor the SEM images allowed us to assess this question because there is no information on the axis perpendicular to the surface. The deviation of the experiments from the simulations for the smaller volumes may be also dependent on this.

2.4. CONCLUSIONS

In this work we have shown a simple method that allowed us to tune the plasmon peak position of single gold nanorods with nanometer accuracy and over the range of 100 nm (300 meV). More importantly, we show that during the etching process the rod-like shape is preserved; this was confirmed both by monitoring the FWHM of the resonance peak and by acquiring SEM images after different reaction times. The experiments allowed us to record the plasmon peak with a relatively high temporal and spectral accuracy, allowing us to stop the reaction when the resonance is at the desired value.

Discrete dipole simulations with an isotropic etching model allowed us to estimate the amount of gold etched from the nanoparticles. The calculations were consistent with the red-shift of the plasmon and the diminishing intensity of the luminescence signal. The general trend of the FWHM is also correctly reproduced, but the obtained values are slightly different. SEM images of the rods confirmed the values obtained from the simulations. Combining these results provides a way of predicting the behaviour of the plasmon peak for different rods.

We observed a broad distribution of the rate at which the plasmon peak shifts for different particles under the same experimental conditions. This can be attributed to the initial differences in aspect ratios and volumes of each particle. Sphere-like particles will show a small shift since the aspect ratio remains constant under isotropic etching. More elongated particles, on the other hand, will have a much steeper increase in aspect ratio while being etched. Intrinsic differences between particles can also be present, producing different shift rates even if particles have the same plasmon resonance. For instance the faceting of the surface or the prescence of left-over CTAB that was not completely washed away or oxidized can induce a slightly anisotropic etching. These differences between particles are impossible to assess by optical means and would require a much more sensitive approach.

The role of the capping agent has largely been studied and has always been held responsible for the observations both in chemical etching[25] and for photothermal reshaping[19]. Avoiding the presence of the passivating layers is impossible in suspension, since gold nanoparticles would aggregate. Our results provide evidence that supports previous observations regarding the effect of the curvature and the accessibility of KCN to the surface of the particle.

REFERENCES

[1] C. Sönnichsen, T. Franzl, T. Wilk, G. von Plessen, J. Feldmann, O. Wilson, and P. Mulvaney, *Drastic Reduction of Plasmon Damping in Gold Nanorods,* Phys. Rev. Lett. **88**, 077402 (2002).

[2] M. Yorulmaz, S. Khatua, P. Zijlstra, A. Gaiduk, and M. Orrit, *Luminescence quantum yield of single gold nanorods.* Nano Lett. **12**, 4385 (2012).

[3] P. Zijlstra, P. M. R. Paulo, and M. Orrit, *Optical detection of single non-absorbing molecules using the surface plasmon resonance of a gold nanorod.* Nat. Nanotechnol. **7**, 379 (2012).

[4] S. T. Sivapalan, B. M. Devetter, T. K. Yang, T. van Dijk, M. V. Schulmerich, P. S. Carney, R. Bhargava, and C. J. Murphy, *Off-resonance surface-enhanced Raman spectroscopy from gold nanorod suspensions as a function of aspect ratio: not what we thought.* ACS Nano **7**, 2099 (2013).

[5] T. Zhao, K. Yu, L. Li, T. Zhang, Z. Guan, N. Gao, P. Yuan, S. Li, S. Q. Yao, Q.-H. Xu, and G. Q. Xu, *Gold nanorod enhanced two-photon excitation fluorescence of photosensitizers for two-photon imaging and photodynamic therapy.* ACS Appl. Mater. Interfaces **6**, 2700 (2014).

[6] P. Zijlstra and M. Orrit, *Single metal nanoparticles: optical detection, spectroscopy and applications,* Reports Prog. Phys. **74**, 106401 (2011).

[7] S. Khatua, P. M. R. Paulo, H. Yuan, A. Gupta, P. Zijlstra, and M. Orrit, *Resonant plasmonic enhancement of single-molecule fluorescence by individual gold nanorods.* ACS Nano **8**, 4440 (2014).

[8] A. D. McFarland, M. a. Young, J. a. Dieringer, and R. P. Van Duyne, *Wavelength-scanned surface-enhanced Raman excitation spectroscopy.* J. Phys. Chem. B **109**, 11279 (2005).

[9] A. M. Alkilany, L. B. Thompson, S. P. Boulos, P. N. Sisco, and C. J. Murphy, *Gold nanorods: Their potential for photothermal therapeutics and drug delivery, tempered by the complexity of their biological interactions,* Adv. Drug Deliv. Rev. **64**, 190 (2012).

[10] L. Vigderman, B. P. Khanal, and E. R. Zubarev, *Functional gold nanorods: Synthesis, self-assembly, and sensing applications,* Adv. Mater. **24**, 4811 (2012).

[11] S. Lal, S. Link, and N. J. Halas, *Nano-optics from sensing to waveguiding,* Nat. Photonics **1**, 641 (2007).

[12] G. V. Hartland, *Coherent Excitation of Vibrational Modes in Metallic Nanoparticles,* Annu. Rev. Phys. Chem. **57**, 403 (2006).

[13] P. V. Ruijgrok, P. Zijlstra, A. L. Tchebotareva, and M. Orrit, *Damping of acoustic vibrations of single gold nanoparticles optically trapped in water.* Nano Lett. **12**, 1063 (2012).

[14] J. Butet, J. Duboisset, G. Bachelier, I. Russier-Antoine, E. Benichou, C. Jonin, and P. F. Brevet, *Optical second harmonic generation of single metallic nanoparticles embedded in a homogeneous medium,* Nano Lett. **10**, 1717 (2010).

[15] M. Lippitz, M. A. Van Dijk, and M. Orrit, *Third-harmonic generation from single gold nanoparticles,* Nano Lett. **5**, 799 (2005).

[16] P. Olk, J. Renger, M. T. Wenzel, and L. M. Eng, *Distance dependent spectral tuning of two coupled metal nanoparticles,* Nano Lett. **8**, 1174 (2008).

[17] P. A. Kossyrev, A. Yin, S. G. Cloutier, D. a. Cardimona, D. Huang, P. M. Alsing, and J. M. Xu, *Electric field tuning of plasmonic response of nanodot array in liquid crystal matrix,* Nano Lett. **5**, 1978 (2005).

[18] S. Link, C. Burda, B. Nikoobakht, and M. A. El-Sayed, *Laser-Induced Shape Changes of Colloidal Gold Nanorods Using Femtosecond and Nanosecond Laser Pulses,* J. Phys. Chem. B **104**, 6152 (2000).

[19] Y. Horiguchi, K. Honda, Y. Kato, N. Nakashima, and Y. Niidome, *Photothermal reshaping of gold nanorods depends on the passivating layers of the nanorod surfaces,* Langmuir **24**, 12026 (2008).

[20] E. Carbó-Argibay, B. Rodríguez-González, J. Pacifico, I. Pastoriza-Santos, J. Pérez-Juste, and L. Liz-Marzán, *Chemical Sharpening of Gold Nanorods: The Rod-to-Octahedron Transition,* Angew. Chemie **119**, 9141 (2007).

[21] J. Rodríguez-Fernández, J. Pérez-Juste, P. Mulvaney, and L. M. Liz-Marzán, *Spatially-directed oxidation of gold nanoparticles by Au(III)-CTAB complexes.* J. Phys. Chem. B **109**, 14257 (2005).

[22] N. R. Jana, L. Gearheart, S. O. Obare, and C. J. Murphy, *Anisotropic Chemical Reactivity of Gold Spheroids and Nanorods,* Langmuir **18**, 922 (2002).

[23] C. K. Tsung, X. Kou, Q. Shi, J. Zhang, M. H. Yeung, J. Wang, and G. D. Stucky, *Selective shortening of single-crystalline gold nanorods by mild oxidation,* J. Am. Chem. Soc. **128**, 5352 (2006).

[24] W. Ni, X. Kou, Z. Yang, and J. Wang, *Tailoring longitudinal surface plasmon wavelengths, scattering and absorption cross sections of gold nanorods,* ACS Nano **2**, 677 (2008).

[25] H. Yuan, K. P. F. Janssen, T. Franklin, G. Lu, L. Su, X. Gu, H. Uji-i, M. B. J. Roeffaers, and J. Hofkens, *Reshaping anisotropic gold nanoparticles through oxidative etching: the role of the surfactant and nanoparticle surface curvature,* RSC Adv. **5**, 6829 (2015).

[26] B. Nikoobakht and M. A. El-Sayed, *Preparation and Growth Mechanism of Gold Nanorods (NRs) Using Seed-Mediated Growth Method,* Chem. Mater. **15**, 1957 (2003).

[27] A. M. Funston, C. Novo, T. J. Davis, and P. Mulvaney, *Plasmon coupling of gold nanorods at short distances and in different geometries,* Nano Lett. **9**, 1651 (2009).

[28] J. B. Snow, S. X. Qian, and R. K. Chang, *Stimulated Raman scattering from individual water and ethanol droplets at morphology-dependent resonances.* Opt. Lett. **10**, 37 (1985).

[29] K. K. Caswell, J. N. Wilson, U. H. F. Bunz, and C. J. Murphy, *Preferential end-to-end assembly of gold nanorods by biotin- streptavidin connectors,* J. Am. Chem. Soc. **125**, 13914 (2003).

[30] S. Link, M. B. Mohamed, and M. a. El-Sayed, *Simulation of the Optical Absorption Spectra of Gold Nanorods as a Function of Their Aspect Ratio and the Effect of the Medium Dielectric Constant,* J. Phys. Chem. B **103**, 3073 (1999).

[31] a. Wokaun, J. P. Gordon, and P. F. Liao, *Radiation damping in surface-enhanced Raman scattering,* Phys. Rev. Lett. **48**, 957 (1982).

[32] L. Pauling, *Atomic Radii and Interatomic Distances in Metals,* J. Am. Chem. Soc. **69**, 542 (1947).

3

BACKGROUND SUPPRESSION IN IMAGING GOLD NANORODS THROUGH DETECTION OF ANTI-STOKES EMISSION

Metallic nanoparticles have opened the possibility of imaging, tracking and manipulating biological samples without time limitations. Their low photoluminescence quantum yield however, makes them hard to detect under high background conditions. In this study we show that it is possible to image gold nanorods by detecting their anti-Stokes emission under resonant excitation. We show that even in the membrane of a cell containing the fluorescent dye ATTO647N, the signal-to-background ratio of the anti-Stokes emission can be higher than 10, while it is impossible to image the particles with the Stokes emission. The main advantage of this technique is that it does not require any major change in existing fluorescence imaging setups, only the addition of an appropriate short-pass filter in the detection path.

This chapter has been published in Biophysical Journal 111, 2492-2499 (2016).

3.1. INTRODUCTION

HIGH-resolution microscopy has become an indispensable tool for studying biological samples both in vitro and in vivo[1]. Fluorescent organic dyes are commonly employed to such ends because of their reduced size and high quantum yield[2]. Fluorophores, however, have an inherent constraint in the possible observation time, since molecules eventually bleach under intense illumination[3]. Even the most photostable dyes cannot be imaged at saturation for longer than few tens of seconds. Gold nanoparticles on the other hand are almost indefinitely stable[4] and open up many original applications including photothermal therapy[5] and imaging[6].

As gold nanoparticles do not blink nor bleach[7, 8],they are ideal candidates for labelling[9], tracking[10] and manipulating[11] biological samples over extended periods of time. Moreover it has been shown that with the proper size and coating, they do not interfere with cells' functioning[12], allowing not only *in vitro* but also *in vivo* studies. Compared to organic dyes, gold nanoparticles are much larger and their emission quantum yield is much smaller, in the order of 10^{-6}[13]. This minute value is compensated by an absorption cross section several orders of magnitude larger than that of molecules[14], therefore the brightness of gold nanoparticles is comparable to that of fluorescent molecules under the same illumination intensity.

Since the absorption cross section of the particles scales as their volume, detecting smaller particles in presence of background requires a specific approach. Several techniques have been proposed, including two-photon excitation[6], photothermal heterodyne detection[15] and interferometric detection[16]. Each of these methods is useful but their operation requires dedicated setups and a high level of expertise. A method that allows to image gold nanoparticles with a high background rejection and that is readily implementable in current confocal and wide-field microscopes would provide great benefits.

Gold nanoparticles exhibit a collective oscillation of conduction electrons called surface plasmon resonance[17]. This resonance strongly depends on the shape of the particles[18, 19]. Spheres with radius roughly between 5 and 80 nm will have a resonance between 520 nm and 560 nm; more elongated particles such as nano-rods or bipyramids[20] exhibit red-shifted longitudinal resonances that reach wavelengths of 800 nm or longer[21]. It is important to note that tuning the shape of the particles can be easily achieved by synthesis and that relatively narrow size distributions can be obtained[22].

The plasmon is responsible for enhanced absorption and scattering cross sections[23] of particles for specific wavelengths but it is also responsible for enhanced photoluminescence emission in the spectral region of the plasmon resonance. In this work luminescence is referred to all the emission arising from a nanoparticle at wavelengths different than the excitation wavelength. Because of the absence of a gap in the excited states spectrum of gold nanoparticles, their photoluminescence excitation spectra overlaps their emission spectrum[13], a very different situation from the Stokes-shifted emission of fluorescent molecules and semiconductor nanocrystals. Upon excitation of gold nanoparticles at their plasmon resonance maximum, most of the emission will be concentrated in a narrow spectral region around the excitation. A portion of the luminescence emission will therefore have the same wavelength than the excitation, making it indistinguishable

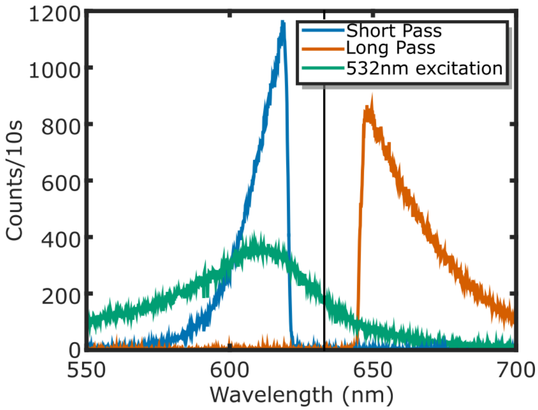

Figure 3.1: Luminescence spectra of a single gold nanorod. Green curve: emission upon excitation with a 532 nm laser. Red curve: Stokes emission upon excitation with a resonant 633 nm HeNe laser. Blue curve: anti-Stokes emission under the same 633 nm excitation.

from elastic scattering. But this region of the spectrum will be blocked by the filters that, in fluorescence detection experiments, prevent direct excitation light from reaching the detectors.

It is also possible to excite the particles off-resonance with a shorter wavelength laser (for instance through interband transitions with 532 nm) and the emission will be mostly concentrated around the longitudinal plasmon resonance of nanorods at longer wavelengths. This is the closest situation to the behavior of a fluorophore, in which the Stokes-shifted emission can be easily detected by introducing a long-pass filter. The drawback, however, is that the cross section of particles is much smaller at this wavelength and can only be compensated by increasing the excitation power.

Figure 3.1 shows typical spectra of a gold nanorod under different excitation wavelengths. The green curve is the one-photon-excited luminescence spectrum around the longitudinal plasmon resonance, observed while irradiating with 532 nm laser; the full spectrum of the longitudinal plasmon is clearly observable with its resonance at 620 nm. The particle can also be excited at or close to its resonance, where its absorption cross section is maximum.

Figure 3.1 shows the emission spectra upon excitation at 633 nm, depicted as the vertical black line. The red curve is the Stokes-shifted emission; the spectral shape of this emission overlaps with the one observed exciting at 532 nm. Exciting in resonance is more efficient and therefore the emission is much brighter. The blue curve in fig. 3.1 displays the anti-Stokes emission at shorter wavelengths. In this case the spectral shape doesn't resemble that of the plasmon resonance. The exponential-like decay of the anti-Stokes spectrum can be modelled with Boltzmann statistics[24] of the bath (phonons and electrons) energy levels that are present in gold nanoparticles at room temperature. In both cases it is clear from the shape of spectra that the filters block an important part of the emission close to the plasmon maximum.

This work focuses in the exploitation of the anti-Stokes luminescence[25] for imaging of gold nanorods in biologically relevant conditions. This scheme benefits from the

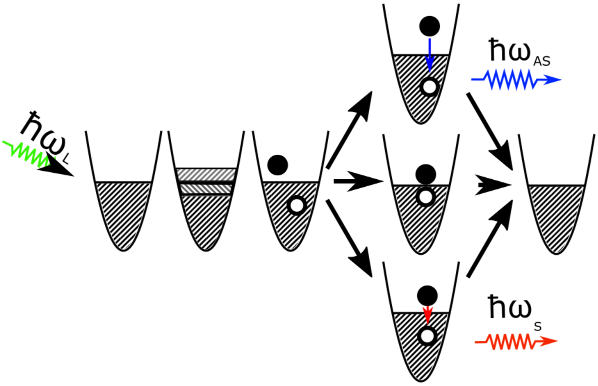

Figure 3.2: Schematic of the anti-Stokes luminescence arising from a single gold nanorod. After excitation with a photon, a collective oscillation of electrons is generated. Once the coherence is lost, the state can be described as an electron-hole pair. Three scenarios are possible: electron and hole may recombine radiatively after one of more interactions with the thermal baths of lattice phonons and charge carrier thermal excitations: i) if the energy difference between electron and hole states is lower than the initial one after excitation we obtain Stokes emission upon a radiative recombination; ii) if electron and hole transiently increase their energy difference at the bath's expense before recombining radiatively, we observe anti-Stokes emission; iii) if electron and hole recombine non radiatively, their energy difference is transferred to the baths and no photon is emitted. The latter process is the most probable one.

enhanced absorption cross section of the particles, their high photo-stability and fairly narrow emission spectra. When exciting in resonance with the plasmon, a short-pass filter can be introduced allowing the observation of only the anti-Stokes emission. This procedure highly reduces the background arising from self-fluorescence and Raman-scattering from cells, most of it being Stokes-shifted. Reducing the background therefore opens the possibility of imaging and tracking smaller particles or using lower excitation powers.

The anti-Stokes emission mechanism[24] is depicted in Figure 3.2 and can be described as follows: an absorbed photon generates a collective oscillation of the conduction electrons. After a fast loss of the coherence[26], the state of the particle can be described as an electron-hole pair. The hole and/or the electron can interact with thermal baths, i.e. with phonons of the gold lattice[27] or thermally excited charge carriers[28]. There are three possibilities after the interaction with baths: i) Electron and hole loose energy to the bath before recombining radiatively, giving rise to Stokes-shifted emission. ii) The interactions with baths can transiently increase the energy difference between electron and hole; if then they recombine radiatively, the emitted photon will have higher energy (shorter wavelength) than the incoming photon[29]. Or iii) electron and hole can recombine non-radiatively, transferring their whole energy to the lattice.

The probability of a radiative recombination of electrons and holes is low, as can be experimentally determined by the very low emission quantum yield of the photoluminescence[13, 20, 26]. Anti-Stokes emission stems from electron-hole recombination events after the electron-hole pair has transiently gained energy from the lattice, i.e., before it thermalizes. Even if the anti-Stokes scenario is unlikely, it is frequent enough as to observe an intensity in the range of 10^3 counts per second on an avalanche photodiode with excitation powers around 16 kW/cm^2. Such relatively high detection rates require enhancement of the emission probability through the proximity of the plasmon resonance[30].

The main advantage of the approach presented in this work is the simplicity of its implementation. With any confocal or wide-field setup enabling resonant excitation of gold nano-particles, one can exploit the anti-Stokes photoluminescence by inserting a proper short-pass filter in the detection path. As we will see below, single gold nanoparticles can be detected even in higher background conditions such as a stained cell, or a highly self-fluorescent sample.

3.2. EXPERIMENTAL METHOD

Images of gold nanorods were recorded by sample scanning employing a XYZ piezo stage (PI Nano Cube) in a home-built confocal microscope, sketched in Figure B.1a. The objective employed was an oil-immersion Olympus 60X NA 1.4 that allowed a high efficiency in both exciting the particles and collecting their emission. The luminescence arising from the particles was filtered and detected by either an avalanche photodiode or a liquid-nitrogen-cooled CCD-spectrometer (Acton 500i). An example of an image can be seen in Figure B.1b. To detect the anti-Stokes luminescence, a 633 nm short-pass filter (Semrock) was added to the detection path together with a 633 nm notch filter. Both filters were needed simultaneously since neither of them was able to entirely block the excitation light from the detectors. The Stokes luminescence was collected replacing the short-pass filter with a 633 nm long-pass (Semrock).

Gold nanorods were synthesized by following the standard seeded-growth method[22]. The average size of the nanorods was 50 nm × 23 nm and their SPR was located at around 650 nm in water. Figure B.2 shows the extinction spectrum of a suspension of the nanoparticles after synthesis and Fig. B.4 shows a TEM image of the rods.

Two different laser wavelengths were employed. A CW 532 nm laser (CNI) was used to excite the transverse plasmon and the full longitudinal plasmon spectrum was collected. Single nanorods exhibit a narrow Lorentzian-shaped luminescence spectrum as displayed in Figure B.1c. A second CW laser (Thorlabs HeNe) with a wavelength of 633 nm allowed us to excite the particles in resonance and collect either the Stokes or the anti-Stokes emission depending on the analysis filters. Both lasers were focused to a diffraction-limited spot through the high NA objective.

Figure 3.3 shows a scatter plot of the Stokes and anti-Stokes emission intensities of 75 gold nanorods against their plasmon peak position. The anti-Stokes emission was calculated by integrating the recorded spectra at wavelengths shorter than the excitation laser, while the opposite was done for the Stokes. This can also be directly measured by recording the emission intensity after a short pass or long pass filter. The large dispersion of the points observed can be attributed to the distribution of sizes of the rods inherent to the synthesis method[31] (bigger particles will have a bigger cross section) and probably to different photoluminescence quantum yields for different individual particles. Because the particles were first deposited on glass directly and because they were excited with circularly polarized light, their orientation shouldn't influence their photoluminescence intensity.

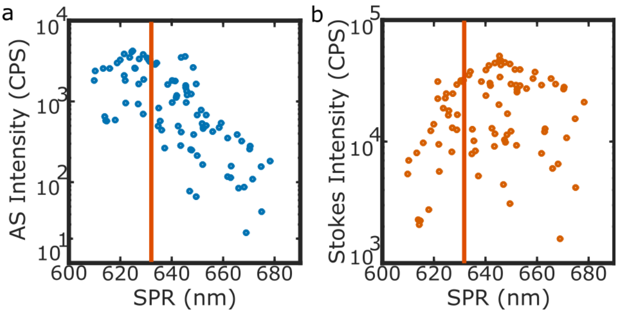

Figure 3.3: Emission intensity of different gold nanorods as a function of their plasmon peak position. The data are plotted for the anti-Stokes (a) and Stokes (b) sides of the emission; the orange vertical line at 633 nm is the wavelength of the laser. The anti-Stokes intensity was obtained by integrating the emission at wavelengths shorter than the laser, while the opposite was done for the Stokes. The spread in intensities for similar peak positions can be attributed to variations in sizes and, possibly, to different quantum yields of the different individual particles. The maximum emission for the anti-Stokes is obtained when the plasmon is slightly blue shifted from the excitation laser and viceversa for the Stokes emission.

It is possible to observe that the maximum emission intensity for the anti-Stokes appears for those particles with their plasmon slightly blue-shifted from the laser wavelength, while the opposite is observed for the Stokes emission. This means that there is a trade-off between the excitation efficiency and the collection efficiency: exciting in perfect resonance is more efficient, but the filters will eliminate most of the luminescence. Therefore exciting slightly to the blue (red) of the resonance will be beneficial for the (anti-)Stokes imaging.

Particles with a plasmon resonance slightly to the blue of the laser show an anti-Stokes emission roughly 10 times weaker than the Stokes emission. This would imply that the quantum yield of the emission at shorter wavelengths is 10 times smaller than the emission at longer wavelengths and therefore would be in the order of 10^{-7} [13, 20, 32, 33]. The spectral dependence of the anti-Stokes emission however, induces a large under estimation of the total intensity. The exponential shape seen in fig. 3.1 implies that the majority of the emission is concentrated close to the laser excitation wavelength and therefore the filters are blocking it. Careful experiments with narrower filters would allow a better characterization of the quantum yield of the anti-Stokes emission.

To prove that the technique is well suited for imaging particles in biological systems, we deposited HeLa cells on top of the nanorod sample. Firstly, nanoparticles were deposited on clean glass coverslips by spin casting a suspension of gold nanorods as described elsewhere[31]. This procedure ensures that the analysis is performed on single nanorods and therefore that the luminescence signals are not arising from clusters of nanorods. It also allowed us to characterize the nanorod emission both by acquiring spectra and by studying the dependency with excitation power, avoiding the diffusion away from the focus.

Secondly, HeLa cells were plated on top of these samples, and grown overnight until they reached a high confluency. Although the obtained images are not equivalent to images of gold nanorods residing in the cytoplasm or nucleus of cells, they would resemble very closely images of rods in cell membranes. This simplified protocol only serves the present purpose of optical signal-to-background characterization, and spared us the labour-intensive bio-compatible particle functionalization that would be needed for more relevant biological assays. Figure B.5 shows a typical white light transmission image of the samples. The high confluency ensures that cells uniformly cover the entire observed area, so the studied nanorods are always localized below a cell. We have also acquired images of nanoparticles under cells containing the fluorescent dye ATTO 647N. For this purpose the cells already attached to the coverslips were incubated with 45 pM ATTO 647N for approximately twenty minutes. This set of experiments allowed us to compare Stokes and anti-Stokes emissions under high-background conditions.

3.3. RESULTS AND DISCUSSION

The nanoparticle shown in Fig. 3.1 displays comparable count rates for both the Stokes and anti-Stokes emissions. As explained earlier and shown in Figure 3.3, this is because the excitation laser is slightly red-shifted from the plasmon resonance, the most favorable position for enhancing the anti-Stokes part of the spectrum. Both types of emission are also comparable to the luminescence intensity obtained while exciting at 532 nm. The main difference is the laser intensity employed; the power density for exciting the transverse plasmon with the 532 nm laser was set to 80 kW/cm^2, while for both the anti-Stokes and Stokes, the 633 nm laser was set to 15 kW/cm^2, 5 times less intense. This suggests that the enhancement of absorption cross section at resonance more than compensates the loss of a significant fraction of the luminescence emission in the laser rejection filter, allowing us to use lower powers.

The three curves in Figure 3.1 also show a very distinctive spectral distribution. The luminescence that arises from the 532 nm excitation spans almost 150 nm, from the laser wavelength up to more than 650 nm. The Lorentzian shape confirms that the emission arises from a single nanorod. The long-pass emission (red curve) spans a range of almost 100 nm, from the excitation at 633 nm to above 700 nm. Finally, the anti-Stokes emission, which requires energy extraction from the thermal bath cannot extend much beyond a few k_BT from the excitation energy. This is the narrowest band, extending from the excitation to about 580 nm. The position of the plasmon resonance to the blue of the excitation laser explains the higher peak intensity of the anti-Stokes spectrum compared to the Stokes spectrum, whereas the total integrated Stokes emission is higher than the anti-Stokes's.

Figure 3.4 shows two raster scans of the same $7.5 \times 7.5\,\mu\text{m}^2$ area of the sample with HeLa cells on top of gold nanorods. The left image shows the Stokes emission, where a 633 nm notch and 633 nm long pass filter were employed. The right image corresponds to the anti-Stokes emission, where the same notch and a 633 nm short pass filter were employed; in both cases the irradiation intensity was kept at 30 kW/cm^2 at the sample. Most particles are observed in both Stokes and anti-Stokes images but with different intensities. The main difference between the two images is the background count rate. The Stokes image has an average background count rate around 5k CPS, while the anti-Stokes is below 100 CPS, close to 70 CPS, the dark counts of the detector. Moreover in the Stokes image a structured background can be observed; we attribute this emission to self-fluorescence of the cells. On the other hand, the anti-Stokes image shows a much flatter background and highly distinguishable single particles. Both images display the

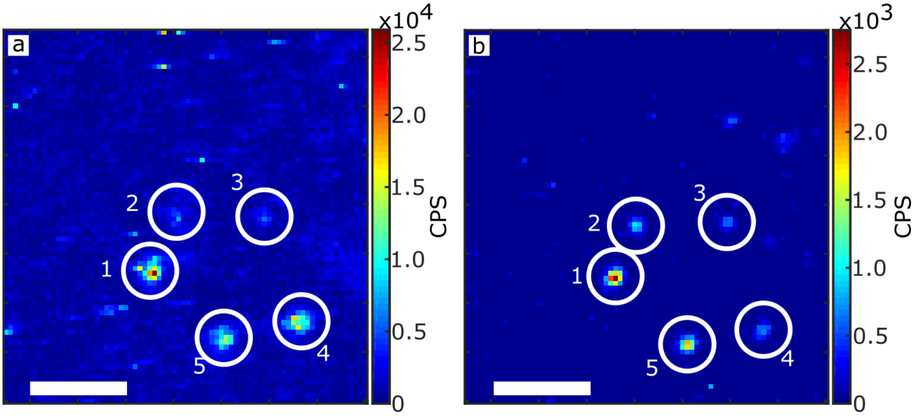

Figure 3.4: Raster scan of a nanorod sample under HeLa cells using (a) a long pass filter and (b) a short pass filter for photoluminescence detection. Some rods can be observed in both images, some others only in the Stokes or anti-Stokes images. Intensities in the Stokes and anti-Stokes emission thus do not necessarily correlate. The scale bar in both figures is 2 μm in length.

count rate obtained after dark count subtraction.

The circled particles in fig. 3.4 show the different possible situations: Particle 1 is the brightest both in Stokes and anti-Stokes, which can be explained if this is a bigger particle. Particles 2 and 3 are barely distinguishable in the Stokes image, while they are clearly visible in the anti-Stokes. This can be attributed to a higher background level in the Stokes case and by a plasmon resonance of particles 2 and 3 to the blue of the laser, favoring the anti-Stokes emission process. Particles 4 and 5 are visible in both, but particle 4 is brighter than 5 in the Stokes image, while the opposite happens in the anti-Stokes. This is due to a plasmon position that favors more one or the other type of emission, as also shown in fig. 3.3. Figure B.6 shows a larger area of the scan, where it is possible to observe more particles both in the Stokes and anti-Stokes configuration.

The use of the anti-Stokes emission is especially valuable when imaging nanoparticles in high background conditions. To this end we incubated the cells with a solution of ATTO 647N. The fluorescent labelling of the cell, even if not specific, resulted in a similar situation to what would be obtained in the case of labelling organelles or the entire cell membrane. This dye was chosen because its absorption maximum is close to 633 nm, the excitation wavelength we employed in these experiments, but also because of its photostability and high quantum yield.

Figure 3.5 shows two raster scans of the samples described above. The right panel shows the anti-Stokes image, in which single particles are clearly distinguishable and marked with a circle. We made sure that the observed spots were nanorods by monitoring their intensity under high illumination conditions and checking that they did not bleach. The left panel shows the Stokes emission, in which no particles can be distinguished from the background. The average background emission in the anti-Stokes image is below 500 CPS, but higher than the dark counts of the detector. The Stokes emission, on the other hand shows an average background intensity around 200 kCPS, two orders of magnitude higher than that observed without the dye.

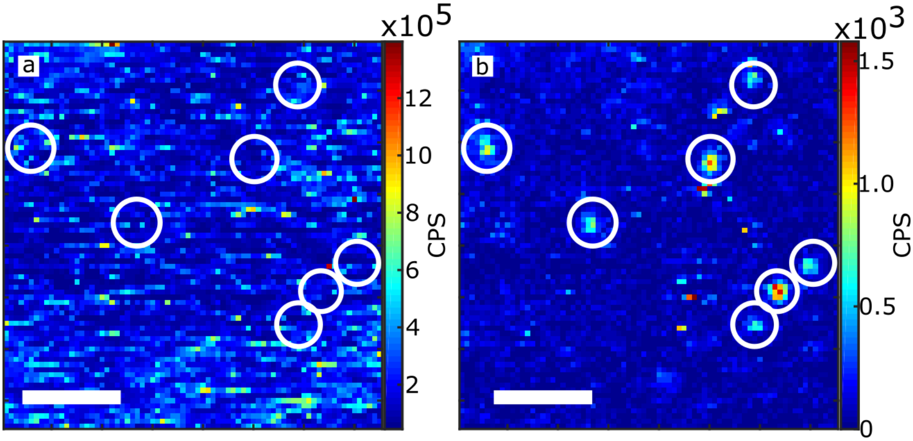

Figure 3.5: Raster scan of a nanorod sample covered by HeLa cells containing the fluorescent dye ATTO 647N, again using (a) a long pass filter and (b) a short pass filter for photoluminescence detection. No clear nanorod signals can be seen in the Stokes images, whereas they are clearly distinguishable in the anti-Stokes image, proving the advantage of the latter for fluorescence background rejection. The scale bar in both figures is 2 μm in length.

These results indicate that the Stokes image deteriorates much faster than the anti-Stokes in the presence of emitting molecules both from the cell itself or from added dyes. The images show regions with higher emission intensities in both configurations, most probably due to a higher concentration of dye in specific regions of the cell. Figure B.7 shows a larger scan, and the difference in background intensities is more evident. At much higher concentrations than the ones shown in this work, the anti-Stokes emission from the dye becomes significant and can overcome the emission rate from individual particles.

Figure 3.6a shows the dependence of the acquired luminescence and the background as functions of excitation power for both the Stokes and anti-Stokes emissions of a particle below a cell without dye. Care was taken in choosing a particle with a resonance close to the excitation laser, to compare Stokes and anti-Stokes luminescence with similar resonant enhancements. The Stokes emission (red curves) shows a linear increase in signal together with a linear increase in background. In this case the signal-to-background ratio reaches a value of 6. The anti-Stokes emission (blue curves) however shows a much steeper increase of the signal than the background, reaching a signal-to-background ratio of 12. Of course, particles with a plasmon resonance to the blue of the laser wavelength show an even larger ratio of anti-Stokes to Stokes emission.

Figure 3.6b shows the same type of curves as 3.6a, for a different particle under cells that contained ATTO 647N. In this case the background prevented the acquisition of luminescence spectra; the particle chosen to draw the figure is representative of the average behavior. We see that in the Stokes case the particle's signal is barely larger than the fluorescence background from the dye. On the other hand, the anti-Stokes luminescence shows an enhanced contrast, reaching a signal-to-background ratio of more than 20 for this particular nanorod. The background level observed in the Stokes

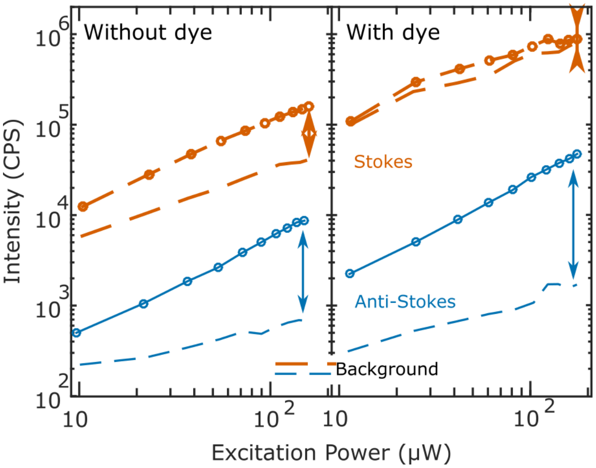

Figure 3.6: Emission intensity (solid lines) and background (broken lines) as functions of excitation intensity for the Stokes (red) and the anti-Stokes (blue) emissions. These data were obtained on two different particles for the right (unstained cells) and left (stained cells) panels. For the unstained cells, the plasmon was chosen close to the laser line, so as to avoid favouring one or the other emission by the resonance effect. Arrows indicate the maximal signal-to-background ratio of each emission in the figure conditions.

image increases much faster with dye content than the anti-Stokes background.

More particles under the same conditions were analyzed and their signal to background ratios are shown in Figure B.8. In this case the irradiation intensity was kept at 30 kW/cm^2. The values of the ratio for Stokes and anti-Stokes under non stained cells is similar and span roughly from 5 to 15. It is however important to note that on average the anti-Stokes emission is 10 times weaker than the Stokes one. It is remarkable that staining the cells with ATTO 647N does not alter significatively the values obtained for the anti-Stokes emission, while the Stokes emission was not separable from the background.

When the cells containing ATTO 647N were used, we observed an increase in the background levels for both Stokes and anti-Stokes emission and these levels also depend on excitation power. This means that the dye shows both components, as is well known from fluorescence hot bands and anti-Stokes Raman scattering. The main difference between nanoparticles and dyes, however, is their quantum yield. While the particles appear to be relatively bright anti-Stokes emitters, in part due to their large absorption cross section, in part due to their plasmon resonance, dyes such as the one employed in this work, are much better Stokes emitters than anti-Stokes. This is the main reason why rods are drowned by the fluorescence background in the Stokes image.

The signal-to-background ratio of the anti-Stokes emission increases with increasing laser excitation powers, going from values close to 2 for 3 kW/cm^2 excitation up to values of 20 for 53 kW/cm^2 as shown in fig 3.6b. However this can't be extrapolated further than the results presented here. It is known that gold nanorods reshape under high irradiation intensities[34]. For high-NA objectives like the one employed in this work, a rule of thumb to prevent reshaping in scanning confocal images is to keep the excitation intensity lower than 150 μW at the back aperture of the objective lens (or equivalently a power density of

$53\,\mathrm{kW/cm^2}$ at the object plane.)

In the presence of a fluorescent dye, the signal-to-background obtained is higher than in the case without dye. This may be a consequence of the selection of particles with a plasmon more favorable to the anti-Stokes than to the Stokes emission, and couldn't be avoided by acquiring luminescence spectra since the background was too high. Although we checked the correct focusing on the sample plane both by optimizing the reflection on the glass/water interface and by employing the anti-Stokes signal, it was never possible to observe single particles under high background conditions in the Stokes configuration.

A major concern for the imaging of nanoparticles in cells is the local increase in temperature, widely exploited in plasmonic photothermal therapy (PPTT)[35]. To calculate the raise in temperature induced by irradiating gold nanoparticles in resonance, we calculated the absorption cross section with the ADDA package[36]. A particle with a length of 50 nm and diameter of 23 nm (the average dimensions of the ones employed in this work) has a maximum absorption cross section of $0.0117\,\mu\mathrm{m}^2$. At an irradiation intensity of $20\,\mathrm{kW/cm^2}$ and assuming all the absorbed energy is dissipated into heat gives a total power of $2.3\,\mu\mathrm{W}$. This value is between 2 and 4 orders of magnitude lower than the reported threshold values for inducing cell death[37, 38].

Moreover we can estimate the temperature of the particle in the steady state by solving the Poisson equation. Assuming a spherical particle of the same volume than the average rod employed in this work and taking into account that the heat conductivity of the particle is much higher than that of the surrounding medium, it is possible to see that the increase in temperature on the surface of the particle follows,

$$\Delta T(r) = \frac{Q_{\mathrm{abs}}}{4\pi\kappa r}$$

Where Q_{abs} is the absorbed power and κ is the heat conductivity of the medium and r is the radius of the particle. By setting κ to $0.45\,\mathrm{W\,m^{-1}\,K^{-1}}$[39], we obtain a temperature increase on the surface of the particle of 25 K at an irradiation intensity of $20\,\mathrm{kW/cm^2}$. Previous studies reported that the threshold temperature for inducing cell destruction is around a mean value of $74\,^o\mathrm{C}$[37] or $50\,^o\mathrm{C}$[40]. In our case the increase in temperature is concentrated locally around the nanoparticle; 50 nm away from the surface the temperature increase of the medium is expected to be below $5\,^o\mathrm{C}$.

As a control we also performed a viability test of the cells after the imaging process. We observed no difference between the cells that were on top of the imaged nanorods and those which were not, as shown in Figure B.9. The black square depicts the region that was imaged under the confocal microscope, while the rest was never irradiated with the laser. The white light transmission image also does not show any distinguishable changes before and after the imaging process. More rigorous tests of the particles inside cells are needed in order to confirm the harmlessness of the method.

3.4. CONCLUSIONS

In this work we have demonstrated that anti-Stokes photoluminescence arising from the excitation in (or close to) the plasmon resonance of a gold nanorod can be exploited to image them in biologically relevant conditions[25]. The comparison between the Stokes and anti-Stokes emissions was possible by using particles immobilized on the substrate, however the technique can be easily extended to imaging in fixed cells, *in vivo* or even for tracking particles in real time[6].

Extending this technique to wide-field should be possible considering the laser powers employed in this work. EMCCDs provide enough gain[41] to easily detect single nanoparticles, while at the same time the background is sufficiently low to give a high contrast. This extension of the technique would open the possibility to track at higher frame rates than achievable by confocal imaging.

The lower count rate of the anti-Stokes compared to the Stokes emission can be a drawback in such applications as localization[42]. This technique's accuracy depends on the number of photons detected, and is given by $\approx 1/\sqrt{N}$, where N is the number of photons collected. The count rates obtained in this work are close to 1.5 kCPS, enough in many applications.

We have shown that the signal-to-background ratio of the anti-Stokes emission is higher than that of the Stokes emission. In the case of HeLa cells not containing a fluorescent dye, typical values can be around 10 and 5 respectively for a particle with a resonance at the laser wavelength. For HeLa cells containing ATTO 647N the difference is much more pronounced, since most of the particles will have a Stokes emission comparable or lower than the background, while in the anti-Stokes the signal-to-background ratio can still be higher than 10.

The main advantage of the technique presented in this work is that it can be easily implemented in any commercial or home-built microscope. It does not require a high investment in equipment or time, since filters are normally available for common laser wavelengths and there is no further need of modifying any experimental configuration already existent. Moreover all the data analysis techniques employed in confocal or wide-field images for localization, tracking, etc. do not have to be modified.

REFERENCES

[1] W. E. Moerner, *New directions in single-molecule imaging and analysis,* Proc. Natl. Acad. Sci. **104**, 12596 (2007).

[2] J. W. Lichtman and J.-A. Conchello, *Fluorescence microscopy,* Nat. Methods **2**, 910 (2005).

[3] N. C. Shaner, P. A. Steinbach, and R. Y. Tsien, *A guide to choosing fluorescent proteins,* Nat. Methods **2**, 905 (2005).

[4] N. R. Jana, L. Gearheart, and C. J. Murphy, *Wet Chemical Synthesis of High Aspect Ratio Cylindrical Gold Nanorods,* J. Phys. Chem. B **105**, 4065 (2001).

[5] A. M. Alkilany, L. B. Thompson, S. P. Boulos, P. N. Sisco, and C. J. Murphy, *Gold nanorods: Their potential for photothermal therapeutics and drug delivery, tempered by the complexity of their biological interactions,* Adv. Drug Deliv. Rev. **64**, 190 (2012).

[6] B. van den Broek, B. Ashcroft, T. H. Oosterkamp, and J. van Noort, *Parallel Nanometric 3D Tracking of Intracellular Gold Nanorods Using Multifocal Two-Photon Microscopy,* Nano Lett. **13**, 980 (2013).

[7] J. Pérez-Juste, I. Pastoriza-Santos, L. M. Liz-Marzán, P. Mulvaney, J. Perezjuste, I. Pastorizasantos, L. Lizmarzan, and P. Mulvaney, *Gold nanorods: Synthesis, characterization and applications,* Coord. Chem. Rev. **249**, 1870 (2005).

[8] M. B. Mohamed, V. Volkov, S. Link, and M. A. El-Sayed, *The 'lightning' gold nanorods: fluorescence enhancement of over a million compared to the gold metal,* Chem. Phys. Lett. **317**, 517 (2000).

[9] S. Yao, H. H. Cai, M. Liu, and P. H. Yang, *Fluorescent labeling of cellular targets and multicolor imaging with gold nanorods,* Dye. Pigment. **101**, 286 (2014).

[10] K. M. Spillane, J. Ortega-Arroyo, G. de Wit, C. Eggeling, H. Ewers, M. I. Wallace, and P. Kukura, *High-speed single-particle tracking of GM1 in model membranes reveals anomalous diffusion due to interleaflet coupling and molecular pinning.* Nano Lett. **14**, 5390 (2014).

[11] A. S. Urban, T. Pfeiffer, M. Fedoruk, A. a. Lutich, and J. Feldmann, *Single-step injection of gold nanoparticles through phospholipid membranes.* ACS Nano **5**, 3585 (2011).

[12] N. Lewinski, V. Colvin, and R. Drezek, *Cytotoxicity of nanopartides,* Small **4**, 26 (2008).

[13] M. Yorulmaz, S. Khatua, P. Zijlstra, A. Gaiduk, and M. Orrit, *Luminescence quantum yield of single gold nanorods.* Nano Lett. **12**, 4385 (2012).

[14] S. Link, M. B. Mohamed, and M. a. El-Sayed, *Simulation of the Optical Absorption Spectra of Gold Nanorods as a Function of Their Aspect Ratio and the Effect of the Medium Dielectric Constant,* J. Phys. Chem. B **103**, 3073 (1999).

[15] S. Berciaud, D. Lasne, G. Blab, L. Cognet, and B. Lounis, *Photothermal heterodyne imaging of individual metallic nanoparticles: Theory versus experiment,* Phys. Rev. B **73**, 045424 (2006).

[16] F. Ignatovich and L. Novotny, *Real-Time and Background-Free Detection of Nanoscale Particles,* Phys. Rev. Lett. **96**, 013901 (2006).

[17] A. Bouhelier, R. Bachelot, G. Lerondel, S. Kostcheev, P. Royer, and G. P. Wiederrecht, *Surface Plasmon Characteristics of Tunable Photoluminescence in Single Gold Nanorods,* Phys. Rev. Lett. **95**, 267405 (2005).

[18] E. Dulkeith, T. Niedereichholz, T. Klar, J. Feldmann, G. von Plessen, D. Gittins, K. Mayya, and F. Caruso, *Plasmon emission in photoexcited gold nanoparticles,* Phys. Rev. B **70**, 205424 (2004).

[19] S. Link and M. a. El-Sayed, *Shape and size dependence of radiative, non-radiative and photothermal properties of gold nanocrystals,* Int. Rev. Phys. Chem. **19**, 409 (2000).

[20] W. Rao, Q. Li, Y. Wang, T. Li, and L. Wu, *Comparison of Photoluminescence Quantum Yield of Single Gold Nanobipyramids and Gold Nanorods,* ACS Nano **9**, 2783 (2015).

[21] L. L. T. Ngoc, J. Wiedemair, A. van den Berg, and E. T. Carlen, *Plasmon-modulated photoluminescence from gold nanostructures and its dependence on plasmon resonance, excitation energy, and band structure,* Opt. Express **23**, 5547 (2015).

[22] B. Nikoobakht and M. A. El-Sayed, *Preparation and Growth Mechanism of Gold Nanorods (NRs) Using Seed-Mediated Growth Method,* Chem. Mater. **15**, 1957 (2003).

[23] W. Ni, X. Kou, Z. Yang, and J. Wang, *Tailoring longitudinal surface plasmon wavelengths, scattering and absorption cross sections of gold nanorods,* ACS Nano **2**, 677 (2008).

[24] Y. He, K. Xia, G. Lu, H. Shen, Y. Cheng, Y.-c. Liu, K. Shi, Y.-F. Xiao, and Q. Gong, *Surface enhanced anti-Stokes one-photon luminescence from single gold nanorods,* Nanoscale **7**, 577 (2015).

[25] L. Jiang, I. W. Schie, J. Qian, S. He, and T. Huser, *Coherent Anti-Stokes Emission from Gold Nanorods and its Potential for Imaging Applications,* ChemPhysChem **14**, 1951 (2013).

[26] C. Sönnichsen, T. Franzl, T. Wilk, G. von Plessen, J. Feldmann, O. Wilson, and P. Mulvaney, *Drastic Reduction of Plasmon Damping in Gold Nanorods,* Phys. Rev. Lett. **88**, 077402 (2002).

[27] Z. Lin, L. V. Zhigilei, and V. Celli, *Electron-phonon coupling and electron heat capacity of metals under conditions of strong electron-phonon nonequilibrium,* Phys. Rev. B - Condens. Matter Mater. Phys. **77**, 1 (2008).

[28] C. K. Sun, F. Vallée, L. H. Acioli, E. P. Ippen, and J. G. Fujimoto, *Femtosecond-tunable measurement of electron thermalization in gold,* Phys. Rev. B **50**, 15337 (1994).

[29] J. Huang, W. Wang, C. J. Murphy, and D. G. Cahill, *Resonant secondary light emission from plasmonic Au nanostructures at high electron temperatures created by pulsed-laser excitation.* Proc. Natl. Acad. Sci. U. S. A. **111**, 906 (2014).

[30] B. Neupane, L. Zhao, and G. Wang, *Up-Conversion Luminescence of Gold Nanospheres When Excited at Nonsurface Plasmon Resonance Wavelength by a Continuous Wave Laser.* Nano Lett. (2013), 10.1021/nl401505p.

[31] P. Zijlstra and M. Orrit, *Single metal nanoparticles: optical detection, spectroscopy and applications,* Reports Prog. Phys. **74**, 106401 (2011).

[32] Y. Cheng, G. Lu, Y. He, H. Shen, J. Zhao, K. Xia, and Q. Gong, *Luminescence Quantum Yields of Gold Nanoparticles Varying with Excitation Wavelength,* Nanoscale , 2188 (2015).

[33] Y. Fang, W.-S. Chang, B. Willingham, P. Swanglap, S. Dominguez-Medina, and S. Link, *Plasmon emission quantum yield of single gold nanorods as a function of aspect ratio.* ACS Nano **6**, 7177 (2012).

[34] Y. Liu, E. N. Mills, and R. J. Composto, *Tuning optical properties of gold nanorods in polymer films through thermal reshaping,* J. Mater. Chem. **19**, 2704 (2009).

[35] X. Huang, P. K. Jain, I. H. El-Sayed, and M. A. El-Sayed, *Plasmonic photothermal therapy (PPTT) using gold nanoparticles,* Lasers Med. Sci. **23**, 217 (2008).

[36] M. A. Yurkin and A. G. Hoekstra, *The discrete-dipole-approximation code ADDA: Capabilities and known limitations,* J. Quant. Spectrosc. Radiat. Transf. **112**, 2234 (2011).

[37] X. Huang, P. K. Jain, I. H. El-Sayed, and M. A. El-Sayed, *Determination of the Minimum Temperature Required for Selective Photothermal Destruction of Cancer Cells with the Use of Immunotargeted Gold Nanoparticles,* Photochem. Photobiol. **82**, 412 (2006).

[38] X. H. Huang, I. H. El-Sayed, W. Qian, and M. a. El-Sayed, *Cancer cell imaging and photothermal therapy in the near-infrared region by using gold nanorods,* J. Am. Chem. Soc. **128**, 2115 (2006).

[39] C. Sturesson and S. Andersson-Engels, *A mathematical model for predicting the temperature distribution in laser-induced hyperthermia. Experimental evaluation and applications,* Phys. Med. Biol. **40**, 2037 (1995).

[40] D. O'Neal, L. R. Hirsch, N. J. Halas, J. Payne, and J. L. West, *Photo-thermal tumor ablation in mice using near infrared-absorbing nanoparticles,* Cancer Lett. **209**, 171 (2004).

[41] D. Dussault and P. Hoess, *Noise performance comparison of ICCD with CCD and EMCCD cameras,* in *Opt. Sci. Technol. SPIE 49th Annu. Meet.*, edited by E. L. Dereniak, R. E. Sampson, and C. B. Johnson (International Society for Optics and Photonics, 2004) p. 195.

[42] S. J. Sahl and W. E. Moerner, *Super-resolution fluorescence imaging with single molecules.* Curr. Opin. Struct. Biol. **23**, 778 (2013).

4

GOLD NANORODS AS NANO-THERMOMETERS

Nano-thermometry is a challenging field that can open the door to very intriguing results ranging from biology and medicine to material sciences. Gold nanorods are excellent candidates to act as nanoprobes because they are reasonably bright emitters upon excitation with a monochromatic source. Moreover gold nanoparticles are already used in photothermal therapy as efficient transducers of electromagnetic radiation into heat. In this work we show that the spectrum of the anti-Stokes emission from gold nanorods irradiated in resonance can be used to measure the absolute temperature of the nanoparticles. The procedure does not require any previous calibration and can be easily implemented in any microscope capable of acquiring emission spectra. We show that the luminescence spectrum of single gold nanorods closely follows Bose-Einstein statistics. We model the emission considering interactions of the electrons and holes created upon absorption of a photon with thermal excitations in the metal, in particular phonons.

4.1. INTRODUCTION

MOST physical, chemical and biological processes depend on temperature. Together with the miniaturization of devices and the advent of nanotechnology the need for measuring temperature with high spatial accuracy started to emerge. Notably in biology[1, 2] and medicine[3] measuring and controlling temperature at a single cell level will provide not only insight into intracellular processes but it will also contribute to a better understanding of the mechanisms involved in proposed new therapies such as photothermal tumor ablation[4] or controlled drug delivery[5, 6].

Probes with distinctive spectral features are ideal candidates for temperature measurements since they provide high spatial accuracy while far-field optics allow a non-contact readout. Some of the proposed strategies include structures that undergo a conformational change upon an increase in temperature[7], thus inducing variations in fluorescence intensity of a dye molecule embedded into them. Also cleverly designed fluorescent probes[8] in which the ratio of particular emission peaks depends on temperature allow a high accuracy and can be used for intracellular thermometry.

The use of anti-Stokes fluorescence emission from lanthanide ions has been studied for several years[9] and can be used to determine temperature with high accuracy. However organic dyes show a very low amount of emitted photons with a higher energy than the excitation energy, rendering their use in biological conditions very challenging. Recently Surface Enhanced Raman Spectroscopy (SERS) allowed to measure changes induced by temperature down to single molecules[10], but a careful calibration of the measurements is crucial.

At a cellular level measuring temperature has been subject to extensive debate[1, 11]. Many cellular processes may be subject to temperature variations, including heat generation at mitochondria. However the measured temperature changes[1] are in the order of 10^5 times higher than the expected values drawn from theoretical models[12]. Moreover new applications in photothermal therapy require locally increasing the temperature in order to induce the death of specific cells in a tissue[5, 13]. Many of these methods employ metallic nanoparticles as heat sources[4, 14] but rely on models[15] or on ad-hoc calibrations to estimate the temperatures reached[16]. Therefore a method that allows both to increase the local temperature and to monitor it will be of great interest in a broad range of fields.

Gold nanoparticles continue to receive a great amount of attention because of their unique optical properties[17]. The collective oscillation of conduction electrons, also known as plasmon, shows a resonance in the visible to near infra-red wavelengths. This resonance can be tuned by changing the shape of the particles[18] and will be responsible for a large absorption and scattering cross section at the resonance wavelength. It is therefore simple to detect nanoparticles in a dark field scattering[19] configuration or via photothermal imaging[20]. Detecting the particles through their luminescence[21] is also possible; their low quantum yield[22–25], in the order of 10^{-5} is compensated by the enhanced cross section. Moreover the luminescence signal is stable over time; gold nanoparticles do not blink nor bleach, therefore are useful labelling agents for processes that require extended periods of observation[26].

Different metallic nano-objects are being introduced as agents for photothermal therapy or drug delivery[5, 13, 27]. One of the advantages of gold nanoparticles is the possibility of tuning their resonance to the near infra-red range, where the penetration of light into tissues can be of several centimeters[3–5, 13, 14, 28]. Moreover the particles can be used not only for treatment, but also for imaging[5, 15]. In this work we propose that the anti-Stokes luminescence of gold nanorods and nanospheres can be used to measure their temperature with relatively high accuracy.

Luminescence of metallic nanoparticles has been the object of extensive study in recent years. Since the first observation of luminescence from bulk gold[29], different groups have tried to quantitatively describe the observed properties[30, 31], such as the quantum yield[22–25, 32] and the emission spectrum[33]. The cross section of different geometries can be calculated employing different computer packages[34–36], obtaining a vary good agreement between calculations and what is experimentally achievable.

Luminescence from single gold nanoparticles can be observed when irradiating them with a monochromatic source. Gold nanorods present two distinct resonance energies, namely the transverse and the longitudinal plasmon resonance. These particles can therefore be excited efficiently at one of those energies; the transverse resonance corresponds to a wavelength of 532 nm and will give rise to a broad emission with a peak at the longitudinal plasmon energy. Conversely it is possible to excite the particles with a wavelength matching the longitudinal plasmon resonance. In this case the excitation benefits from an enhanced absorption cross section, but the emission that overlaps the plasmon resonance will be mostly blocked by the filters needed to prevent direct excitation light from reaching the detectors.

In this work luminescence refers to the emission from nanoparticles observed at energies different from the excitation energy. Normally it is expected that after absorption of a photon, the electrons in the particle will relax and the emitted photon will appear at lower energies than the excitation. If this is the case, the emission is called Stokes-shifted; however gold nanoparticles when excited in resonance also present a significant emission at higher energies called anti-Stokes emission[37–39].

The mechanism we propose to explain the luminescence from gold nanoparticles is based on the radiative recombination of electrons and holes that are created upon the absorption of an incident photon[29, 32]. The emission will be enhanced by the presence of the surface plasmon acting as an antenna[30]. At the same time, the probability of the interaction of the electron or hole with a thermal bath (a phonon or a carrier) before recombining can give rise to an emitted photon with a higher energy than the excitation photon's[40–42].

A monochromatic photon with energy $\hbar\omega_\mathrm{L}$ incident on the particle will give rise to a collective oscillation of the gas of conduction electrons called plasmon. The lifetime of the oscillation can be measured in pulsed experiments or calculated from the inverse of the linewidth and is in the order of 10 fs[43]. The plasmon decays by forming a pair of hot electron and hole with an internal energy equal to the plasmon energy[44–46].

The hot electron and hole cool down by exchanging energy with the lattice on a timescale of $\tau \approx 1\,\mathrm{ps}$[47]. Before this happens, electron and hole have a small probability of recombining radiatively, i.e. of re-emitting their high electronic energy as a photoluminescence photon. If they have interacted only with static surfaces, their energy will be the same and therefore the emitted photon will have the same energy as the incoming photon, and will not contribute to the measured photoluminescence (as it will be blocked by the notch filter.) If, on the other hand, they have interacted with a phonon or a thermally excited electron or hole, they may have lost or acquired energy before recombining.

Electron and hole can interact with baths upon recombination, either by creation or annihilaton of a phonon. In both cases the energy available upon recombination cannot much exceed $\hbar\omega_L + k_B T$. It has to be noted that in the hypothesis of a single-photon absorption at low excitation power, the temperature T is that of the baths before absorption, i.e. the temperature of the medium surrounding the particle. This is different from pulsed experiments, in which the electron gas temperature can be orders of magnitude higher than room temperature[48].

Radiative recombination gives rise to weakly emitting sources spectrally and spatially distributed throughout the particle over a broad frequency band with an exponential cutoff at $\hbar\omega_\mathrm{L} + k_\mathrm{B} T$. The weak recombination emission can be greatly enhanced by the surface plasmon resonance, acting as an antenna. With this model the following predictions can be made. Firstly the emission spectrum must follow the plasmon spectrum if the excitation laser is well above the plasmon resonance as shown in Figure 4.1 in the results. If the excitation falls within the plasmon resonance, the spectrum is expected to follow the plasmon spectrum multiplied by a Bose-Einstein statistics factor arising from phonon population. This factor should be proportional to $\bar{n}$ for anti-Stokes and $\bar{n}+1$ for Stokes processes, where

$$\bar{n} = \left(\exp\frac{\hbar\omega}{k_B T} - 1\right)^{-1}. \tag{4.1}$$

With this model, it can also be predicted that the emission should be polarized; for the longitudinal plasmon of gold nanorods this polarization coincides with the longitudinal axis of the particle[37]. Moreover, the lifetime should be determined by the lifetime of hot electrons and holes and should be significantly shorter than the thermalization time of the carriers. If this was not the case, some interactions would be enough to reduce the carriers' energy and therefore the electron and hole wouldn't have enough energy to produce an optical photon. Finally, only the presence of hot carriers is required in the model. As the wavevectors are randomly distributed at all times, the recombination probability remains constant at all stages of relaxation. Therefore excitation well above the plasmon resonance should excite the photoluminescence with nearly the same efficiency as just above the plasmon resonance[25]. Differences in the distribution of electrons and holes appear if the excitation energy allows interband transitions[44, 49].

In this work we propose to use the anti-Stokes luminescence emission from gold nanoparticles to determine their temperature. According to the model just described, the anti-Stokes emission follows the following form,

$$I(\omega) = \mathrm{I}_\mathrm{SPR}(\omega)\cdot\left(\exp\frac{\hbar(\omega-\omega_\mathrm{L})}{k_\mathrm{B} T} - 1\right)^{-1} \tag{4.2}$$

where I is the intensity, ω is the angular frequency of the photons, ω_L is the frequency of the laser, $\hbar$ is Planck's constant, k_B the Boltzmann constant. I_SPR is the surface plasmon resonance that can be obtained by exciting the particle at energies higher than the resonance or, ideally, by looking at the scattering spectrum. Even if these two spectra are not identical, they overlap in the range of wavelengths comprising the maximum of the emission and longer[24]; in the results section a lengthier discussion will be given. The only remaining free parameter is the temperature T (plus a normalization constant not included in eqn. 4.2.) This means that carefully fitting the emission spectra excited at two frequencies ($\nu \gg \nu_{\mathrm{SPR}}$ and $\nu \approx \nu_{\mathrm{SPR}}$) allows us to extract the absolute temperature of the particles without any previous calibration.

4.2. EXPERIMENTAL METHOD

All the measurements in this work were performed with a home-built confocal microscope equipped with an APD and a spectrometer (Acton 500i). Samples were mounted in a flow cell that allowed us to increase the temperature of the medium up to $60\,^{o}C$ and to monitor it through a Pt100 resistance thermometer placed 1 mm away from the observation area.

Samples were prepared by spin casting a suspension of nanoparticles onto clean coverslips. Different particles were employed in this work. Nanorods with average dimensions of 21 nm × 50 nm and a plasmon resonance around 650 nm were synthesized following the seeded-growth method[50]; spheres with radii between 30 nm and 60 nm were purchased from BBI International. We employed a 532 nm (CNI) laser for characterizing the nanorods' plasmon and for exciting spheres close to resonance. A 633 nm HeNe (Thorlabs) was employed to excite the nanorods in resonance.

Room temperature measurements were performed using a $60X$, NA 1.4 oil immersion objective (Olympus). This provided high excitation and collection efficiency. At higher temperatures an air-spaced objective, $60X$, NA 0.9 (Olympus) was employed to avoid the presence of a heat sink directly in contact to the observed area. With this objective both the excitation and collection efficiencies are significantly lower. The lower excitation efficiency can be compensated increasing the excitation power, the lower collection however is inherent to the method and can be compensated only by increasing the exposure time.

To compensate for the drift of the setup while increasing the temperature, we developed a computer program to continuously track a reference particle. The same program was responsible for recording the temperature and triggering the spectrometer. In this way complete data sets were acquired at different temperatures, including spectra while exciting at 532 nm, at 633 nm with different laser intensities and the temperature measured by the Pt100. A spectrum with 532 nm laser excitation was taken after every cycle to ensure that the particle was not reshaping due to higher excitation powers.

The intensity of the lasers was controlled via the voltage applied to an AOM in the optical path. Several accumulations of the spectra at the same laser intensity were recorded. This not only allowed us to lower the noise of the measurements because of a longer exposure time, but also allowed us to remove bright pixels generated by cosmic rays. Having several accumulations is also useful to monitor changes in the intensity of the spectra during the acquisition itself. These changes can be due to a drift of the setup while measuring or to a reshaping of the particle. The reshaping can be confirmed by comparing the spectra acquired with the 532 nm laser[51]. In case reshaping was observed, the measurements where rejected. In the case of drift of the setup, the particular data set was not taken into account. For the purposes of this work the excitation intensity is crucial for characterizing the method; if the particle is not in focus it would result in an over estimation of the excitation power.

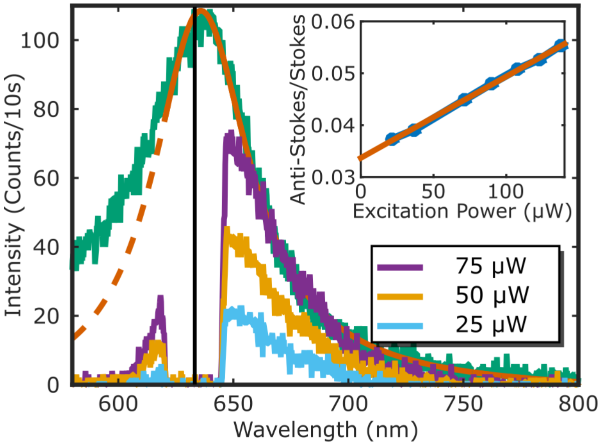

Figure 4.1: Luminescence spectra of a single gold nanorod. The green curve is the emission under 532 nm excitation. In red is the fitting by a lorentzian; the dashed part is the region that was not considered for the fitting. The other curves are the emission of the same particle under 633 nm irradiation at three different powers. The inset shows the anti-Stokes-to-Stokes ratio as a function of the excitation power, overlapped with a linear fit in red.

To calculate the heating of the particles the absorption cross section has to be computed. For the case of nanorods, the ADDA package was employed[34]. Spheres' cross section can be calculated from Mie theory. Once the dissipated power is known, the parameters can be either used in a Comsol model or the heat equation can be analytically solved, approximating the rods by spheres with the same total area.

4.3. RESULTS

The proposed model for the anti-Stokes emission requires to know the plasmon spectrum (I_{SPR} function in equation 4.2) of the particle in order to fit the emission at shorter wavelengths and extract the particle temperature. It has been shown that both scattering and luminescence spectra roughly overlap over a broad range of wavelengths[24]. Therefore exciting gold nanorods with 532 nm allows to record the longitudinal plasmon spectra, as shown in the green solid curve of Figure 4.1. The peak was fitted by a single lorentzian, shown in red in the Figure; the dashed part of the curve depicts the spectral region that was not considered for the fitting. It has to be recalled that the luminescence spectrum is not a perfect lorentzian since there is a broadband contribution to the luminescence arising between the excitation wavelength and the plasmon peak[52]. This appears as an asymmetry in the emission spectrum, particularly visible for wavelengths smaller than 625 nm. The results of this fitting will be employed for the I_{SPR} function defined in equation 4.2.

The other curves in Fig. 4.1 show the luminescence emission of the same nanorod while irradiating with a 633 nm laser at different powers, ranging from 25 μW to 75 μW at the back aperture of the objective. The vertical black line shows the wavelength of the laser. The Stokes part of the spectrum at longer wavelengths than the excitation

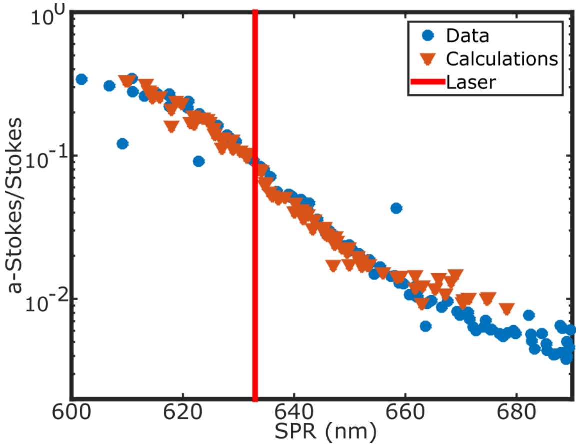

Figure 4.2: Ratio of the anti-Stokes to Stokes emission under 633 nm excitation as function of the resonance wavelength of each particle. The blue circles are experimental results, while the red triangles are the results of the calculations with equation 1.2. There is a very good agreement between experiment and calculations. Particles with a resonance to the blue of the laser (vertical red line) have an increased anti-Stokes emission.

shows the same shape as the plasmon emission observed under 532 nm excitation, apart from a normalization factor. From the figure it can readily be seen that the shape of the anti-Stokes emission, at shorter wavelengths than excitation, is exponential-like and doesn't follow the lorentzian shape of the Stokes emission. The dip between Stokes and anti-Stokes is caused by the notch filter that prevents direct excitation light from reaching the detectors.

The inset of Fig. 4.1 shows the anti-Stokes-to-Stokes ratio of the integrated luminescence for different laser excitation intensities. It is possible to see that even with a linear behavior, the anti-Stokes intensity increases more rapidly with laser excitation power than the Stokes emission. We already exploited this phenomenon to image gold nanorods in high-background conditions[39]. Moreover it shows that the anti-Stokes emission depends on laser excitation power differently from its Stokes counterpart.

Figure C.2 shows the intensity of the Stokes (red) and anti-Stokes (blue) emission for several excitation powers. In both cases the linear fit in logarithmic scale has a slope close to 1, being 0.88 for the Stokes and 1.20 for the anti-Stokes, confirming that both types of emission are single-photon processes. The behavior is independent of the plasmon resonance position. It is important to note that the excitation intensity cannot be increased much beyond what is shown because nanorods would start reshaping towards a more spherical shape at higher laser powers.

Figure 4.2 shows the ratio of the anti-Stokes to Stokes emission for 90 nanorods with different plasmon resonances and under 633 nm excitation; the blue circles are experimental data. The horizontal axis of the figure is the surface plasmon resonance (SPR) of each particle. The vertical red line marks the laser wavelength. The particles shown in the plot had resonances between 600 nm and 690 nm; the ones showing the maximum ratio of anti-Stokes to Stokes are those with a resonance to the blue of the laser. For these particles the plasmon is enhancing preferably the anti-Stokes emission. For

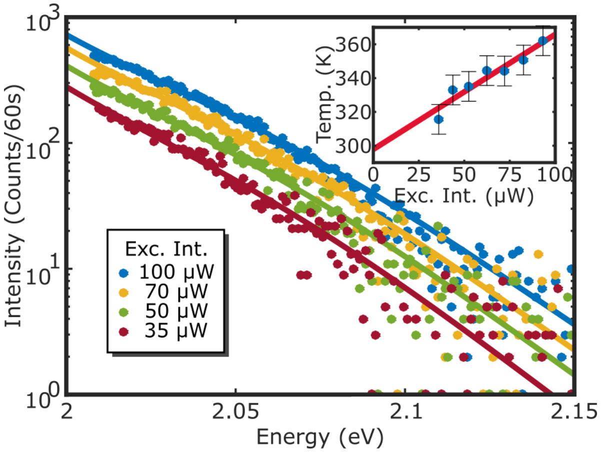

Figure 4.3: Anti-Stokes emission at different irradiation powers with the corresponding fits by equation 4.2. There is an excellent agreement between data and model. The inset shows the extracted temperature at each power (blue dots) and a linear extrapolation of the data to 0 μW excitation power. The value obtained for room temperature was 293 K while the measured value was 296 K.

particles with a resonance at the laser wavelength the anti-Stokes and the Stokes emission have similar enhancement and show a ratio close to 10%.

Figure 4.2 also shows the results of calculations as the red triangles. A very good overlap between the measured and the calculated data can be observed. The absorption cross section of several particles was calculated with the ADDA package. Each calculated absorption spectrum was fitted by a lorentzian and used as $\mathrm{I_{SPR}}(\omega)$ in eqn. 4.2. The absorption cross section also allowed us to estimate the temperature of the particle assuming a diffraction limited laser spot and from this to calculate the anti-Stokes emission spectrum using the full eqn. 4.2. The Stokes emission was calculated assuming a lorentzian spectrum overlapping the absorption. Both anti-Stokes and Stokes emissions are proportional to the excitation power, so that this term cancels out when computing the ratio. For this calculation no free parameters were assumed and the transmission of the filters was taken into account.

By fitting the anti-Stokes part of the spectra shown in Fig. 4.1 with equation 4.2 it is possible to extract the temperature of the particle at each excitation power. Figure 4.3 shows the results of this procedure. The spectra shown were recorded at 4 different excitation intensities while the full lines are the fits; there is an excellent agreement between data and model. For every anti-Stokes measurement we have also acquired the full plasmon spectrum while exciting with a 532 nm laser before and after the temperature extraction. Having the full plasmon spectrum allowed us to calculate the parameters of I_{SPR} from equation 4.2 and also to verify that the particle didn't reshape while being excited at resonance.

The inset in fig. 4.3 shows the temperatures resulting from the fits at different irradiation intensities (blue dots). It is remarkable that the absolute temperatures of the particle were extracted without any previous calibration. As expected, the temperature of the nanorod is proportional to the excitation intensity, or equivalently to the absorbed energy.

From these data it is also possible to calculate the temperature at 0 μW excitation power, i.e. room temperature, by extrapolating the results of a linear fit. The value we obtained in this case is 293 ± 6 K, while room temperature was 296 K, a 2% accuracy.

The accuracy of the obtained temperature depends to a great extent on the plasmon resonance. The first step in the fitting of spectra is the determination of the term I_{SPR} in equation 4.2. This is achieved by fitting a lorentzian to the emission spectrum obtained while irradiating with a 532 nm laser. In figure 4.1 it is possible to observe that the emission spectrum is not perfectly lorentzian and therefore the fitting results will be sensitive to the portion of the spectrum selected. Depending on the wavelength range selected, the parameters of the lorentzian fit (its width and peak position) can slightly change and this will give rise to different temperatures when fitting the anti-Stokes emission spectrum.

Equation 4.2 shows that if the particle plasmon resonance is red shifted with respect to the 633 nm laser, the term I_{SPR} will have a smaller effect on the temperature extracted. When the resonance is to the red of the laser, the term I_{SPR} will slowly vary in the region where the anti-Stokes emission is observed. Therefore small changes in the parameters of the lorentzian fit will have a small effect on the temperature extracted. However, particles that are not in resonance with the excitation laser will present a lower emission due to a smaller absorption cross section and to a lower enhancement of the anti-Stokes emission (see for example figure 4.2). A balance between the amount of collected light and the uncertainty produced by the correct determination of the plasmon resonance has to be reached depending on each application. The error bar in figure 4.3 and in the following figures is the result of the estimation of the temperature uncertainty because of variations in the plasmon resonance fit.

As expected from the model, the anti-Stokes emission should depend not only on the particle's intrinsic properties but also on the temperature of the surrounding medium[53]. The samples were therefore mounted in a flow cell that allowed us to change the temperature and to measure it with a Pt100 resistance thermometer. In this set of experiments we employed a dry objective and therefore the laser powers are higher to compensate for the lower excitation efficiency. At each temperature several spectra were acquired at different 633 nm excitation powers and also a spectrum of the plasmon before and after each measurement in order to monitor any possible reshaping of the particles during the experiment.

Figure 4.4 shows the extracted temperature of a particle at varying excitation powers and at different water temperatures. The blue circles are the results of the measurement at 20 ^{o}C, while the green crosses are at 40 ^{o}C and the yellow squares at 60 ^{o}C. The full lines are the calculated temperatures for a particle with plasmon overlapping the measured one and assuming a diffraction-limited focus spot. For the dimensions of the particle, the mean values from TEM images were used and the length was adjusted to obtain the same resonance. There is a remarkable agreement between the calculation and the measured values. Moreover it is possible to extrapolate the temperature at zero excitation power for each case as was explained earlier. The results are shown in the inset of the figure for each temperature. The red line with slope 1 is a guide to the eye.

Figure 4.4 clearly shows that the extracted temperature varies with the temperature of the surrounding medium. More strikingly the method does not require any previous calibration nor adjustment. The values obtained with the extrapolation to 0 μW excitation

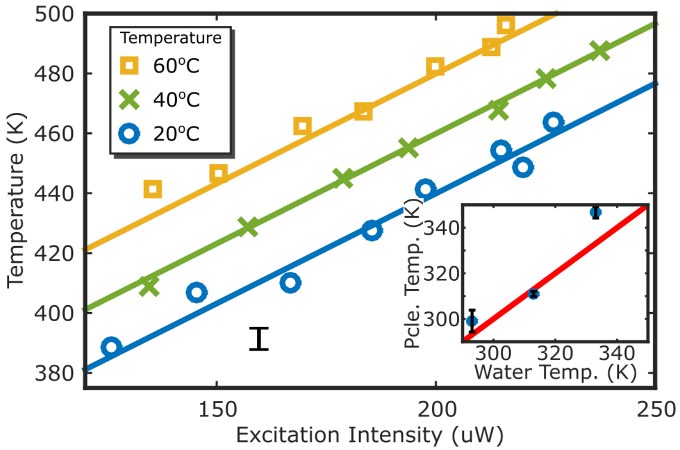

Figure 4.4: Extracted temperatures at different excitation powers and at different flow cell temperatures. The full lines are the results of the calculated temperatures. The inset shows the extrapolated temperature at zero excitation power.

power were 299 ± 8 K, 311 ± 3 K and 347 ± 6 K for water temperatures of 293 K, 313 K and 333 K respectively. The very good agreement between the temperatures obtained from fitting the anti-Stokes emission and the water temperatures measured by the Pt100 thermometer is remarkable. The calibration-free procedure would allow us to perform the same measurements in any other setup and could act as a reference for calibration of other nano thermometers.

It is also possible to keep the excitation intensity constant and to vary the temperature of the surrounding medium. Figure 4.5 shows the extracted temperature from the fitting with equation 4.2 as a function of the temperature of the medium. The red line is showing the water temperature and acts as a guide to the eye. The Figure clearly shows an increase in the extracted temperature while increasing the temperature of the flow cell. The range of explored temperatures was from 296 K to 320 K. This range is enough to observe a change in the anti-Stokes emission spectrum. At higher temperatures the stability of the setup plays a crucial role in maintaining the particle in focus during the spectra acquisition time. Longer exposure times and therefore lower excitation intensities can be employed if particles are actively maintained in focus.

Particles that can withstand higher excitation powers and that have a well-defined plasmon resonance are of great interest, because they would allow to employ a single wavelength and also to reduce the exposure times to record the spectra. A well defined plasmon resonance also lowers the uncertainties associated with the initial lorentzian fit needed for the term I_{SPR} in equation 4.2. In principle gold nanospheres fulfill these requirements. They are known to withstand much higher excitation powers without reshaping nor melting[54]. Moreover the plasmon resonance of spheres shifts only slightly with radius, therefore it is possible to predict it using Mie theory and to eliminate the need of a second laser beam. Sphere samples however always show a shape distribution that cannot be neglected[55] and that induces deviations of the observed resonance from

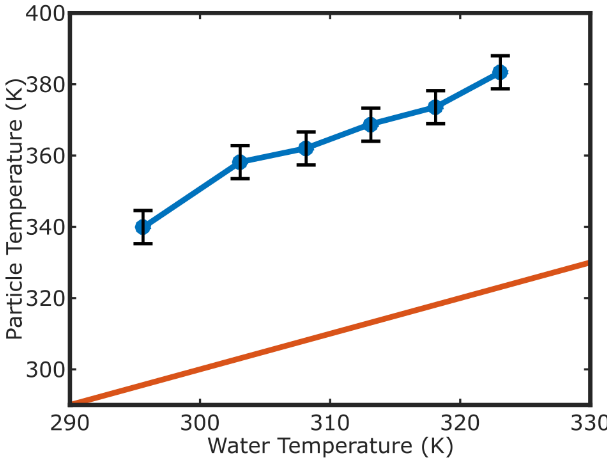

Figure 4.5: Temperature of a single nanorod under the same 633 nm excitation conditions, but at different medium temperatures.

Mie's model.

Figure 4.6 shows the normalized luminescence spectra of three nanospheres of diameters 60 nm, 40 nm and 30 nm under 532 nm excitation. As for the nanorods, two very distinctive parts of the spectrum are distinguishable, the Stokes spectrum at longer wavelengths and the anti-Stokes spectrum at shorter ones. From Mie theory we would have expected a blue shift of the resonance whith decreasing radius of the particles; however the 30 nm sphere seems to be the most red-shifted. This is most likely due to small anisotropies of the particles, giving rise to slightly different plasmon resonances. The inset in Fig.4.6 shows a detail of the anti-Stokes emission for the three spheres without any further normalization. It has to be pointed out, however, that the excitation intensities were 1.2 mW, 2.0 mW and 3.6 mW to compensate for the lower cross sections of the smaller particles.

Spheres not only have a smaller cross section than nanorods of the same volume, but their quantum yield is also one order of magnitude lower than that of rods[24]. The weaker emission from these particles can be compensated by increasing the excitation power. The maximum power that can be employed is given by either reaching the melting temperature of gold or by inducing a phase transition of the surrounding liquid. The first would induce an irreversible change in shape of the particles[56] the latter would induce a change in the refractive index of the medium and therefore would induce a shift in the plasmon resonance[54].

Figure 4.7 shows the extracted temperature of the three particles while increasing the medium temperature. It is possible to see that the small 30 nm diameter sphere is 150 K hotter than both the 40 nm and 60 nm. The three curves show an increasing trend, but in this case the variation of medium temperature amounts to less than 5% the temperature of the particles. The extracted temperature is several tens of degrees above what would be expected from the heat equation, considering the absorption cross section given by Mie theory. The reason for the discrepancies between the measured values and the expected

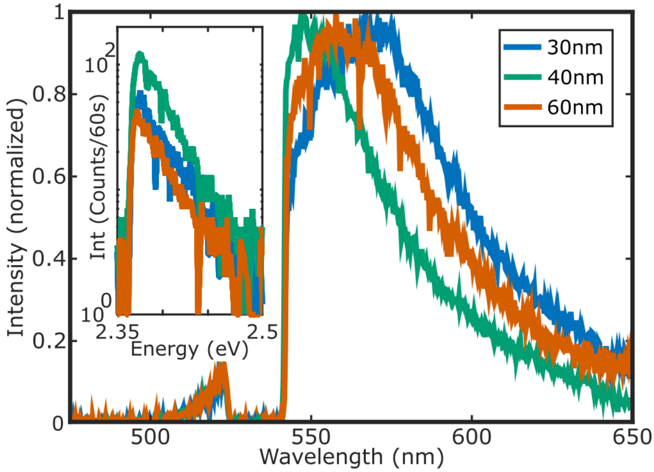

Figure 4.6: Normalized luminescence spectra of spheres with diameters of 60 nm, 40 nm and 30 nm under 532 nm excitation. The inset shows the detail of the anti-Stokes emission without normalization. The excitation powers for the three particles were 1.2 mW, 2.0 mW and 3.6 mW respectively.

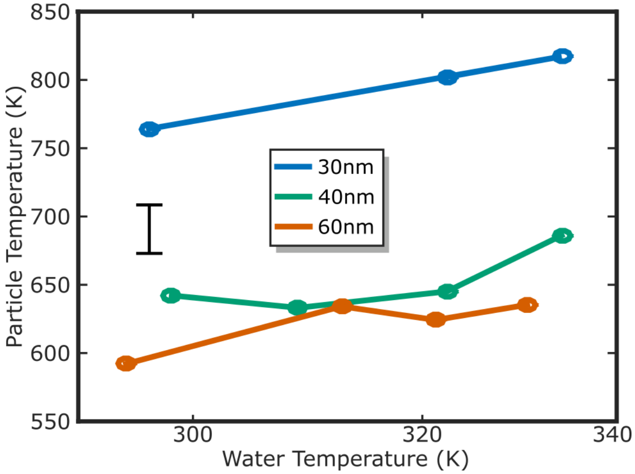

Figure 4.7: Extracted temperature from the same particles as in fig. 4.6 at different medium temperatures.

values can be accounted for by the computation of the plasmon resonance term I_{SPR} in eqn. 4.2.

As explained earlier for nanorods, the fitting of the anti-Stokes emission is highly sensitive to the plasmon position relative to the laser employed. In the case of nanospheres, the resonance is slightly shifted to the red from the 532 nm laser. Small errors in the determination of the plasmon resonance will generate larger errors in the temperature extracted. The differences between the plasmon observed in fig. 4.6 and the results of Mie scattering calculations most likely are due to particles that are not spherical. If this was the case, the calculated cross section and plasmon resonance will not coincide with the particles under study, leading to larger errors.

The use of spheres would be beneficial for some applications that require higher excitation powers or smaller particles. The intrinsic heterogeneity of the samples, however, prevents the use of a single wavelength for the measurements. Ideally, white light scattering of single gold nanospheres would provide the information on the plasmon resonance needed for the correct fitting of the anti-Stokes emission.

4.4. CONCLUSIONS

Being able to control and monitor temperature at the nanoscale is of utmost importance in different fields ranging from photothermal therapy[5] to nano fabrication[57]. In this work we have shown a simple procedure that allows us to measure the temperature of single gold nanorods and nanospheres irradiated under a monochromatic continuous laser and without any previous calibration. The level of accuracy of the temperature measurement depends on several factors, but for nanorods it can be estimated to be better than 6 K and for nanospheres around 15 K.

The model employed for describing the anti-Stokes emission takes into account the plasmon, responsible for enhancing the emission, as well as Bose-Einstein statistics to explain the distribution of the excited states of the particles. It has been shown that the correct characterization of the plasmonic resonance is fundamental for the proper extraction of temperature, specially in cases where the excitation wavelength is red-detuned from the resonance.

Particles with a resonance to the red of the excitation wavelength would be more reliable in the temperature extraction procedure, but would also exhibit a lower emission towards shorter wavelengths. The trade-off between both effects and the possibility to fully characterize the plasmon resonance, will determine the specific particles that are better suited for each application.

In this work we have also explored the possibility of employing gold nanospheres. Since these particles do not reshape under higher excitation powers it is possible to compensate their lower cross section by increasing the irradiation intensity. However, their quantum yield is at least one order of magnitude smaller than that of rods, giving an overall lower photoluminescence intensity. Samples with a narrow shape distribution such as bipyramids[58] would be ideal candidates to temperature extraction since their plasmon can be measured or determined from theory, avoiding the need of a second excitation source.

We have observed the anti-Stokes emission from particles with three different diameters. It was already possible to see that the heterogeneity in the shape of the particles induces plasmon resonances different from the ones predicted from Mie theory. The variation in the temperature extracted from the anti-Stokes spectra while increasing the medium's temperature falls within the experimental error. The obtained temperatures however are much higher than predicted from the heat equation. The samples normally have a distribution of sizes and shapes, assuming a perfectly spherical particle leads to an incorrect determination of the plasmon resonance that propagates into the determination of the surface temperature.

The main advantage of the proposed method is that it doesn't require any calibration, since the only free parameter of the model is the absolute temperature of the nanoparticle under study. Moreover the recording of the anti-Stokes spectrum is readily achievable in any confocal microscope with a coupled spectrometer. A 6 K accuracy may suffice for several applications; it is important to point out that this value can be improved in different ways: by carefully selecting the particles that show the most favorable plasmon resonance; by determining the plasmon resonance through white-light scattering, avoiding the uncertainty in the fit; by increasing the exposure times to increase the signal-to-noise ratio; finally an ad-hoc calibration of the temperature can be performed.

REFERENCES

[1] J.-M. Yang, H. Yang, and L. Lin, *Quantum Dot Nano Thermometers Reveal Heterogeneous Local Thermogenesis in Living Cells,* ACS Nano **5**, 5067 (2011).

[2] C. Hrelescu, J. Stehr, M. Ringler, R. A. Sperling, W. J. Parak, T. A. Klar, and J. Feldmann, *DNA Melting in Gold Nanostove Clusters,* J. Phys. Chem. C **114**, 7401 (2010).

[3] Y. Li, A. M. Gobin, G. W. Dryden, X. Kang, D. Xiao, S. P. Li, G. Zhang, and R. C. G. Martin, *Infrared light-absorbing gold/gold sulfide nanoparticles induce cell death in esophageal adenocarcinoma,* Int. J. Nanomedicine **8**, 2153 (2013).

[4] A. M. Gobin, M. H. Lee, N. J. Halas, W. D. James, R. A. Drezek, J. L. West, M. Gobin, M. H. Lee, N. J. Halas, W. D. James, R. A. Drezek, and J. L. West, *Near-Infrared Resonant Nanoshells for Combined Optical Imaging and Photothermal Cancer Therapy,* Nano Lett. **7**, 1929 (2007).

[5] X. H. Huang, I. H. El-Sayed, W. Qian, and M. a. El-Sayed, *Cancer cell imaging and photothermal therapy in the near-infrared region by using gold nanorods,* J. Am. Chem. Soc. **128**, 2115 (2006).

[6] S. Huo, S. Jin, X. Ma, X. Xue, K. Yang, A. Kumar, P. C. Wang, J. Zhang, Z. Hu, and X.-J. Liang, *Ultrasmall Gold Nanoparticles as Carriers for Nucleus-Based Gene Therapy Due to Size-Dependent Nuclear Entry,* ACS Nano **8**, 5852 (2014).

[7] S. Ebrahimi, Y. Akhlaghi, M. Kompany-Zareh, and A. Rinnan, *Nucleic Acid Based Fluorescent Nanothermometers.* ACS Nano (2014), 10.1021/nn5036944.

[8] F. Vetrone, R. Naccache, A. Zamarrón, A. Juarranz de la Fuente, F. Sanz-Rodríguez, L. Martinez Maestro, E. Martín Rodriguez, D. Jaque, J. García Solé, and J. A. Capobianco, *Temperature sensing using fluorescent nanothermometers,* ACS Nano **4**, 3254 (2010), http://dx.doi.org/10.1021/nn100244a .

[9] F. Auzel, *Upconversion and Anti-Stokes Processes with f and d Ions in Solids,* Chem. Rev. **104**, 139 (2004).

[10] E. A. Pozzi, A. B. Zrimsek, C. M. Lethiec, G. C. Schatz, M. C. Hersam, and R. P. Van Duyne, *Evaluating Single-Molecule Stokes and Anti-Stokes SERS for Nanoscale Thermometry,* J. Phys. Chem. C **119**, 21116 (2015).

[11] M. Suzuki, V. Zeeb, S. Arai, K. Oyama, and S. Ishiwata, *The 10ˆ5 gap issue between calculation and measurement in single-cell thermometry,* Nat. Methods **12**, 802 (2015).

[12] M. K. Sato, M. Toda, N. Inomata, H. Maruyama, Y. Okamatsu-Ogura, F. Arai, T. Ono, A. Ishijima, and Y. Inoue, *Temperature Changes in Brown Adipocytes Detected with a Bimaterial Microcantilever,* Biophys. J. **106**, 2458 (2014).

[13] X. Huang, P. K. Jain, I. H. El-Sayed, and M. A. El-Sayed, *Plasmonic photothermal therapy (PPTT) using gold nanoparticles,* Lasers Med. Sci. **23**, 217 (2008).

[14] L. R. Hirsch, R. J. Stafford, J. A. Bankson, S. R. Sershen, B. Rivera, R. E. Price, J. D. Hazle, N. J. Halas, and J. L. West, *Nanoshell-mediated near-infrared thermal therapy of tumors under magnetic resonance guidance.* Proc. Natl. Acad. Sci. U. S. A. **100**, 13549 (2003), arXiv:0008204 [cond-mat] .

[15] T. Zhao, K. Yu, L. Li, T. Zhang, Z. Guan, N. Gao, P. Yuan, S. Li, S. Q. Yao, Q.-H. Xu, and G. Q. Xu, *Gold Nanorod Enhanced Two-Photon Excitation Fluorescence of Photosensitizers for Two-Photon Imaging and Photodynamic Therapy,* ACS Appl. Mater. Interfaces **6**, 2700 (2014).

[16] J. S. Donner, S. a. Thompson, C. Alonso-Ortega, J. Morales, L. G. Rico, S. I. C. O. Santos, and R. Quidant, *Imaging of Plasmonic Heating in a Living Organism,* ACS Nano **7**, 8666 (2013).

[17] P. Zijlstra and M. Orrit, *Single metal nanoparticles: optical detection, spectroscopy and applications,* Reports Prog. Phys. **74**, 106401 (2011).

[18] A. Carattino, S. Khatua, and M. Orrit, *In situ tuning of gold nanorod plasmon through oxidative cyanide etching,* Phys. Chem. Chem. Phys. **18**, 15619 (2016).

[19] M. Hu, C. Novo, A. Funston, H. Wang, H. Staleva, S. Zou, P. Mulvaney, Y. Xia, and G. V. Hartland, *Dark-field microscopy studies of single metal nanoparticles: understanding the factors that influence the linewidth of the localized surface plasmon resonance,* J. Mater. Chem. **18**, 1949 (2008).

[20] S. Berciaud, D. Lasne, G. Blab, L. Cognet, and B. Lounis, *Photothermal heterodyne imaging of individual metallic nanoparticles: Theory versus experiment,* Phys. Rev. B **73**, 045424 (2006).

[21] A. Tcherniak, S. Dominguez-Medina, W.-S. Chang, P. Swanglap, L. S. Slaughter, C. F. Landes, and S. Link, *One-Photon Plasmon Luminescence and Its Application to Correlation Spectroscopy as a Probe for Rotational and Translational Dynamics of Gold Nanorods,* J. Phys. Chem. C **115**, 15938 (2011).

[22] Y. Fang, W.-S. Chang, B. Willingham, P. Swanglap, S. Dominguez-Medina, and S. Link, *Plasmon emission quantum yield of single gold nanorods as a function of aspect ratio.* ACS Nano **6**, 7177 (2012).

[23] W. Rao, Q. Li, Y. Wang, T. Li, and L. Wu, *Comparison of Photoluminescence Quantum Yield of Single Gold Nanobipyramids and Gold Nanorods,* ACS Nano **9**, 2783 (2015).

[24] M. Yorulmaz, S. Khatua, P. Zijlstra, A. Gaiduk, and M. Orrit, *Luminescence quantum yield of single gold nanorods.* Nano Lett. **12**, 4385 (2012).

[25] Y. Cheng, G. Lu, Y. He, H. Shen, J. Zhao, K. Xia, and Q. Gong, *Luminescence Quantum Yields of Gold Nanoparticles Varying with Excitation Wavelength,* Nanoscale , 2188 (2015).

[26] H. Wang, T. B. Huff, D. A. Zweifel, W. He, P. S. Low, A. Wei, and J.-X. Cheng, *In vitro and in vivo two-photon luminescence imaging of single gold nanorods,* Proc. Natl. Acad. Sci. **102**, 15752 (2005).

[27] B. Kang, M. M. Afifi, L. a. Austin, and M. a. El-Sayed, *Exploiting the nanoparticle plasmon effect: observing drug delivery dynamics in single cells via Raman/fluorescence imaging spectroscopy.* ACS Nano **7**, 7420 (2013).

[28] D. O'Neal, L. R. Hirsch, N. J. Halas, J. Payne, and J. L. West, *Photo-thermal tumor ablation in mice using near infrared-absorbing nanoparticles,* Cancer Lett. **209**, 171 (2004).

[29] A. Mooradian, *Photoluminescence of metals,* Phys. Rev. Lett. **22**, 185 (1969).

[30] M. B. Mohamed, V. Volkov, S. Link, and M. A. El-Sayed, *The 'lightning' gold nanorods: fluorescence enhancement of over a million compared to the gold metal,* Chem. Phys. Lett. **317**, 517 (2000).

[31] M. Beversluis, A. Bouhelier, and L. Novotny, *Continuum generation from single gold nanostructures through near-field mediated intraband transitions,* Phys. Rev. B **68**, 1 (2003).

[32] E. Dulkeith, T. Niedereichholz, T. Klar, J. Feldmann, G. von Plessen, D. Gittins, K. Mayya, and F. Caruso, *Plasmon emission in photoexcited gold nanoparticles,* Phys. Rev. B **70**, 205424 (2004).

[33] S. Link and M. A. El-Sayed, *Shape and size dependence of radiative, non-radiative and photothermal properties of gold nanocrystals,* Int. Rev. Phys. Chem. **19**, 409 (2000).

[34] M. A. Yurkin and A. G. Hoekstra, *The discrete-dipole-approximation code ADDA: Capabilities and known limitations,* J. Quant. Spectrosc. Radiat. Transf. **112**, 2234 (2011).

[35] B. T. Draine and P. J. Flatau, *Discrete-Dipole Approximation For Scattering Calculations,* J. Opt. Soc. Am. A **11**, 1491 (1994).

[36] A. F. Oskooi, D. Roundy, M. Ibanescu, P. Bermel, J. Joannopoulos, and S. G. Johnson, *Meep: A flexible free-software package for electromagnetic simulations by the FDTD method,* Comput. Phys. Commun. **181**, 687 (2010).

[37] Y. He, K. Xia, G. Lu, H. Shen, Y. Cheng, Y.-c. Liu, K. Shi, Y.-F. Xiao, and Q. Gong, *Surface enhanced anti-Stokes one-photon luminescence from single gold nanorods,* Nanoscale **7**, 577 (2015).

[38] L. Jiang, I. W. Schie, J. Qian, S. He, and T. Huser, *Coherent Anti-Stokes Emission from Gold Nanorods and its Potential for Imaging Applications,* ChemPhysChem **14**, 1951 (2013).

[39] A. Carattino, V. I. Keizer, M. J. Schaaf, and M. Orrit, *Background Suppression in Imaging Gold Nanorods through Detection of Anti-Stokes Emission,* Biophys. J. **111**, 2492 (2016).

[40] J. H. Hodak, A. Henglein, and G. V. Hartland, *Electron-phonon coupling dynamics in very small (between 2 and 8 nm diameter) Au nanoparticles,* J. Chem. Phys. **112**, 5942 (2000).

[41] A. Giri, J. T. Gaskins, B. M. Foley, R. Cheaito, and P. E. Hopkins, *Experimental evidence of excited electron number density and temperature effects on electron-phonon coupling in gold films,* J. Appl. Phys. **117**, 044305 (2015).

[42] A. Arbouet, C. Voisin, D. Christofilos, P. Langot, N. D. Fatti, F. Vallée, J. Lermé, G. Celep, E. Cottancin, M. Gaudry, M. Pellarin, M. Broyer, M. Maillard, M. P. Pileni, and M. Treguer, *Electron-Phonon Scattering in Metal Clusters,* Phys. Rev. Lett. **90**, 177401 (2003).

[43] C. Sönnichsen, T. Franzl, T. Wilk, G. von Plessen, J. Feldmann, O. Wilson, and P. Mulvaney, *Drastic Reduction of Plasmon Damping in Gold Nanorods,* Phys. Rev. Lett. **88**, 077402 (2002).

[44] R. Sundararaman, P. Narang, A. S. Jermyn, W. a. Goddard III, and H. a. Atwater, *Theoretical predictions for hot-carrier generation from surface plasmon decay,* Nat. Commun. **5**, 5788 (2014).

[45] M. L. Brongersma, N. J. Halas, and P. Nordlander, *Plasmon-induced hot carrier science and technology,* Nat. Nanotechnol. **10**, 25 (2015).

[46] A. Manjavacas, J. G. Liu, V. Kulkarni, and P. Nordlander, *Plasmon-Induced Hot Carriers in Metallic Nanoparticles,* ACS Nano **8**, 7630 (2014).

[47] V. K. Pustovalov, *Theoretical study of heating of spherical nanoparticle in media by short laser pulses,* Chem. Phys. **308**, 103 (2005).

[48] G. Baffou, P. Berto, E. Bermúdez Ureña, R. Quidant, S. Monneret, J. Polleux, and H. Rigneault, *Photoinduced Heating of Nanoparticle Arrays,* ACS Nano **7**, 6478 (2013).

[49] A. M. Brown, R. Sundararaman, P. Narang, W. A. Goddard, and H. A. Atwater, *Ab initio phonon coupling and optical response of hot electrons in plasmonic metals,* Phys. Rev. B **94**, 075120 (2016), arXiv:1602.00625 .

[50] B. Nikoobakht and M. A. El-Sayed, *Preparation and Growth Mechanism of Gold Nanorods (NRs) Using Seed-Mediated Growth Method,* Chem. Mater. **15**, 1957 (2003).

[51] Y. Liu, E. N. Mills, and R. J. Composto, *Tuning optical properties of gold nanorods in polymer films through thermal reshaping,* J. Mater. Chem. **19**, 2704 (2009).

[52] G. T. Boyd, Z. H. Yu, and Y. R. Shen, *Photoinduced luminescence from the noble metals and its enhancement on roughened surfaces,* Phys. Rev. B **33**, 7923 (1986).

[53] A. Konrad, F. Wackenhut, M. Hussels, A. J. Meixner, and M. Brecht, *Temperature Dependent Luminescence and Dephasing of Gold Nanorods,* J. Phys. Chem. C **117**, 21476 (2013).

[54] L. Hou, M. Yorulmaz, N. R. Verhart, and M. Orrit, *Explosive formation and dynamics of vapor nanobubbles around a continuously heated gold nanosphere,* New J. Phys. **17**, 13050 (2015).

[55] Y.-J. Lee, N. B. Schade, L. Sun, J. a. Fan, D. R. Bae, M. M. Mariscal, G. Lee, F. Capasso, S. Sacanna, V. N. Manoharan, and G.-R. Yi, *Ultrasmooth, highly spherical monocrystalline gold particles for precision plasmonics.* ACS Nano **7**, 11064 (2013).

[56] P. Zijlstra, J. W. M. Chon, and M. Gu, *White light scattering spectroscopy and electron microscopy of laser induced melting in single gold nanorods,* Phys. Chem. Chem. Phys. **11**, 5915 (2009).

[57] M. Fedoruk, M. Meixner, S. Carretero-Palacios, T. Lohmüller, and J. Feldmann, *Nanolithography by Plasmonic Heating and Optical Manipulation of Gold Nanoparticles,* ACS Nano **7**, 7648 (2013).

[58] M. Pelton, J. E. Sader, J. Burgin, M. Liu, P. Guyot-Sionnest, and D. Gosztola, *Damping of acoustic vibrations in gold nanoparticles,* Nat. Nanotechnol. **4**, 492 (2009).

5

PLASMON DAMPING AS A FUNCTION OF TEMPERATURE

The fundamental property of metallic nanoparticles is the presence of a localized surface plasmon resonance. This resonance gives rise to very intriguing and useful properties such as sub-wavelength field confinement, increase in the efficiency of creation of hot carriers, large absorption and scattering cross sections. In this work we show that the plasmon resonance width increases linearly with temperature in the range from $293\,K$ *to* $350\,K$. *This can be used to measure temperature employing far field optics and can have many applications in different fields.*

5.1. INTRODUCTION

MEASURING temperature at the nanoscale is one of the main open challenges in biology[1], specially when focused into the promising fields of photothermal[2, 3] and photodynamic therapy[4]. The first method normally employs small nanoparticles to efficiently convert irradiation energy into heat in very localized environments[5], thus making it possible to address specific cells[3, 6]. The latter employs the nanoparticles as small antennas, utilizing the enhanced near field to produce singlet oxygen that in turn will induce cell apoptosis[7] or to induce drug delivery after irradiation[8].

Successfully designing and implementing new therapies requires not only a careful understanding of the mechanisms involved, but also needs tools to measure and validate the hypotheses. For instance, little is reported in literature regarding the critical temperatures needed for inducing cell death[2]. Much less is reported regarding the effect of a single nanoparticle in or in the vicinity of a cell.

Measuring temperature in cells has been recently subject to debate, mainly because measurements contradict the expected thermodynamic values[1, 9, 10]. Therefore new techniques that can shine light into these matters are very valuable. Moreover these techniques should be easy to implement in existing setups and ideally should not interfere with the environment to be measured.

Biologically relevant questions however are not the only open concerns regarding temperature at the nanoscale. For instance the temperature of a nanoparticle in an optical tweezer can be estimated from models[11] or by indirect measurements. Two different approaches include looking at the rotational diffusion coefficient[12] or by seeing changes in a lipid bilayer standing in the vicinity[5, 13]. These methods are specific to some experiments and can't be easily generalized.

The mentioned therapies are not the only research areas where nanoparticles have become very promising tools. In particular gold nanoparticles have been successfully employed as biosensors[14, 15], labels[16, 17], nanoantennas[18, 19] and are currently under investigation for solar energy conversion[20]. The main property for such broad range of applications resides in the presence of a localized surface plasmon resonance (LSPR) that strongly depends on the shape of the particles[21]. Normally this resonance will lie between 2.34 eV (530 nm) for spheres and in the near infrared for more elongated particles.

The plasmon resonance on one hand is responsible for high electromagnetic field enhancements near tips or protrusions[22, 23]. Because of this, nanoparticles currently are employed as nanometer-sized antennas useful both for Raman scattering (SERS)[24] and also for enhanced fluorescence[25, 26] experiments. On the other hand, the plasmon resonance energy is highly sensitive to the refractive index[27] of the medium surrounding the particles. This phenomenon is exploited for instance in nanosensors that rely in minute changes in the plasmon resonance to detect down to single molecules[14].

The energy (or equivalently the wavelength) of the resonance is not the only useful parameter for sensing applications. The resonance's width is also dependent on surrounding conditions[28, 29] and therefore can be exploited. In this work we propose the use of the FWHM of the resonance as a parameter to measure temperature changes of the immersion medium. In order to achieve a better understanding of the phenomenon it is important to determine the different parameters that explain the resonance's linewidth of the plasmon.

In literature the main mechanisms involved in the description of the damping of the plasmon resonance are electron-phonon scattering, electron-surface scattering, radiative damping and electron-electron scattering[30–32]. Interband damping can be neglected if the resonance energies are low enough, which is the case for the nanorods we studied. Each one of the mentioned terms contributes additively to the total plasmon damping; electron-phonon scattering however is the only one that shows a strong dependence on temperature[28, 29]. From the Debye model of phonons and a Fermi distribution of the conduction electrons it is possible to calculate the damping term attributed to electron-phonon interaction $\Gamma_{\text{e-ph}}$ as[33],

$$\Gamma_{\text{e-ph}} = \frac{\hbar}{\tau_0}\left[\frac{2}{5} + 4\left(\frac{T}{\Theta_D}\right)^5 \int_0^{\Theta_D/T} \frac{z^4}{e^z - 1}\,\mathrm{dz}\right] \tag{5.1}$$

where $\tau_0 = 30\,\text{fs}$[28], $\Theta_D = 170\,\text{K}$[34]. It is important to note that this equation is valid in the case $T < \Theta_D$, in which mostly acoustic phonon modes are occupied. For temperatures $T > \Theta_D$ and by following a simple model for metals it is possible to simplify eqn. 5.1 into[35]

$$\Gamma_{\text{e-ph}} = \lambda \frac{k_\text{B} T}{\hbar} \tag{5.2}$$

where λ is a constant depending on the metal, and k_B is Boltzmann's constant. Equations 5.1 and 5.2 are derived in the limit $E_f \gg \hbar\omega \gg k_\text{B} T$, where E_f is the Fermi energy and $\hbar\omega$ is the plasmon resonance energy. For gold, $E_f = 5.53\,\text{eV}$, and at room temperature $k_\text{B} T = 0.026\,\text{eV}$. For nanoparticles with resonances at around 1.91 eV as the ones employed in this work, both conditions are satisfied. The coefficient λ is assumed to be a constant of the metal, but it could also be an intrinsic property of each particle.

Previous work done at low temperatures on bulk gold[33], gold nanorods[29] and gold bipyramids[28] showed a good agreement of the model in equation 5.1 with the experimental results. On average it was found that the electron-phonon damping increases with a rate of 0.1 meV/ K for temperatures above the Debye temperature, independently of the geometry. Nanorods or bipyramids normally have plasmon resonances below 2 eV and therefore interband damping mechanisms can be discarded. [36, 37]

Figure 5.1 shows white light scattering spectra of a single gold nanorod at 293 K and 333 K with the corresponding lorentzian fits. The plasmonic resonance centered around 1.857 eV is clearly visible. The FWHM of the fit at 333 K is 3.6 meV larger than at 293 K; this increase in width is of about 3% over a 40 K temperature change. The inset of the figure shows a SEM image of a cluster of the typical particles employed in this work.

Measuring the plasmonic resonance of single gold nanorods can be achieved not only by detecting white light scattering spectra but also by exciting their luminescence[29]. It has to be kept in mind, however, that measuring scattering spectra benefits from the enhanced cross section at the resonant wavelengths without being affected by the very low quantum yield of the luminescence[38]. This in turn will allow us to use much lower excitation powers and shorter acquisition times.

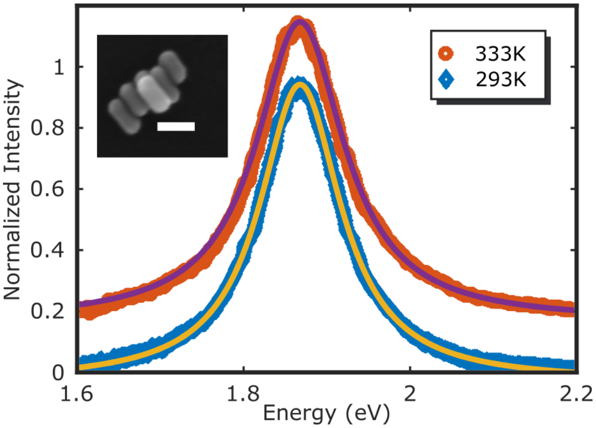

Figure 5.1: Normalized scattering spectra of a single gold nanorod at 293 K and at 333 K with corresponding lorentzian fits. The offset between the curves is for clarity. The FWHM increases by 3.6 meV upon a temperature change of 40 K. The inset shows a SEM image of some nanorods from the same batch. The scale bar is 50 nm.

5.2. EXPERIMENTAL METHOD

The experiments were performed in a home-built confocal microscope. The samples were mounted on a flow cell that allowed to raise the temperature of the medium up to 60 ^{o}C. A dry objective (Olympus 60× NA0.9) was employed to avoid the presence of a heat sink close to the observed area. To acquire white light scattering spectra the particles were immersed in index matching oil, therefore achieving a dark-field configuration without changes to the optics. Nanorods with average dimensions 20 nm × 50 nm, as shown in the inset of fig. 5.1 were spin coated on top of a clean coverslip. As a result, the number of dimers or clusters is below 1% of the observed diffraction-limited bright spots.

Spectra were recorded with an Acton 500-i spectrometer. Exposure times were on average of two seconds. This short time was possible because the collected scattered intensity is of the order of 10^5 counts per second with a laser-driven white light source (Energetiq).

Two different kinds of experiments were performed. Firstly spectra of a single nanorod were acquired continuously while varying the temperature in cycles, as shown in Figure 5.2. From 19 ^{o}C the temperature was increased to 60 ^{o}C and then freely cooled down. For the first analyzed particle the procedure was repeated three times in order to study fluctuations in the results given by the higher temperatures. Two more particles were studied in the same manner, but each was subject to one thermal cycle only. In every case, after each spectrum a background was recorded in the vicinity of the particle.

Secondly many particles were analyzed to improve the statistics of the results. In this set of experiments, each particle's spectrum was acquired consecutively. Also backgrounds in different regions of the sample were recorded. After the iteration on all particles was finished, the temperature was changed to a fixed value and the operation was repeated. In this way we have recorded the scattering spectrum of more than 200 particles at 9 different temperatures ranging from 19 ^{o}C to 58 ^{o}C. The first 5 measurements were done while increasing the temperature, while the last 4 were done when cooling down to

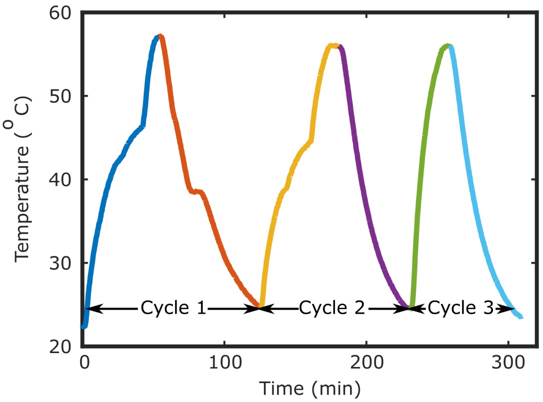

Figure 5.2: Example of the temperature cycle employed for studying a single gold nanorod. Spectra of the particle and of the background were acquired in intervals of approximately 10 s

room temperature.

In order to compensate for the drift of the setup while changing the temperature, a special computer program to control the setup was written. In the first set of experiments, it continuously refocused on the studied particle and triggered the spectrometer. The same program monitored and recorded the temperature of the flow-cell by measuring the resistance of a previously calibrated Pt100 thermometer, placed 1 mm away from the observed area. Only in the first cycle both the warming up and cooling down were done in steps, as can be seen in the Fig. 5.2, in order to slowly test the procedure.

In the second experiment, a reference particle was used for compensating the drift while changing temperature; the relative positions of the other particles were calculated accordingly. In every case an automatic refocusing procedure was applied before triggering the spectrometer, ensuring the correct positioning of the desired particle in the center of the beam. With this procedure, approximately 80 particles can be studied at 9 different temperatures in under 6 hours. Measuring the local temperature in the vicinity of the particles is important since the PID loop used to control the flow-cell temperature can have drifts of up to 4 ^{o}C.

5.3. RESULTS

The particle shown in Figure 5.1 was analyzed while continuously changing the temperature of the flow cell as described earlier. Figure 5.3 shows the FWHM (full width at half maximum) of the plasmon resonance as a function of temperature. Each row in the figure corresponds to every temperature cycle in Fig. 5.2, the first cycle on top and the last at the bottom. In every plot, the red dots show the part of the cycle with an increasing temperature. The blue crosses show the results when cooling down to room temperature.

In Fig. 5.3 it is possible to observe that during the first cycle there is a linear relationship between the plasmon resonance's width and temperature. In this cycle the plasmon broadens at a rate of 0.34 meV/ K. During the second cycle the broadening of the resonance is slightly less pronounced, at a rate of 0.23 meV/ K. During the third cycle the

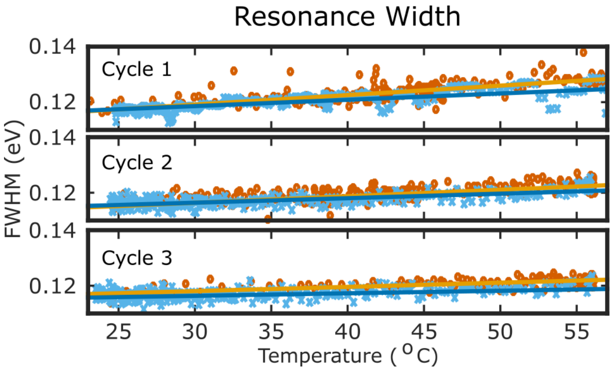

Figure 5.3: Plasmon width for one particle at varying temperatures. From top to bottom, each plot represents a thermal cycle, going from room temperature to 60 ^{o}C (red circles) and cooling down afterwards (blue crosses). It can be seen that after the second cycle the width increases reproducibly with temperature.

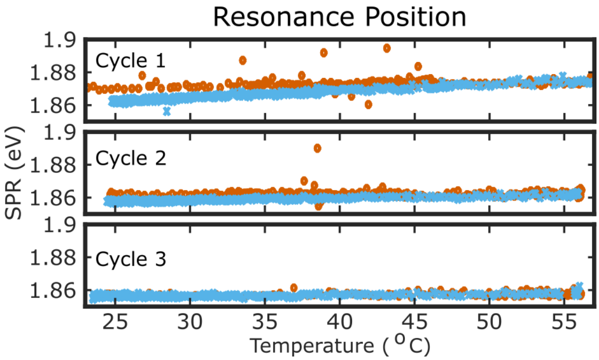

Figure 5.4: Resonance position for one particle at varying temperatures. From top to bottom, each plot represents a thermal cycle, going from room temperature to 60 ^{o}C (red circles) and cooling down afterwards (blue crosses). It can be seen that after the second cycle there is no variation of the plasmon resonance position, thus no reshaping of the particle.

broadening of the plasmon shows a rate of 0.15 meV/ K. The results of the linear fittings of the FWHM of the plasmon while changing temperature are summarized in table 5.1. The values correspond to the slope of the line for the increasing and the decreasing part of the cycle separately. The cooling down part of the third cycle gives a measured rate of 0.09 meV/ K. This value is in good agreement with the expected broadening rate of 0.1 meV/ K reported earlier[28, 29] and expected from bulk gold measurements.

However the resonance damping rate is not the only parameter changing with temperature. Figure 5.4 shows that the resonance energy also shifts when changing the temperature of the immersion oil. The resonance goes from 1.869 eV at room temperature to 1.877 eV at 58 ^{o}C. More strikingly, when cooling down the resonance energy diminishes to 1.862 eV. The second cycle presents the same behavior but much less pronounced than during the first one. In the third cycle the resonance does not depend on temperature and is stable around 1.856 eV, indicating the the rods don't reshape significantly in our

Cycle	B_i(meV/K)	B_d(meV/K)	Particle	B_i(meV/K)	B_d(meV/K)
1	0.34	0.23	2	0.27	0.23
2	0.23	0.16	3	0.08	0.02
3	0.15	0.09			

Table 5.1: Summary of the results of the linear fittings for particles 1 (on the left). 2 and 3 (on the right). B_i and B_d are the results for the *i*ncreasing and *d*ecreasing part of the temperature cycles.

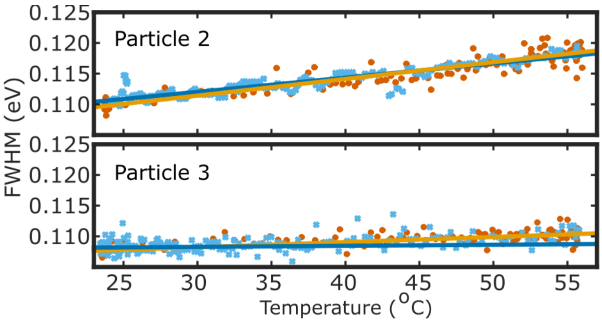

Figure 5.5: Plasmon width for two particles, going from room temperature to 60 ^{o}C (red circles) and cooling down afterwards (blue crosses). Both particles show a broadening of the plasmon proportional to temperature, but the rates are different.

conditions.

Normally plasmon shifts are related to changes in the refractive index of the medium surrounding the nanoparticles. This phenomenon is used, for instance, in photothermal imaging[39, 40] or in biosensors[14] as described in the introduction. The fact that in the first cycle there is a non-reversible plasmon shift suggests that either the medium or the surface of the particle (or both) changed in a permanent way after reaching higher temperatures. This can be due to a deterioration of the immersion oil, or to an adsorption/desorption of molecules from the particle's surface, effectively changing the refractive index in the surroundings of the nanorod. Discriminating these two mechanisms would require further studies that are out of the scope of this work.

Thermal reshaping of the nanoparticles can be ruled out since it would have induced a blue-shift of the resonance[41, 42], while we observe an overall red-shift. Moreover, the temperatures reached in this work are much lower than those needed for observing changes in shape of the nanorods. However, it is important to note that the plasmon broadening still occurs in the third temperature cycle when no resonance shift is observed. Therefore the broadening is not caused by changes in the medium but by intrinsic properties of the nanoparticles, as proposed in the introduction.

We performed the same experiment on two more particles. The measurements were carried on right after the third cycle of particle 1 in order to preserve the same experimental conditions and to avoid possible changes in the immersion oil as explained earlier. The surface plasmon resonance of both particles did not shift during their temperature cycles. This shows that the changes induced either on the surface of the particle or of the immersion oil at higher temperatures have a persistence of at least few hours.

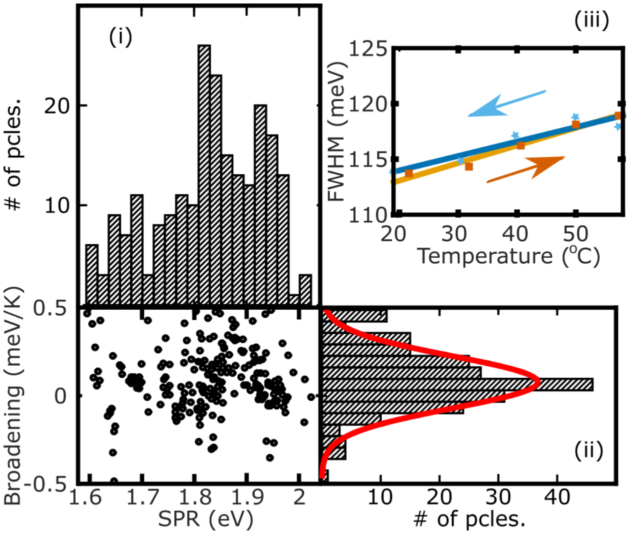

Figure 5.6: Plasmon broadening rate as a function of initial resonance position. Main panel shows the results for 220 different nanorods. Panel (i) is the histogram of the distribution of resonance energies found. Panel (ii) shows the distribution of broadening rates for all the particles and its fit by a gaussian as a solid red curve. Panel (iii) shows an example of the fitting for one particle; red squares correspond to increasing temperatures while blue crosses correspond to the decreasing.

The FWHM of the resonances of these two particles are shown in Figure 5.5. The slopes of every fit are summarized in table 5.1 on the right columns. Particle 2 shows a broadening rate higher than particle 1 while particle 3 shows a rate lower than expected. The heterogeneity in nanorod samples normally accounts for large variations in the observables. For instance quantum yield measurements[38] or the rate of chemical etching[43] of the surface of the particles show a broad distribution of values. To further investigate the differences between particles and to study if there is a relationship between the broadening rates and the plasmon resonance, we performed the same analysis on 220 different particles.

As described earlier, we acquired the scattering spectrum of several particles at different temperatures. The top right panel Figure 5.6 shows the result of the procedure for one of the particles as en example. The red squares show the FWHM of the plasmon resonance while increasing the temperature and the blue crosses correspond to the cooling down to room temperature. The linear fits have slopes of 0.14 meV/ K and 0.13 meV/ K respectively. Compared to the results shown in Figs. 5.3 and 5.5, spectra were not acquired continuously but after the temperature was stabilized at a certain value. At each temperature, spectra of several nanorods were acquired.

From the slopes of the linear fits of all the particles analyzed it is possible to construct the scatter plot of broadening rates and resonance energies for all the nanoparticles. This is shown in the bottom left panel of Figure 5.6. The particles analyzed had resonances varying from 1.6 eV to 2 eV, and the distribution of energies is shown in the top left histogram of Fig.5.6. The most frequent resonance is around 1.81 eV. The distribution of resonance energies is also an indication of the dispersion of shapes of the samples and is inherent to wet chemical synthesis methods.

The broadening rates of the 220 studied particles are summarized in the histogram at the bottom right in fig. 5.6. The gaussian fit of the distribution has the center at 0.08 meV/ K with a standard deviation of 0.3 meV/ K. This is in good agreement with the expected broadening rate of 0.1 meV/ K. The measurements were performed after some thermal cycles and no change in the plasmon resonance energy was observed while increasing or decreasing the temperature. This implies that the broadening rates differ from particle to particle because of inherent properties and not because of differences generated by the immersion oil used.

From Figure 5.6 it is possible to discard any significant dependence of the plasmon broadening rate on the plasmon's resonance position if this is kept below the interband transition energy. The model proposed in the introduction accounts for the broadening of the plasmon in terms of the electron-phonon coupling in gold and can account for the average behavior observed. It is important to note, however, that particles with resonances to the red normally have narrower plasmons[30]. Therefore the sensitivity of the broadening will be higher for particles with lower resonance energies.

The distribution of rates shown in Fig. 5.6 also includes particles that show a narrowing of the plasmon resonance while the temperature increases. Approximately 27% of the studied nanorods present a negative broadening rate. The model of electron-phonon coupling proposed in this work does not account for this phenomenon, nor for the different broadening rates for different particles. It is possible that the uncertainty in the determination of the plasmon width is responsible in part for this. The expected plasmon width change with a temperature increase of 40 K is of about 4 meV, or 4% of the FWHM of the resonance of the particles.

5.4. CONCLUSIONS

Measuring temperature at the nanoscale is challenging. Available techniques rely on spectral changes of fluorophores[44] or quantum dots[1, 9]. Here we show that scattering properties of gold nanoparticles can also be used as temperature sensors. One of the main advantages is that the scattering cross section of gold nanoparticles is on the order of $10^3\,\mathrm{nm}^2$, and therefore the powers needed for measuring the spectrum as well as the integration times can be low.

Electron-phonon coupling in gold is one of the parameters responsible for the broad plasmonic resonance of nanoparticles. This is also the only parameter that depends strongly on temperature and can be modeled with a simple linear relation for temperatures in the range that we studied, between 293 K and 350 K. It is therefore expected that the plasmon width depends linearly on temperature as was shown in this work.

Particles were studied in detail, acquiring continuously spectra while increasing and decreasing the immersion medium's temperature and showed a broadening of their resonances with various rates. The electron-phonon coupling model does not allow us to explain this behavior; however we have also observed that the resonance energy changes with temperature and a persistent red-shift is observed. This is attributed to changes in the refractive index of the medium surrounding the particles, either due to the immersion oil changing in a non reversible way or to some modification of the surface chemistry of the particles (for instance because of adsorption of molecules present in the oil). The plasmon shift however disappears after some thermal cycles, but the plasmon broadening remains.

In the situation when no resonance shift with increasing or decreasing temperature is observed, we have investigated the differences in the broadening rates from particle to particle. Spectra of more than 200 nanorods were studied, allowing us to discard a possible relationship of the rates with the resonance position. It was found that the broadening rates have a distribution centered around 0.08 meV/K, while the value expected from bulk measurements is 0.1 meV/K[33]. The standard deviation of the distribution of rates is 0.3 meV/K.

The model proposed in this work cannot account for the distribution of rates observed. However it has to be noted that when working with gold nanoparticles, the distribution of values of selected quantities can be of up to one order of magnitude. For example, quantum yield measurements[38], surface chemistry[43], plasmon induced reactions[45] are some of the examples of the high variability observed from particle to particle. This variability also makes single-particle studies important since many of the phenomena can be hidden in bulk measurements[34].

With the measured average broadening rate, reaching sensitivities of 1 K imply detecting changes in the plasmon width of 0.08 meV, less than 0.1% of the total width. The error in the fitting of the scattering spectrum is mainly given by the amount of light collected. Longer exposure times can lead to lower errors and therefore higher sensitivities. On the other hand, detecting several particles at the same time can lead to increasing the temperature sensitivity. Without any previous calibration, the broadening of the plasmon can be used at best to detect temperature changes, but not the absolute temperature of the sample.

REFERENCES

[1] J.-M. Yang, H. Yang, and L. Lin, *Quantum Dot Nano Thermometers Reveal Heterogeneous Local Thermogenesis in Living Cells,* ACS Nano **5**, 5067 (2011).

[2] X. Huang, P. K. Jain, I. H. El-Sayed, and M. A. El-Sayed, *Determination of the Minimum Temperature Required for Selective Photothermal Destruction of Cancer Cells with the Use of Immunotargeted Gold Nanoparticles,* Photochem. Photobiol. **82**, 412 (2006).

[3] L. R. Hirsch, R. J. Stafford, J. A. Bankson, S. R. Sershen, B. Rivera, R. E. Price, J. D. Hazle, N. J. Halas, and J. L. West, *Nanoshell-mediated near-infrared thermal therapy of tumors under magnetic resonance guidance.* Proc. Natl. Acad. Sci. U. S. A. **100**, 13549 (2003), arXiv:0008204 [cond-mat] .

[4] J. L. West and N. J. Halas, *Engineered nanomaterials for biophotonics applications: improving sensing, imaging, and therapeutics.* Annu. Rev. Biomed. Eng. **5**, 285 (2003).

[5] H. Ma, P. Tian, J. Pello, P. M. Bendix, and L. B. Oddershede, *Heat Generation by Irradiated Complex Composite Nanostructures.* Nano Lett. **14**, 612 (2014).

[6] X. Huang, P. K. Jain, I. H. El-Sayed, and M. A. El-Sayed, *Plasmonic photothermal therapy (PPTT) using gold nanoparticles,* Lasers Med. Sci. **23**, 217 (2008).

[7] D. Hone, P. Walker, and R. Evans-Gowing, *Generation of cytotoxic singlet oxygen via phthalocyanine-stabilized gold nanoparticles: A potential delivery vehicle for photodynamic therapy,* Langmuir , 2985 (2002).

[8] Y. Cheng, A. C. Samia, J. D. Meyers, I. Panagopoulos, B. Fei, and C. Burda, *Highly efficient drug delivery with gold nanoparticle vectors for in vivo photodynamic therapy of cancer,* J. Am. Chem. Soc. **130**, 10643 (2008).

[9] R. Tanimoto, T. Hiraiwa, Y. Nakai, Y. Shindo, K. Oka, N. Hiroi, and A. Funahashi, *Detection of Temperature Difference in Neuronal Cells.* Sci. Rep. **6**, 22071 (2016).

[10] J. S. Donner, S. a. Thompson, C. Alonso-Ortega, J. Morales, L. G. Rico, S. I. C. O. Santos, and R. Quidant, *Imaging of Plasmonic Heating in a Living Organism,* ACS Nano **7**, 8666 (2013).

[11] P. Ruijgrok, N. Verhart, P. Zijlstra, a. Tchebotareva, and M. Orrit, *Brownian Fluctuations and Heating of an Optically Aligned Gold Nanorod,* Phys. Rev. Lett. **107**, 1 (2011).

[12] J. Trojek, L. Chvátal, and P. Zemánek, *Optical alignment and confinement of an ellipsoidal nanorod in optical tweezers: a theoretical study.* J. Opt. Soc. Am. A. Opt. Image Sci. Vis. **29**, 1224 (2012).

[13] a. S. Urban, M. Fedoruk, M. R. Horton, J. O. Rädler, F. D. Stefani, and J. Feldmann, *Controlled nanometric phase transitions of phospholipid membranes by plasmonic heating of single gold nanoparticles.* Nano Lett. **9**, 2903 (2009).

[14] P. Zijlstra, P. M. R. Paulo, and M. Orrit, *Optical detection of single non-absorbing molecules using the surface plasmon resonance of a gold nanorod.* Nat. Nanotechnol. **7**, 379 (2012).

[15] M. A. Beuwer, M. W. J. Prins, and P. Zijlstra, *Stochastic protein interactions monitored by hundreds of single-molecule plasmonic biosensors,* Nano Lett. **15**, 3507 (2015).

[16] K. M. Spillane, J. Ortega-Arroyo, G. de Wit, C. Eggeling, H. Ewers, M. I. Wallace, and P. Kukura, *High-speed single-particle tracking of GM1 in model membranes reveals anomalous diffusion due to interleaflet coupling and molecular pinning.* Nano Lett. **14**, 5390 (2014).

[17] J. Conde, J. Rosa, J. M. de la Fuente, and P. V. Baptista, *Gold-nanobeacons for simultaneous gene specific silencing and intracellular tracking of the silencing events.* Biomaterials **34**, 2516 (2013).

[18] J. a. Schuller, E. S. Barnard, W. Cai, Y. C. Jun, J. S. White, and M. L. Brongersma, *Plasmonics for extreme light concentration and manipulation.* Nat. Mater. **9**, 193 (2010).

[19] C. Leduc, S. Si, J. Gautier, M. Soto-Ribeiro, B. Wehrle-Haller, A. Gautreau, G. Giannone, L. Cognet, and B. Lounis, *A highly specific gold nanoprobe for live-cell single-molecule imaging.* Nano Lett. **13**, 1489 (2013).

[20] K. R. Catchpole and A. Polman, *Plasmonic solar cells.* Opt. Express **16**, 21793 (2008).

[21] P. Zijlstra and M. Orrit, *Single metal nanoparticles: optical detection, spectroscopy and applications,* Reports Prog. Phys. **74**, 106401 (2011).

[22] M. Beversluis, A. Bouhelier, and L. Novotny, *Continuum generation from single gold nanostructures through near-field mediated intraband transitions,* Phys. Rev. B **68**, 1 (2003).

[23] M. B. Mohamed, V. Volkov, S. Link, and M. A. El-Sayed, *The 'lightning' gold nanorods: fluorescence enhancement of over a million compared to the gold metal,* Chem. Phys. Lett. **317**, 517 (2000).

[24] S. T. Sivapalan, B. M. Devetter, T. K. Yang, T. van Dijk, M. V. Schulmerich, P. S. Carney, R. Bhargava, and C. J. Murphy, *Off-resonance surface-enhanced Raman spectroscopy from gold nanorod suspensions as a function of aspect ratio: not what we thought.* ACS Nano **7**, 2099 (2013).

[25] H. Yuan, S. Khatua, P. Zijlstra, M. Yorulmaz, and M. Orrit, *Thousand-fold enhancement of single-molecule fluorescence near a single gold nanorod.* Angew. Chem. Int. Ed. Engl. **52**, 1217 (2013).

[26] S. Khatua, P. M. R. Paulo, H. Yuan, A. Gupta, P. Zijlstra, and M. Orrit, *Resonant plasmonic enhancement of single-molecule fluorescence by individual gold nanorods.* ACS Nano **8**, 4440 (2014).

[27] J. Prasad, I. Zins, R. Branscheid, J. Becker, A. H. R. Koch, G. Fytas, U. Kolb, and C. Sönnichsen, *Plasmonic Core-Satellite Assemblies as Highly Sensitive Refractive Index Sensors,* J. Phys. Chem. C **119**, 5577 (2015).

[28] M. Liu, M. Pelton, and P. Guyot-Sionnest, *Reduced damping of surface plasmons at low temperatures,* Phys. Rev. B **79**, 035418 (2009).

[29] A. Konrad, F. Wackenhut, M. Hussels, A. J. Meixner, and M. Brecht, *Temperature Dependent Luminescence and Dephasing of Gold Nanorods,* J. Phys. Chem. C **117**, 21476 (2013).

[30] C. Sönnichsen, T. Franzl, T. Wilk, G. von Plessen, J. Feldmann, O. Wilson, and P. Mulvaney, *Drastic Reduction of Plasmon Damping in Gold Nanorods,* Phys. Rev. Lett. **88**, 077402 (2002).

[31] C. Novo, D. Gomez, J. Perez-Juste, Z. Zhang, H. Petrova, M. Reismann, P. Mulvaney, and G. V. Hartland, *Contributions from radiation damping and surface scattering to the linewidth of the longitudinal plasmon band of gold nanorods: a single particle study,* Phys. Chem. Chem. Phys. **8**, 3540 (2006).

[32] M. Hu, C. Novo, A. Funston, H. Wang, H. Staleva, S. Zou, P. Mulvaney, Y. Xia, and G. V. Hartland, *Dark-field microscopy studies of single metal nanoparticles: understanding the factors that influence the linewidth of the localized surface plasmon resonance,* J. Mater. Chem. **18**, 1949 (2008).

[33] J. A. McKay and J. A. Rayne, *Temperature dependence of the infrared absorptivity of the noble metals,* Phys. Rev. B **13**, 673 (1976).

[34] S. Link and M. a. El-Sayed, *Size and Temperature Dependence of the Plasmon Absorption of Colloidal Gold Nanoparticles,* J. Phys. Chem. B **103**, 4212 (1999).

[35] C. Kittel, *Introduction to solid state physics* (Wiley, 1995).

[36] R. Sundararaman, P. Narang, A. S. Jermyn, W. a. Goddard III, and H. a. Atwater, *Theoretical predictions for hot-carrier generation from surface plasmon decay,* Nat. Commun. **5**, 5788 (2014).

[37] A. Manjavacas, J. G. Liu, V. Kulkarni, and P. Nordlander, *Plasmon-Induced Hot Carriers in Metallic Nanoparticles,* ACS Nano **8**, 7630 (2014).

[38] M. Yorulmaz, S. Khatua, P. Zijlstra, A. Gaiduk, and M. Orrit, *Luminescence quantum yield of single gold nanorods.* Nano Lett. **12**, 4385 (2012).

[39] S. Berciaud, D. Lasne, G. Blab, L. Cognet, and B. Lounis, *Photothermal heterodyne imaging of individual metallic nanoparticles: Theory versus experiment,* Phys. Rev. B **73**, 045424 (2006).

[40] A. Gaiduk, M. Yorulmaz, P. V. Ruijgrok, and M. Orrit, *Room-Temperature Detection of a Single Molecule's Absorption by Photothermal Contrast,* Science (80-.). **330**, 353 (2010).

[41] Y. Liu, E. N. Mills, and R. J. Composto, *Tuning optical properties of gold nanorods in polymer films through thermal reshaping,* J. Mater. Chem. **19**, 2704 (2009).

[42] Y. Horiguchi, K. Honda, Y. Kato, N. Nakashima, and Y. Niidome, *Photothermal reshaping of gold nanorods depends on the passivating layers of the nanorod surfaces,* Langmuir **24**, 12026 (2008).

[43] A. Carattino, S. Khatua, and M. Orrit, *In situ tuning of gold nanorod plasmon through oxidative cyanide etching,* Phys. Chem. Chem. Phys. **18**, 15619 (2016).

[44] C. F. Chapman, Y. Liu, G. J. Sonek, and B. J. Tromberg, *THE USE OF EXOGENOUS FLUORESCENT PROBES FOR TEMPERATURE MEASUREMENTS IN SINGLE LIVING CELLS,* Photochem. Photobiol. **62**, 416 (1995).

[45] L. Osinkina, S. Carretero-Palacios, J. Stehr, A. a. Lutich, F. Jäckel, and J. Feldmann, *Tuning DNA Binding Kinetics in an Optical Trap by Plasmonic Nanoparticle Heating.* Nano Lett. , 1 (2013).

6

CONCLUSIONS & OUTLOOK

6.1. GENERAL CONCLUSIONS

THIS thesis is a collection of heterogeneous results that range from etching of single gold nanorods to studying their anti-Stokes luminescence. Gold nanoparticles have been in the spotlight for almost two decades because of their optical properties[1]. They are ideal candidates for labelling[2] applications and also as biosensors[3]. Many properties of the nanoparticles have been already characterized but there is still a large number of them that needs to be addressed; this thesis provides several illustrations of this need.

Wet chemical synthesis of nanorods yields a high degree of heterogeneity between individual particles[4]. This was already observed in our group when measuring the quantum yield (QY) of particles with different aspect ratios[5]. The values differ by almost one order of magnitude between particles that, up to experimental accuracy, should have been identical. In every chapter of this thesis single-particle results have always been complemented with statistics.

Chapter 2 shows that the mean behavior of single particles is different from what is observed in bulk suspension. Chapters 3 and 4 focus on the anti-Stokes luminescence, a phenomenon greatly overlooked in the past decade. Chapter 5 on plasmon width is again an example of the heterogeneity observed at single-particle level. Experiments similar to these need proper statistics to be complete.

The four chapters of this thesis are but a proof that there is still room for investigation at single-particle level. Many intriguing phenomena can still be left to discover.

6.2. OUTLOOK

Every chapter includes a conclusion regarding the content of the chapter itself. This section on the other hand aims at pointing out what are the different possibilities that every chapter opens for future research.

6.2.1. CYANIDE ETCHING

Chapter 2 shows that is possible to change the shape of gold nanoparticles once immobilized on a glass coverslip. We employed cyanide etching because of its well understood chemistry with gold but the methodology is not limited to it; other reactions are possible alternatives. Moreover we have shown that it is possible to monitor the changes of shape by studying the evolution of the plasmon resonance and therefore the experiments can be performed under an optical microscope.

Other works have focused into the possibility of using the plasmon resonance shift as a detector of minute concentrations of cyanide[6]. At a single particle level we can easily detect μM concentrations and nM should be reachable without changes to the setup. Lowering the concentrations keeping reasonable measurement times reduces to improving the detection of the plasmon shift. However gold nanoparticles are completely etched away after being exposed to cyanide ions for enough time. This would make samples non reusable.

Another interesting opportunity is the ability to change the spacing between particles with sub nanometer accuracy[7]. Gold nanorods are becoming promising nano antennas, and dimers of particles have a much stronger near field. However, controlling the spacing between particles is a major challenge. The results shown in chapter 2 can be extended to dimers, where slow etching of the surface of the particles can be used for tuning the distance between them.

6.2.2. BACKGROUND SUPPRESSION

Chapter 3 shows that it is possible to image gold nanorods in high background conditions by detecting their anti-Stokes emission. The chapter focuses into imaging under living cells but the technique is not limited to biological applications. High background conditions can include working with fluorescent molecules in solution, for example to study enhanced FCS[8]. Background suppression is not the only advantage of anti-Stokes imaging.

A common problem in colocalization studies is the correction for chromatic aberrations and misalignment of different beams. If one desires to colocalize a gold nanorod and a fluorescent dye with absorption in the same spectral region, the anti-Stokes emission provides a way to achieve it with only one excitation laser and one detection path. Employing a single laser beam rules out the possibility of a misalignment of the excitation path; the detection of both channels (anti-Stokes for the rods and Stokes for the dye) can be concentrated over a short spectral range, thus minimizing chromatic aberrations.

Colocalizing gold nanorods and fluorescently labelled proteins can give insight into the different processes that mediate the uptake of gold nanorods[2]. It can also be useful for characterizing the targeting of proteins in living cells. A gold nanorod can be functionalized to bind to specific proteins[9]; the binding efficiency and specificity, however, are difficult to determine *in vivo* if there is a high background signal.

Anti-Stokes detection is not limited to imaging. If used as labels, nanorods can be used for tracking[10] specific proteins for extended periods of time. In living cells, regulatory mechanisms depend on free diffusion and active transport[11]. Tracking of functionalized single nanoparticles can provide important insight into mechanisms that are active over different timescales[12].

6.2.3. TEMPERATURE SENSING WITH ANTI-STOKES LUMINESCENCE

Chapter 4 shows that anti-Stokes luminescence from single nanoparticles can be used for nano-thermometry. This novel result opens many possibilities in the fields of photothermal therapy[13] and nano fabrication[14]. For over 20 years gold nanoparticles have been studied as possible candidates for treating cancer[15]. A large community is focused into using nanoparticles to locally increase the temperature of malignant cells, preserving the healthy ones.

After decades of research, however, there is little insight into the temperature that the nanoparticles have to reach to induce cellular death[16]. The conclusions of chapter 4 clearly show that the technique developed is ready to be implemented in biologically relevant conditions. Being able to actively control and monitor the temperature of nanoparticles in or around cells has never been done before and can yield important answers to the mechanisms that induce cell death.

Moreover the method described in chapter 4 can be used to measure the temperature of nanoparticles in various situations. For instance the characterization of optically trapped nanoparticles normally relies on assumptions of the temperature[17]. Nano bubble generation[18], polymerization at the nanoscale[19], controlled chemical reactions[20], photothermal detection[21] are some of the fields where actually measuring the temperature of the nanoparticles instead of estimating it can provide insight into new phenomena.

An important task for future work should be to characterize different particle geometries. Gold shells[22], bipyramids[23], even spheres of different diameters can be better suited for temperature sensing. Different plasmon resonances and different quantum yields can make other particles better anti-Stokes emitters.

Acquiring spectra as was done in chapter 4 is a slow process; it can take several minutes to obtain a proper signal-to-noise ratio. There is a possibility to shorten the acquisition times by studying the ratio of anti-Stokes to Stokes emission[24]. In principle the Stokes emission is constant with temperature and depends only on the laser power; the anti-Stokes however will be brighter for higher temperatures. Already in figure 4.2 it is possible to observe that the ratio of both types of emission can be easily reproduced by numerical calculations. Preliminary calculations show that the ratio of anti-Stokes to Stokes changes with temperatures, but experimental data is missing.

6.2.4. PLASMON DAMPING

Chapter 5 shows the relation between the plasmon damping rate and the temperature of the medium surrounding the nanoparticles. The main idea of the chapter was to explore the possibility of using the broadening of the plasmon resonance as an alternative thermometry strategy. Anti-Stokes luminescence has the advantage of not needing a calibration, but the higher laser powers employed induce a temperature rise that can be much higher than the temperature to be detected.

Chapter 5 shows that, on average, the linear relationship between the plasmon full width at half maximum and temperature agrees with the expected value from bulk gold. However there is a big heterogeneity between nanoparticles, not all of them have the same broadening rate. This explains why the broadening was not observed in bulk suspension and also sets a limit to the applicability of this method for temperature measurements.

Since every nanoparticle behaves in slightly a different way when increasing temperature, one needs to build proper statistics to determine how much the temperature of the sample increased or decreased. The statistics can be built either by studying several individual nanoparticles, as was done in this thesis, or by placing a bigger number of particles in the focal spot, as done with quantum dots[25]. The heterogeneity, however, can pose a limit to the applicability of the method. It is possible that other geometries such as bipyramids exhibit a more homogeneous behavior.

REFERENCES

[1] P. Zijlstra and M. Orrit, *Single metal nanoparticles: optical detection, spectroscopy and applications,* Reports Prog. Phys. **74**, 106401 (2011).

[2] C. Leduc, S. Si, J. Gautier, M. Soto-Ribeiro, B. Wehrle-Haller, A. Gautreau, G. Giannone, L. Cognet, and B. Lounis, *A highly specific gold nanoprobe for live-cell single-molecule imaging.* Nano Lett. **13**, 1489 (2013).

[3] P. Zijlstra, P. M. R. Paulo, and M. Orrit, *Optical detection of single non-absorbing molecules using the surface plasmon resonance of a gold nanorod.* Nat. Nanotechnol. **7**, 379 (2012).

[4] Y.-J. Lee, N. B. Schade, L. Sun, J. a. Fan, D. R. Bae, M. M. Mariscal, G. Lee, F. Capasso, S. Sacanna, V. N. Manoharan, and G.-R. Yi, *Ultrasmooth, highly spherical monocrystalline gold particles for precision plasmonics.* ACS Nano **7**, 11064 (2013).

[5] M. Yorulmaz, S. Khatua, P. Zijlstra, A. Gaiduk, and M. Orrit, *Luminescence quantum yield of single gold nanorods.* Nano Lett. **12**, 4385 (2012).

[6] S.-C. Wei, P.-H. Hsu, Y.-F. Lee, Y.-W. Lin, and C.-C. Huang, *Selective detection of iodide and cyanide anions using gold-nanoparticle-based fluorescent probes.* ACS Appl. Mater. Interfaces **4**, 2652 (2012).

[7] A. M. Funston, C. Novo, T. J. Davis, and P. Mulvaney, *Plasmon coupling of gold nanorods at short distances and in different geometries,* Nano Lett. **9**, 1651 (2009).

[8] L. Langguth and a. Femius Koenderink, *Simple model for plasmon enhanced fluorescence correlation spectroscopy,* Opt. Express **22**, 15397 (2014).

[9] K. Li, X. Zhao, B. K Hammer, S. Du, and Y. Chen, *Nanoparticles Inhibit DNA Replication by Binding to DNA: Modeling and Experimental Validation.* ACS Nano (2013), 10.1021/nn402472k.

[10] K. M. Spillane, J. Ortega-Arroyo, G. de Wit, C. Eggeling, H. Ewers, M. I. Wallace, and P. Kukura, *High-speed single-particle tracking of GM1 in model membranes reveals anomalous diffusion due to interleaflet coupling and molecular pinning.* Nano Lett. **14**, 5390 (2014).

[11] E. C. M. Nowack and A. R. Grossman, *Trafficking of protein into the recently established photosynthetic organelles of Paulinella chromatophora,* Proc. Natl. Acad. Sci. **109**, 5340 (2012).

[12] J. Conde, J. Rosa, J. M. de la Fuente, and P. V. Baptista, *Gold-nanobeacons for simultaneous gene specific silencing and intracellular tracking of the silencing events.* Biomaterials **34**, 2516 (2013).

[13] L. R. Hirsch, R. J. Stafford, J. A. Bankson, S. R. Sershen, B. Rivera, R. E. Price, J. D. Hazle, N. J. Halas, and J. L. West, *Nanoshell-mediated near-infrared thermal therapy of tumors under magnetic resonance guidance.* Proc. Natl. Acad. Sci. U. S. A. **100**, 13549 (2003), arXiv:0008204 [cond-mat] .

[14] M. Fedoruk, M. Meixner, S. Carretero-Palacios, T. Lohmüller, and J. Feldmann, *Nanolithography by Plasmonic Heating and Optical Manipulation of Gold Nanoparticles,* ACS Nano **7**, 7648 (2013).

[15] D. O'Neal, L. R. Hirsch, N. J. Halas, J. Payne, and J. L. West, *Photo-thermal tumor ablation in mice using near infrared-absorbing nanoparticles,* Cancer Lett. **209**, 171 (2004).

[16] X. Huang, P. K. Jain, I. H. El-Sayed, and M. A. El-Sayed, *Determination of the Minimum Temperature Required for Selective Photothermal Destruction of Cancer Cells with the Use of Immunotargeted Gold Nanoparticles,* Photochem. Photobiol. **82**, 412 (2006).

[17] P. Ruijgrok, N. Verhart, P. Zijlstra, a. Tchebotareva, and M. Orrit, *Brownian Fluctuations and Heating of an Optically Aligned Gold Nanorod,* Phys. Rev. Lett. **107**, 1 (2011).

[18] L. Hou, M. Yorulmaz, N. R. Verhart, and M. Orrit, *Explosive formation and dynamics of vapor nanobubbles around a continuously heated gold nanosphere,* New J. Phys. **17**, 13050 (2015).

[19] H. Ma, P. Tian, J. Pello, P. M. Bendix, and L. B. Oddershede, *Heat Generation by Irradiated Complex Composite Nanostructures.* Nano Lett. **14**, 612 (2014).

[20] a. S. Urban, M. Fedoruk, M. R. Horton, J. O. Rädler, F. D. Stefani, and J. Feldmann, *Controlled nanometric phase transitions of phospholipid membranes by plasmonic heating of single gold nanoparticles.* Nano Lett. **9**, 2903 (2009).

[21] D. Boyer, P. Tamarat, A. Maali, B. Lounis, and M. Orrit, *Photothermal Imagin of Nanometer-Sized Metal Particles Among Scatterers,* Science (80-.). **297**, 1160 (2002).

[22] A. M. Gobin, M. H. Lee, N. J. Halas, W. D. James, R. A. Drezek, J. L. West, M. Gobin, M. H. Lee, N. J. Halas, W. D. James, R. A. Drezek, and J. L. West, *Near-Infrared Resonant Nanoshells for Combined Optical Imaging and Photothermal Cancer Therapy,* Nano Lett. **7**, 1929 (2007).

[23] W. Rao, Q. Li, Y. Wang, T. Li, and L. Wu, *Comparison of Photoluminescence Quantum Yield of Single Gold Nanobipyramids and Gold Nanorods,* ACS Nano **9**, 2783 (2015).

[24] E. A. Pozzi, A. B. Zrimsek, C. M. Lethiec, G. C. Schatz, M. C. Hersam, and R. P. Van Duyne, *Evaluating Single-Molecule Stokes and Anti-Stokes SERS for Nanoscale Thermometry,* J. Phys. Chem. C **119**, 21116 (2015).

[25] S. Li, K. Zhang, J.-M. Yang, L. Lin, and H. Yang, *Single Quantum Dots as Local Temperature Markers,* Nano Lett. **7**, 3102 (2007).

A

SUPPLEMENTARY INFORMATION FOR: *In situ* TUNING OF GOLD NANOROD PLASMON THROUGH OXIDATIVE CYANIDE ETCHING

A.1. SOLUTION RESULTS

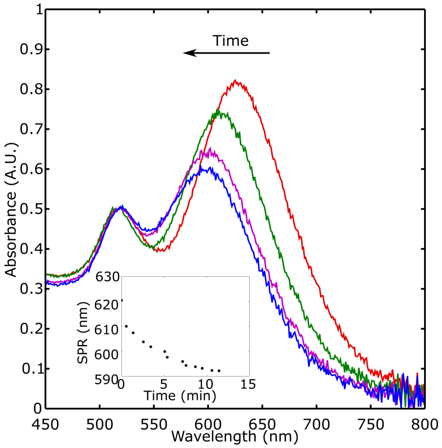

Figure A.1: Extinction spectra of a bulk suspension of gold nanorods dispersed in 100 μM KCN. The curves are displayed at 2 minutes intervals. The inset shows the peak position as a function of time. The curves were normalized to the transverse peak for clarity.

Figure SA.1 shows the behavior of nanorods dispersed in 100 μM KCN. The same sample than for the single-particle experiments was used. We observe a clear blue shift of the longitudinal plasmon resonance, towards the transverse peak at around 530 nm. As stated in the main text, we attribute the blue shift of the peak to a shortening of the long axis of the rods. This is because the CTAB is more efficient in protecting the sides than the tips of the particles. The blue shift does not seem stabilized for the last spectrum. We attribute this to a complete consumption of KCN by excess gold metal in our sample. If more KCN had been added, the blue-shift would probably have continued.

The spectra were acquired in an UV-Vis spectrometer. The first spectrum was acquired with the rods dispersed in water, before adding KCN into the cuvette. Later a solution such that the final concentration was 100 μM was added and a set of automatic spectra was recorded at a fixed interval of time. The peak position was extracted by fitting a double Lorentzian, one with a fixed central wavelength (the transverse resonance) and a second one for the longitudinal plasmon.

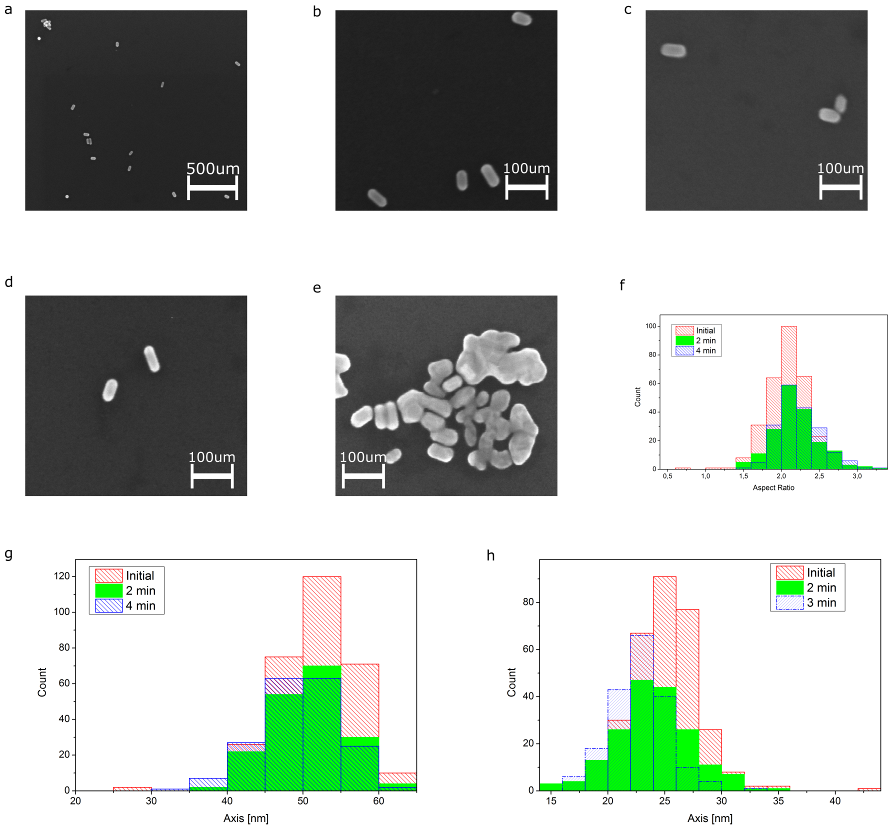

Figure A.2: SEM images of the rods a-b) after synthesis, at different magnifications c) after 2 minutes in 20 μM KCN. d) after 4 minutes in KCN and e) when they were forming clusters. f-h) Histograms of the aspect ratio (f), longitudinal(g) and transverse axis(h) before, after 2 and after 4 minutes in KCN. The distribution of values is too broad to visualize a shift in aspect ratio. Statistics on the values, however, show a slight increase and the data is summarized in table 1.

A.2. SEM IMAGES

Samples for SEM images were prepared by drop casting a suspension of gold nanorods into clean silicon wafers. An initial image of several hundreds of rods was acquired before any etching. The same samples were placed in a solution of KCN for 2 minutes and imaged again. Finally they were submersed again for 2 minutes in KCN and imaged afterwards. In this way, even if it was not possible to track the same particles during the etching process, it was possible to reproduce the conditions in which the reshaping took place on the optical microscope.

Figure SA.2 shows the SEM images of the rods. In SA.2a,b an example of the rods after synthesis and before etching at two different magnificatins. Figures SA.2c and d show the rods after 2 minutes and 4 minutes in 20 μM KCN. Figure SA.2e was acquired after 4 minutes in KCN; the difference on the shape of the particles when they are in contact is notable. It has to be reminded however that the clusters of rods were already formed on the substrate before the etching started. Drop casting a suspension of rods tends to form conglomerates of particles rather than isolated particles as can be easily achieved by spin casting and shown in the optical experiments in the main text.

Histograms in Figures SA.2f-h show the analysis of the aspect ratio, the longitudinal and the transverse axes respectively for each of the cases. Table 1 summarizes the average values found after analyzing approximately 300 particles. The shift is rather small as compared to the standard deviation of the distribution of sizes.

	L (nm)	Sdv (nm)	D (nm)	Sdv (nm)
0min	51	5	24	3
2min	50	5	23	3
4min	49	5	22	2

Table A.1: Summary of the results obtained for 300 different particles while imaging them with an SEM. L and D are the length and diameter respectively. Sdv is the standard deviation of the values

A.3. BACKGROUND SPECTRUM

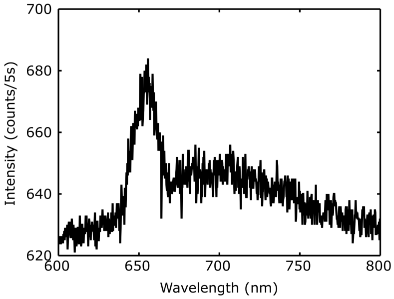

Figure A.3: Spectra from the background while exciting with a 532 nm laser. The peak appearing at 650 nm is attributed to Raman scattering from the O-H stretching modes of water.

Figure SA.3 shows the typical background when exciting with a 532 nm laser. The peak at 650 nm is attributed to Raman scattering from water. Normally this background can be well subtracted from the spectra acquired on particles. For less intense curves however, it is possible to observe a shoulder appearing at this particular wavelength. This indicates a non-additive phenomenon that we attributed to enhanced Raman scattering close to the nanoparticles.

B

SUPPLEMENTARY INFORMATION FOR: BACKGROUND SUPPRESSION IN IMAGING GOLD NANORODS THROUGH DETECTION OF ANTI-STOKES EMISSION

B.1. SETUP

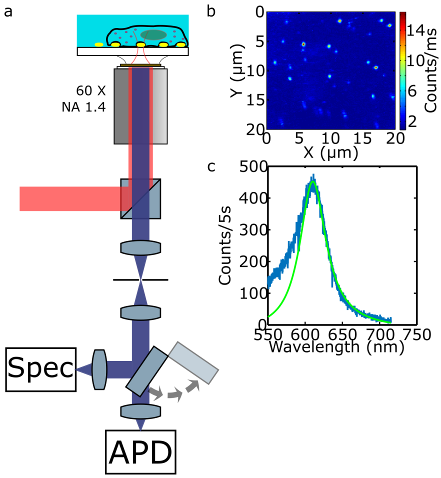

Figure B.1: Experimental setup and examples of observations. a) Simplified schematic of the confocal microscope employed during the measurements. b) A typical 1-photon luminescence raster scan of the sample immersed in water c) luminescence spectrum of a single rod.

Figure B.1 shows the schematic of the confocal microscope employed in the experiments. It is important to note the presence of a 50/50 beamsplitter before the objective. Exchanging it for an appropriate dichroic mirror would increase the collection efficiency. In this work we chose not to do it because the beamsplitter allows to collect both the full emission under 532 nm excitation and the Stokes/anti-Stokes emission under 633 nm without changes in the optical path.

B.2. UV-VIS SPECTRUM

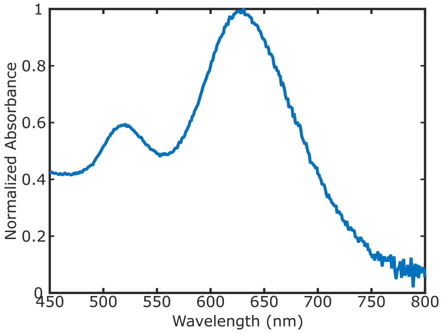

Figure B.2: Normalized extinction spectrum of a suspension of nanorods after synthesis. The resonance maximum is located at 630 nm.

Figure B.2 shows the extinction spectrum of the nanorod samples used throughout this work. Two peaks are clearly distinguishable, one around 630 nm that corresponds to the longitudinal plasmon resonance (LPR) of particles with sizes 50 nm × 23 nm and a second one at around 520 nm. This peak also includes contributions of spheres as by-products of the synthesis of the rods. The transverse plasmon resonance is also located at the same wavelength but is much weaker than the LPR. In a sample consisting exclusively of rods, the transverse resonance would be barely observable in a UV-Vis spectrometer.

B.3. FILTERS

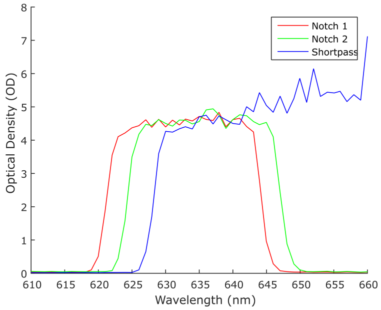

Figure B.3: Transmission spectrum of two notch filters and a short pass filter (Semrock).

The selection of filters plays a crucial role in the signal acquired. Since the main part of the anti-Stokes emission is concentrated around the excitation wavelength, it is important to select filters that have a high transmission close to the laser line. Figure B.3 shows the normalized absorption spectrum of two notch filters and a short pass. Both notch filters are branded as NF03 – 633E – 25 but show a slightly different absorption spectrum, shifted roughly 4 nm from each other. The shortpass filter (branded as SP01 – 633RU – 25) shows the transition to transmission even closer to the laser line.

For many fluorescence applications the exact shape of the transmission spectrum of the filters does not play a crucial role. However for anti-Stokes imaging, since the shape of the emission is exponential-like, minute changes in the transmission spectrum can have a great impact on the signal collected. For example, changing from a detection path with a spectrum like notch 1 to one like shortpass (i.e. shifting in about 7 nm the edge of the filter) increases the collected number of photons by about 50%.

In this work, since only one filter does not provide enough attenuation, care was taken to always employ the notch with the most favorable transmission spectrum in combination with either a shortpass or a longpass filter. Ideally, two shortpass filters would have been the best solution.

B.4. TEM IMAGES OF RODS

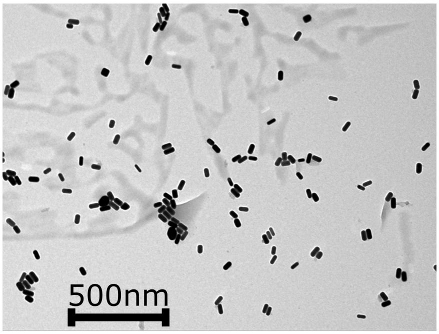

Figure B.4: TEM image of the nanorod sample. The scale bar is 500 μm.

Figure B.4 shows an example TEM image of the gold nanorod sample. Analysis on the dimensions of the particles yield an average length of 50 nm and diameter of 23 nm. This is consistent with the plasmon observed in fig. B.2 and at a single-particle level as in fig. B.1c.

B.5. WHITE LIGHT TRANSMISSION

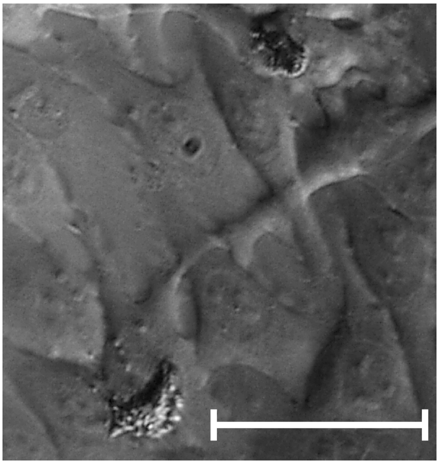

Figure B.5: White light transmission image of the sample with cells deposited on top of the rods. It is possible to observe that they cover entirely the observed region without spacing in between them. The scale bar in the figure is 20 μm in length.

B.6. FULL SCAN WITHOUT DYE

The raster scan shown in Figure B.6 corresponds to a larger area comprising the same region shown in the main text. The majority of the particles has a much larger contrast in

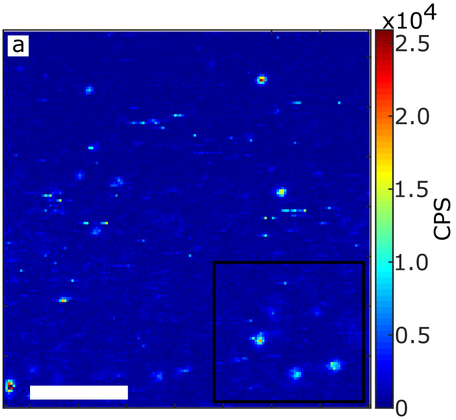

Figure B.6: Raster scan of a nanorod sample under HeLa cells using (a) a long pass filter and (b) a short pass filter for photoluminescence detection. Both scans contain the same region shown in the main text and here marked with a black square. The scale bar in both figures is 4 μm in length.

the anti-Stokes. Moreover it can be noted that the background is flat. In the Stokes image the nanorods are still visible, but the contrast is obviously lower.

B.7. FULL SCAN WITHOUT DYE

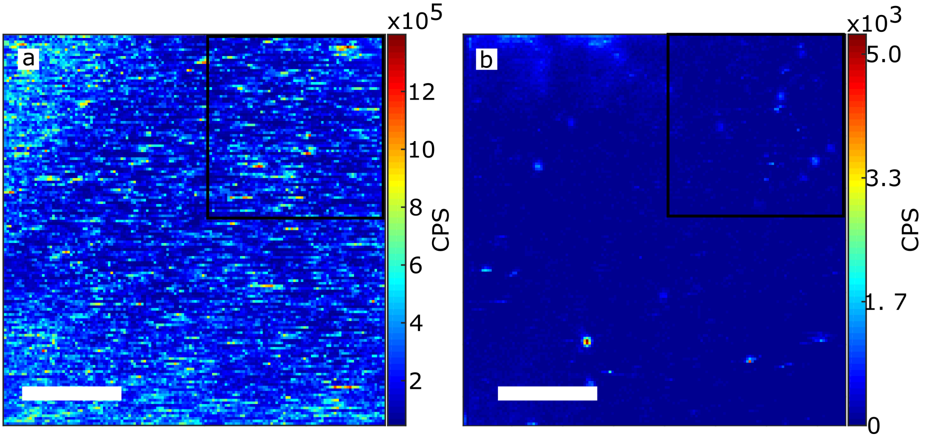

Figure B.7: Raster scan of a nanorod sample under stained HeLa cells using (a) a long pass filter and (b) a short pass filter for photoluminescence detection. Both scans contain the same region shown in the main text and here marked with a black square. The scale bar in both figures is 4 μm in length.

Figure B.7 shows a raster scan of gold nanorods under cells stained with ATTO 647N. Both images comprise the same region shown in the main text, here marked with a black square. No particles can be detected in the Stokes image, while several nanorods are visible in the anti-Stokes image with a high signal-to-background. We note, however, that there is some background appearing in the top left part of the anti-Stokes image. This may be due to an increase of the concentration of ATTO 647N. The incubation procedure does not prevent the accumulation of dye in specific organelles of the cells, and there is no control on the final dye concentration.

B.8. SIGNAL-TO-BACKGROUND OF SEVERAL PARTICLES

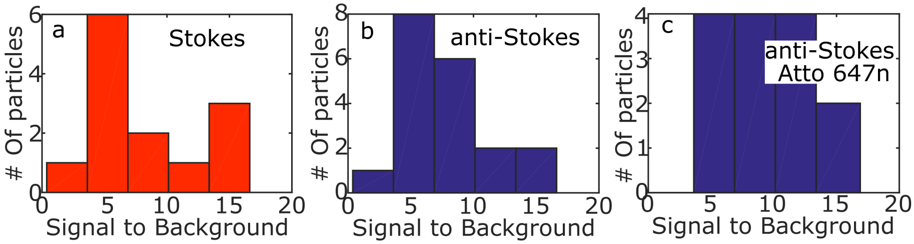

Figure B.8: Histograms of the signal-to-background of several particles irradiated at 30 kW/cm^2. a) Stokes emission under unstained cells, b) same but anti-Stokes emission, c) anti-Stokes under cells stained with ATTO 647N.

Figure B.8 shows the distribution of signal-to-background ratios for several particles. The data were acquired with an irradiation intensity of 30 kW/cm^2. Fig. B.8a shows the distribution for nanoparticles under unstained cells. It is possible to observe a broad distribution of values between ratios of 5 and 15. Fig. B.8b shows the signal-to-background distribution for the anti-Stokes emission, concentrated mainly between 5 and 10. Finally Figure B.8c shows the anti-Stokes signal-to-background ratio of particles under cells stained with ATTO 647N. In this case it is possible to observe a similar distribution of values. Stokes data under stained cells are not presented because it was impossible to detect single nanoparticles under those conditions.

B.9. VIABILITY TEST

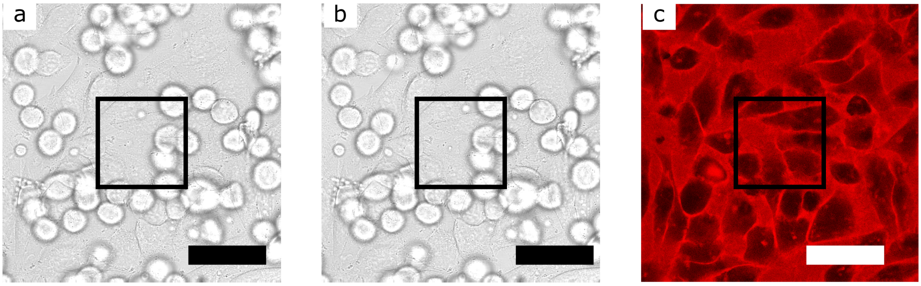

Figure B.9: White light transmission image of the cells, a) before being irradiated with the 633 nm laser, b) after the imaging process and c) viability test. The black square represents the imaged area. The scale bar is 50 μm.

To support the claim of the harmlessness of the method proposed in this work, we performed a standard viability test of the cells after imaging. Figure B.9 shows white light transmission images of the cells. The left figure is before the imaging of the nanorods, the central is after and the rightmost is the result of a viability test with trypan blue. The black square represents the area that was imaged with the confocal microscope. The cells show no change between before and after the procedure. Moreover in Fig. B.9c it is possible to see that the dye did not enter the cells, therefore their membrane was intact after the imaging process.

More rigorous tests of viability after imaging the nanorods inside the cells are needed, but they are outside the scope of this work. On one hand there is enough evidence showing that gold nanoparticles are not toxic for cells[1, 2]. On the other hand two photon imaging[3] or photothermal heterodyne detection[4] of particles inside cells did not destroy them. Continuous wave confocal imaging as presented here however was not studied in detail in the past mainly because of the poor signal-to-background ratio with the normal Stokes configuration.

REFERENCES

[1] T. B. Huff, M. N. Hansen, Y. Zhao, J.-x. Cheng, and A. Wei, *Controlling the Cellular Uptake of Gold Nanorods,* Langmuir **23**, 1596 (2007).

[2] N. Lewinski, V. Colvin, and R. Drezek, *Cytotoxicity of nanopartides,* Small **4**, 26 (2008).

[3] B. van den Broek, B. Ashcroft, T. H. Oosterkamp, and J. van Noort, *Parallel Nanometric 3D Tracking of Intracellular Gold Nanorods Using Multifocal Two-Photon Microscopy,* Nano Lett. **13**, 980 (2013).

[4] C. Leduc, S. Si, J. Gautier, M. Soto-Ribeiro, B. Wehrle-Haller, A. Gautreau, G. Giannone, L. Cognet, and B. Lounis, *A highly specific gold nanoprobe for live-cell single-molecule imaging.* Nano Lett. **13**, 1489 (2013).

C

SUPPLEMENTARY INFORMATION FOR: GOLD NANORODS AS NANO-THERMOMETERS

C.1. COMPARING COMSOL AND A SIMPLE APPROXIMATION FOR TEMPERATURE CALCULATION

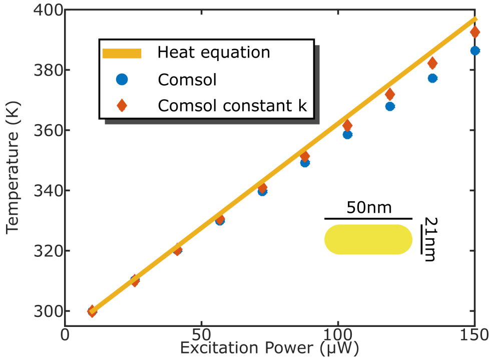

Figure C.1: Calculated temperature for a 21 nm × 50 nm nanorod under different excitation intensities. The full line is the result of the simple model while the dots are the calculated values using Comsol. The circles are with the default heat conductivity and the diamonds are with a constant value.

Throughout the main text the temperature measured with the anti-Stokes emission is compared to the calculated temperature using a simple heat diffusion equation. For spheres, assuming a thermal conductivity much higher than the surrounding medium, the temperature increase is given by

$$\Delta \mathrm{T}(P) = \frac{P}{4\pi k_{\mathrm{water}} R} \tag{C.1}$$

where P is the dissipated power, k_{water} is the heat conductivity of water and R is the radius of the particle. The dissipated power can be easily derived from the cross section of the particle at a given wavelength and the intensity of the focused laser beam. For nanorods we assumed an equivalent radius such that the total area is preserved.

Figure C.1 shows the difference between the results from the equation (full line) and a finite element method calculation using Comsol (dots) for a nanorod of length 50 nm and diameter 21 nm. The cross section and dissipated power were kept the same. The blue circles are the results given by using the built-in material properties of water, i.e. a thermal conductivity that depends on temperature. The diamonds are the results when the thermal conductivity is fixed to $0.61\,\mathrm{W}(\mathrm{m}\cdot\mathrm{K})^{-1}$. The difference is accentuated at higher temperatures.

C.2. LUMINESCENCE POWER DEPENDENCE

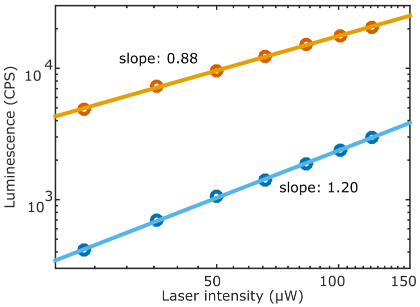

Figure C.2: Stokes and anti-Stokes emission as functions of excitation power. The linear fit in logarithmic scale has a slope of 0.88 and 1.20 respectively, confirming the 1-photon nature of both kinds of emission.

Figure C.2 shows the power dependence of both the Stokes and anti-Stokes luminescence. The fit in logarithmic scale confirms that both processes are due to one-photon absorption.

SUMMARY

Gold nanorods are ideal candidates for complementing fluorophores in labelling applications. The presence of the surface plasmon resonance generates large absorption and scattering cross sections, thus making the detection of single nanoparticles possible under a light microscope. The plasmon of gold nanorods depends on the ratio between their width and length and covers the range between 540 nm for spheres and even above 800 nm for elongated particles, thus almost the entire visible and near-infrared spectrum. The surface plasmon presents great opportunities in (bio-)sensing, enhanced spectroscopies, photothermal therapy and for concentrating light below the diffraction limit.

Chapter 1 of this thesis is a brief overview on fluorescence microscopy and on the basic properties of gold nanoparticles. Microscopy and specifically fluorescence microscopy is the result of a long process of technical improvements in optics and light sources, but also of the labels used to prepare the samples. From simpler molecules to genetically encoded proteins, the wealth of resources available nowadays is remarkable. In this context, gold nanoparticles can find their way because of their stability over time.

The resonance wavelength (or energy) of metallic nanoparticles will be given by their geometry and by the surrounding medium's properties, such as its refractive index. The geometry of the particles is determined during the synthesis procedure, where the average length and width can be tuned. Once the particles are deposited on a substrate, their resonance is already determined. It is possible, however, to induce shape modification to the particles through chemical means.

Previous works have focused on bulk measurements in suspension. In this case, the tips of the particles tend to be more reactive because they are less protected by the surfactants that prevent aggregation of particles. This leads to an anisotropic reaction that slowly transforms elongated particles into spheres and that softens sharp edges or tips, yielding an overall blue-shift of the resonance.

Chapter 2 shows that through well known chemistry between gold and cyanide ions it is possible to induce a red-shift of the plasmon. This is modelled through an isotropic etching of the particles, and a good agreement between calculations and experiments is obtained. The main difference with previous work is the absence of a capping agent on the particles' surface. Controllably changing the shape of nanoparticles is of great importance for experiments where a specific resonance is needed.

When particles are excited by a monochromatic light source, such as a laser, they will emit light at different wavelengths than the excitation wavelength. This emission is generally referred to as luminescence and is commonly used for imaging and tracking nanoparticles under confocal microscopes. When the excitation wavelength coincides with the plasmon resonance, the emission will happen not only at longer wavelengths, i.e. lower energies, but also at shorter wavelengths. This emission is called anti-Stokes emission and possesses intriguing properties.

Chapter 3 shows that it is possible to image gold nanorods in biologically relevant conditions through detection of their anti-Stokes emission. By placing a short-pass filter in the detection path the background level is reduced significantly, while the luminescence signal from the particles remains high. This is valid even for cells stained with a dye with high quantum yield that absorbs light of the same wavelengths as the rods. In these conditions it is not possible to observe any single nanoparticle through conventional Stokes-shifted emission while the anti-Stokes scheme presents a signal-to-background ratio higher than 10.

The technique presented in chapter 3 can be readily implemented in any conventional microscope by the addition of the appropriate filters. It does not require any special operation nor infrastructure. Moreover any data analysis tool for tracking, imaging, centroid extraction, etc. of single labels can readily be implemented without further modifications. The results of chapter 3 can have a major impact in the way nanoparticles are imaged and detected in biological conditions.

During the past two decades there has been an increasing interest in gold nanoparticles as possible agents for medical treatments. The strong interaction between particles and light makes them ideal candidates not only for labelling but also for releasing heat into very localized environments. This simple approach can be used, for instance, to induce death of cancer cells and is normally referred to as plasmonic photo thermal therapy.

Chapter 4 focuses on the characterization of the mechanisms that give rise to anti-Stokes luminescence. Discarding multi-photon processes, photons with higher energies than the excitation energy require interactions with thermal baths. In a nanoparticle electrons and holes can interact with phonons before recombining radiatively. The distribution of phonons in gold follows Bose-Einstein statistics, where the only free parameter is the temperature. We therefore propose in the chapter that anti-Stokes emission can be used for sensing temperature at the nanoscale.

By carefully fitting the luminescence spectra of single gold nanorods and nanospheres it is possible to extract the surface temperature of the particles. The method presented in chapter 4 does not depend on any ad-hoc calibration and can be performed in any confocal microscope with a coupled spectrometer. The chapter shows the increase in temperature with increasing laser powers and also shows the changes that the luminescence spectra undergo when increasing the medium temperature. The calibration-free procedure is a major improvement over previous techniques in the field of nano-thermometry.

Luminescence is not the only method for detecting gold nanorods with an optical microscope. Gold nanoparticles have a large scattering cross section coinciding with the plasmon resonance. Exciting nanoparticles with white light allows one to record the scattering spectra in any confocal microscope coupled to a spectrometer. Since the plasmon damping rate is affected by the surrounding conditions it can also be used to detect changes in temperature. From the mechanisms involved to explain the plasmon damping rate, only electron-phonon coupling is dependent on temperature.

Chapter 5 focuses on the characterization of the plasmon resonance of single gold nanorods at various temperatures. In the range of temperatures studied (between 293 K and 350 K), the plasmon width increases linearly with temperature. The broadening is assigned to an increase in the electron-phonon damping rate. Measuring the broadening of the resonance can then be related to changes in temperature of the surrounding medium. The powers needed for recording scattering spectra are much lower than the ones employed when exciting the luminescence of the particles. However the broad distribution of widths and broadening rates found in the studies of chapter 5 does not allow to perform an absolute temperature measurement but only to measure a relative change.

SAMENVATTING

Gouden nanostaafjes zijn ideale kandidaten om fluoroforen te complementeren als labels. De *surface plasmon resonance* zorgt voor een grote werkzame doorsnede voor absorptie en verstrooiing, waardoor zelfs enkelvoudige nanodeeltjes onder een lichtmicroscoop zichtbaar zijn. Het plasmon van gouden nanostaafjes hangt af van de verhouding tussen hun lengte en breedte, en beslaat de golflengten tussen 540 nm voor sferische deeltjes, tot meer dan 800 nm voor langwerpige staafjes, oftewel bijne het gehele zichtbare en nabij-infrarode spectrum. Het oppervlakteplasmon biedt grote mogelijkheden voor *(bio-)sensing*, geamplificeerde spectroscopie, fotothermische therapie en voor het concenteren van licht voorbij de diffractielimiet.

Hoofdstuk 1 van deze thesis biedt een kort overzicht van fluorescentiemicroscopie en de basiseigenschappen van gouden nanodeeltjes. Microscopie en specifiek fluorescentiemicroscopie zijn resultaten van een lange technische ontwikkeling van de optica en van lichtbronnen, maar ook van de labels die worden gebruikt om de monsters te prepareren. Het scala aan tegenwoordig beschikbare middelen is opmerkelijk: van simpele moleculen tot genetisch geëncodeerde eiwitten. Gouden nanodeeltjes verdienen hun plek tussen deze gereedschappen vanwege hun lange stabiliteit.

De resonantiefrequentie (of energie) van metallische nanodeeltjes wordt bepaald door hun geometrische eigenschappen en door de eigenschappen, zoals de brekingsindex, van het medium waarin ze zich bevinden. De geometrische eigenschappen worden bepaald tijden het synthetiseren van de deeltjes, wanneer de gemiddelde lengte en breedte kunnen worden afgestemd. Wanneer de deeltjes op een substraat worden neergelaten, ligt hun al resonantie vast. Echter, het is mogelijk om de vorm aan te passen via chemische methoden.

Voorgaand werk heeft zich geconcentreerd op bulkmetingen in suspensie. In dit geval zijn de uiteinden van de deeltjes vaak meer reactief, omdat ze minder goed worden beschermd door de surfactanten die het aggregeren van deeltjes voorkomen. Dit leidt tot een anisotropische reactie die langzaam de langwerpige deeltjes tot sferische deeltjes zal reduceren, en die scherpe randen en punten zal eroderen, hetgeen leidt tot een blauwverschuiving van de resonantie.

Hoofdstuk 2 toont aan dat het ook mogelijk is, via welbekende chemische reacties tussen goud en cyanide-ionen, om een roodverschuiving teweeg te brengen. Dit proces kan worden gemodelleerd als het isotropisch etsen van de deeltjes, en we vinden een goede overeenkomst tussen onze berekeningen en experimentele waarnemingen. Het voornaamste verschil met voorgaand werk is de afwezigheid van een surfactant op het oppervlak van de deeltjes. Het beheerst aanpassen van de vorm van nanodeeltjes is van groot belang voor experimenten waar een specifieke resonantie vereist is.

Wanneer deeltjes worden aangeslagen door een monochromatische lichtbron, zoals een laser, zenden ze in het algemeen licht uit bij een andere golflengte dan die van de bron. Dit noemen we luminescentie en dit wordt veel gebruikt voor het afbeelden en volgen van nanodeeltjes onder confocale microscopen. Wanneer de excitatiegolflengte gelijk is aan de resonantiefrequentie van het plasmon, vindt de emissie niet alleen plaats bij langere golflengten, i.e. lagere energieën, maar ook bij kortere golflengten. Dit noemen we anti-Stokes-emissie en dit proces kent intrigerende eigenschappen.

Hoofdstuk 3 toont aan dat het mogelijk is om gouden nanostaafjes te detecteren in biologisch relevante omstandigheden via hun anti-Stokes-emissie. Een short-pass filter in het detectiepad resulteert in een significante onderdrukking van de achtergrondruis, terwijl het luminescentiesignaal hoog blijft. Dit geldt zelfs voor cellen gekleurd met een dye met een hoge *quantum yield* die bij dezelfde golflengte licht absorbeert als de staafjes. Onder dergelijke omstandigheden is het niet mogelijk om losse nanodeeltjes zichtbaar te maken via conventionele Stokes-verschoven emissie, terwijl de anti-Stokesmethode een signaal-ruisverhouding oplevert van meer dan 10.

De techniek gepresenteerd in Hoofdstuk 3 kan eenvoudig worden geïmplementeerd in elke conventionele microscoop door de juiste filters toe te voegen. Er zijn geen speciale operaties of infrastructuur voor nodig. Bovendien kunnen analyse-tools voor het volgen, afbeelden, extraheren van zwaartepunten, etc. van enkelvoudige labels worden gebruikt zonder aanpassingen. De resultaten van Hoofdstuk 3 kunnen een grote impact hebben op de manier waarop nanodeeltjes worden gedetecteerd en afgebeeld in biologische omstandigheden.

Gedurende de laatste twee decennia is er een groeiende interesse geweest in gouden nanodeeltjes als mogelijke middelen in medische behandelingen. De sterke interactie tussen de deeltjes en licht maakt ze ideaal geschikt niet alleen als labels, maar ook om zeer gelokaliseerd warmte los te laten. Deze simpele toepassing kan bijvoorbeeld worden gebruikt om de dood van kankercellen te induceren, en wordt over het algemeen plasmonische fotothermische therapie genoemd.

Hoofdstuk 4 is gericht op het karakteriseren van de mechanismen die anti-Stokes luminescentie veroorzaken. Behalve in processen waar meerdere fotonen mee gemoeid zijn, moet het systeem in contact staan met een thermisch reservoir om fotonen met een hogere energie dan de excitatie-fotonen uit te kunnen zenden. In een nanodeeltjes kunnen electronen en gaten ook met fononen interacteren, voordat ze recombineren en licht uitzenden. De distributie van fononen in goud volgt de Bose-Einsteinstatistiek, waarbij de temperatuur de enige vrije parameter is. We stellen daarom in Hoofdstuk 4 voor dat anti-Stokes-emissie ook kan worden gebruikt om op de nanoschaal temperaturen te meten.

Door zorgvuldig de luminescentiespectra van enkelvoudige gouden nanostaafjes en nanosferen te meten is het mogelijk om de oppervlaktetemperatuur van de deeltjes te bepalen. Het ad-hoc kalibreren van de methode uit Hoofdstuk 4 is niet nodig, en de methode kan worden uitgevoerd met elke confocale microscoop met een gekoppelde spectrometer. In dit hoofdstuk laten we zien hoe de temperatuur toeneemt met toenemend laservermogen, en de veranderingen die de luminescentiespectra ondergaan wanneer we de temperatuur van het medium verhogen.

Deze kalibratievrije methode is een grote verbetering ten op zichte van voorgaande technieken in de nanothermometrie. De resultaten uit dit hoofdstuk kunnen een significante impact hebben op een opkomende gemeenschap die een van de meest dringende gezondheidskwesties van onze tijd probeert aan te pakken.

Luminescentie is niet de enige manier om gouden nanostaafjes te detecteren met een optische microscoop. Gouden nanodeeltjes hebben een grote verstrooiingsdoorsnede die samenvalt met de plasmonresonantie. Wanneer we nanodeeltjes aanslaan met wit licht kunnen we de verstrooiingsspectra meten in elke confocale microscoop met een gekoppelde spectrometer. Omdat de demping van het plasmon afhangt van de eigenschappen van het medium, kan ook dit worden aangewend om veranderingen in temperatuur te meten. Van de mechanismen die een rol spelen in deze demping hang alleen de koppeling tussen electronen en fononen af van de temperatuur.

Hoofdstuk 5 is gericht op het karakteriseren van de plasmonresonantie van enkelvoudige gouden nanostaafjes bij verschillende temperaturen. Bij de temperaturen die we hebben bestudeerd (tussen 293 K en 350 K) neemt de breedte van de resonantiepiek lineair toe met de temperatuur. Deze verbreding kennen we toe aan een versterkte electron-fonondemping. Het meten van deze verbreding kan daarom worden gerelateerd aan temperatuurveranderingen in het omringende medium. Het meten van verstrooiingsspectra kost veel minder vermogen dan het exciteren van de lumeniscentie van de deeltjes. Echter, in de studies van Hoofdstuk 5 vinden we dusdanig brede verdelingen van piekbreedtes, dat het meten van de absolute temperatuur niet mogelijk is, en we deze methode slechts kunnen aanwenden om veranderingen in temperatuur te meten.

CURRICULUM VITÆ

Aquiles Carattino was born on May 7th, 1986 in Buenos Aires, Argentina. From March 2004 until December 2010 he studied physics at the University of Buenos Aires. His undergraduate research project was carried on under supervision of Prof. Pedro Aramendía and focused on the emission anisotropy of nile red molecules embedded in polymer thin films. After his studies, he started working as Research Assistant at Tenaris, world leader in the production of seamless steel tubes in Campana, Argentina. In October 2012 he joined the group of Prof. Michel Orrit at Leiden University to start his PhD project on the luminescence of single gold nanorods.

LIST OF PUBLICATIONS

5. Araoz, B., **Carattino, A.**, Tauber, D., Von Borczyskowski, C. & Aramendia, P. F., *Influence of the glass transition on rotational dynamics of dyes in thin polymer films: Single-molecule and ensemble experiments*. J. Phys. Chem. A 118, 10309-10317 (2014).

4. **Carattino, A.**, Khatua, S. & Orrit, M., *In situ tuning of gold nanorod plasmon through oxidative cyanide etching*. Phys. Chem. Chem. Phys. 18, 15619-15624 (2016).

3. **Carattino, A.**, Keizer, V. I. P., Schaaf, M. J. M. & Orrit, M., *Background Suppression in Imaging Gold Nanorods through Detection of Anti-Stokes Emission*. Biophys. J. 111, 2492-2499 (2016).

2. **Carattino, A.** & Orrit, M., *Gold nanorods as nano-thermometers: Anti-Stokes Luminescence* (Manuscript in preparation)

1. **Carattino, A.** & Orrit, M., *Plasmon damping of gold nanorods at variable temperatures* (Manuscript in preparation)

ACKNOWLEDGMENTS

The last four years of work have been marked by the help and support of many friends and colleagues to whom I want to express my most sincere gratitude. Most of the work in this thesis wouldn't have been possible without them.

Prof. Michel Orrit, my supervisor, deserves a big part of the credit for what has been done in this last four years. His support and guidance were crucial for the completion of this thesis. I learned a lot in these past years thanks to his insightful knowledge over a broad range of topics.

At the beginning of my research, dr. Pedro Navarro and dr. Saumyakhanti Khatua, two fellow members of the group, were of great importance both for scientific discussion and for me to integrate into the group. I am also grateful to the members of the project in which my PhD was framed, including dr. Aimee Boyle for the majority of the nanorod samples employed throughout the thesis, Veer Keizer for the help preparing the samples with cells that led to chapter 3 and Sara Carozza for several insightful discussions.

I am also very grateful to dr. Martín Caldarola, with whom I have shared many hours in the same dark, cold lab. Long discussions with him triggered different approaches and ideas, some of which are reflected in this thesis. He is not only a colleague but also a good friend, whose support has extended beyond the walls of the university.

I am indebted to Ferry Kruidenberg whose bachelor project gave the initial push to the software to control the setup. I am also indebted to Irina Komen, whose MSc project was part of a very challenging idea that finally didn't find its way into this thesis.

The MoNOS group has provided the perfect setting for conducting research, and I am grateful to all the members, especially to Henriëtte van Leeuwen for taking care of so much paperwork. I also thank Marco Tompitak for the translation of the summary.

Of course nothing of what happened during these last four years would have been possible without the endless love and support from my family.